Valter Bruno Reis e Silva

Polymer Electrolyte Membrane Fuel Cells: Activation Analysis and Operating Conditions Optimization

Dissertation presented for the degree of

Doctor of Philosophy in Chemical and Biological Engineering

by

Porto University

Supervisors:

Adélio Miguel Magalhães Mendes

Luis Miguel Palma Madeira

LEPAE – Chemical Engineering Department
Faculty of Engineering
University of Porto

Porto, August 2009

Acknowledgements

I would like to express my gratitude to the Portuguese Foundation for Science and Technology (FCT) for the Ph D grant, reference SFRH/BD/18159/2004, and for the financial support through the projects PTDC/EQU-EQU/70574/2006, POCTI/EQU/38075/2001 and POCTI/EQU/45225/2002.

I would also like to acknowledge to my supervisors Prof. Adélio Mendes and Prof. Miguel Madeira for giving me the opportunity and conditions to perform the present work and for their helpful scientific suggestions and recommendations.

Finally, I would like to express all my admiration and gratitude to my wonderful and beloved wife and parents for their encouragement and unconditional support.

Contents

Part III

3. DMFC Behaviour During an Activation Process

4. Targeting an Improved DMFC Performance Using an Optimized Activation Procedure

Part V

---

7. General Conclusions and Future Work

Figure Captions

Table Captions

Abstract

The present dissertation aimed at understanding the phenomena occurring during an activation procedure of a proton exchange membrane fuel cell (PEMFC), as well as the optimization of the activation procedure of a direct methanol fuel cell (DMFC). A design of experiments approach was employed for obtaining the operating conditions that maximize the efficiency and power density of a DMFC.

Whenever a membrane electrode assembly (MEA) is inserted in a PEMFC, it does not reach the best performance immediately after starting up. Actually, the PEMFC needs to be activated. Activation procedures can be understood as all the actions that can bring the MEA to its highest and stabilized performance. In this work we distinguish between pre-treatment and *in situ* activation procedures. Pre-treatment procedures include all actions carried over a fresh MEA, including the proton exchange membrane (PEM) and electrodes, while *in situ* activation procedures are actions used to improve the performance of a MEA when the fuel cell is on a working state; in the present study loading cycles were employed for the *in situ* activation.

The effect of the pre-treatment actions was followed performing proton conductivity, methanol crossover and swelling experiments. The changes induced in the MEA by the *in situ* activation procedure were followed performing a set of *in situ* electrochemical experiments, namely polarization curves, electrochemical impedance spectroscopy (EIS) and cyclic voltammetry (CV).

Hydrogen fuel cells were firstly characterized to obtain a deeper knowledge about the changes that both the proton exchange membrane (Nafion 112) and catalyst layers experience during an activation procedure. Then, similar activation procedures were

applied to a DMFC and the changes experienced by the MEA (equipped with a Nafion 112 membrane) were fully characterized.

To optimize the power density obtained by the DMFC submitted to an activation procedure, a design of experiments (DoE) methodology was applied (*in situ* activation). Simultaneously, several standard pre-treatments were compared and coupled to the optimized *in situ* activation procedure, allowing the selection of the best activation protocol.

The effect of the activation procedure was also studied in a DMFC equipped with MEAs using proton exchanges membranes of different natures: sulfonated poly(ether ether ketone) (sPEEK) (42 % of sulfonation degree), plain and loaded with zirconium oxide (2.5 wt.% and 5.0 wt.%), and Nafion 112, 1135 and 117.

Finally, the DoE methodology was also applied to obtain the operating conditions of a DMFC (steady state) that maximize the efficiency and the power density.

Sumário

O presente trabalho teve como objectivo compreender os fenómenos que ocorrem durante um procedimento de activação de uma célula de combustível de electrólito de membrana polimérica ("Polymer Electrolyte Membrane Fuel Cell – PEMFC"), assim como a optimização de um procedimento de activação de uma célula de combustível alimentada a metanol ("Direct Methanol Fuel Cell – DMFC"). As condições operatórias que maximizam a eficiência e a densidade de potência de uma DMFC foram obtidas utilizando um planeamento factorial de experiências.

Sempre que um conjunto membrana - eléctrodo ("Membrane Electrode Assembly – MEA") é inserido numa PEMFC não atinge seu máximo desempenho imediatamente. De facto, a célula de combustível de electrólito de membrana polimérica necessita de ser activada. A activação pode ser compreendida como todos os procedimentos que conduzem a MEA a um desempenho máximo. Neste trabalho distinguir-se-á pré-tratamento de activação *in situ*.

O pré-tratamento inclui todos os procedimentos efectuados na membrana de permuta protónica ("Proton Exchange Membrane – PEM") e eléctrodos de uma nova MEA, enquanto por activação *in situ* entende-se todas as acções que levam ao melhoramento do desempenho de uma MEA quando em operação numa célula de combustível.

O procedimento de activação foi realizado submetendo a MEA a um pré-tratamento e a uma activação *in situ*. Foram realizadas experiências de determinação de condutividade protónica, permeação de metanol através da membrana e inchamento da membrana para seguir os efeitos do pré-tratamento. As alterações induzidas na MEA pelo procedimento de activação *in situ* foram seguidas através da determinação de curvas de polarização e

pelo uso de técnicas electroquímicas, nomeadamente, espectroscopia de impedância electroquímica e voltametria cíclica.

As células de combustível alimentadas a hidrogénio foram caracterizadas, em primeiro lugar, para obter um conhecimento mais profundo acerca das alterações que a membrana de permuta protónica (Nafion 112) e as camadas catalíticas sofrem durante o procedimento de activação. De seguida, os procedimentos de activação foram aplicados a uma DMFC e as alterações sofridas por uma MEA foram caracterizadas.

Foi aplicada uma metodologia de planeamento factorial ("Design of Experiments – DoE") para optimizar a densidade de potência obtida por uma DMFC submetida a um procedimento de activação.

Simultaneamente, foram comparados alguns pré-tratamentos padrão referidos na literatura, os quais foram incorporados no procedimento optimizado de uma activação *in situ*, permitindo deste modo a selecção do melhor protocolo de activação.

Foi também estudado o efeito de um procedimento de activação numa DMFC equipada com MEAs montadas com membranas de permuta protónica de naturezas diferentes: poli (éter éter cetona) sulfonada com um grau de sulfonação de 42 %, simples e incorporada com óxido de zircónio (2,5 % e 5,0 % em m/m) e Nafion 112, 1135 e 117.

Finalmente, foi também aplicada uma metodologia de planeamento factorial de experiências para obter as condições operatórias que maximizam a eficiência e a densidade de potência de uma DMFC em estado estacionário.

Part I

1. Proton Exchange Membrane Fuel Cells: an Overview

1.1. Introduction

Nowadays, global environment issues such as atmospheric pollution and global warming are even more a source of deep concern [1 - 3], meanwhile the world energy production demand is rising steadily [3, 4]. On the other hand, it is well known that the conventional power generation supply, based on fossil fuels, is limited and these fuels are expected to be fully depleted in the next years (40 - 100 years) [5]. An alternative approach considers the use of renewable sources to produce and store the energy needed [6]. Renewable sources such as hydroelectric power [7, 8], biomass [9], solar [10], wind [10] and geothermal energy [11] are now being investigated to produce mainly electricity, but is also being investigated the use of bio-fuels [12 - 16] such as bio-diesel [13, 14], bio-ethanol [15] or bio-methanol [16]. All these technologies have advantages and disadvantages, depending on the region and on the local peculiarities [6].

Due to their near zero pollutants emission and potentially high energy efficiencies, fuel cells are growing of interest, assuming a crucial role on the search and development of new energy production systems [17]. Fuel cells are devices which produce energy in the form of electricity, similarly to batteries. However, unlike batteries, a fuel cell does not run down or require recharging; it only needs to be refuelled.

Fuel cells can be used advantageously in the portable [6, 18, 19], transportation [6, 17, 20 - 22] or stationary sectors [6, 21, 23]. Portable power solutions like cellular phones, video cameras, personal digital assistants (PDAs) or laptops, among others, are easily found everywhere. The portable power solutions face significant challenges such as to provide more power and power for longer periods of time. Fuel cells show some

advantages comparing with the direct competitors: easy recharging, compactness, low noise and are easily scalable, being also able to produce different amounts of power.

In the transportation sector, the fuel cells allow a new range of power use from scooters to trucks or other vehicles [6]. On the other hand, the fuel cells are also expected to handle efficiently with the environmental issues associated to transportation, which requires minimal emissions [17]. Finally, fuel cells also show better efficiencies than other competing technologies. The fuel cell's efficiency is not limited by the Carnot Cycle as it occurs with combustion engines. For example, a proton exchange membrane fuel cell fed with hydrogen has a maximum possible efficiency of 83 % when operating at 25 ºC [22].

In the stationary sector, fuel cells can be used as power back-up when the power goes down or to power residences or businesses in remote areas [6].

Despite the considerable advantages related with the use of fuel cells, they also show serious drawbacks. The major barrier to the widespread use of fuel cells is their high cost when compared with the available technologies. Additional limitations of fuel cells are related to their durability, room temperature compatibility and ability to produce good performances right after starting or restarting after a resting period [24]. The use of the fuel cell technology is intimately related with the ability to develop technological solutions that minimize or solve these drawbacks.

1.1.1. Different Types of Fuel Cells

Currently, there are five main types of fuel cells:

- Polymer electrolyte membrane fuel cell (PEMFC)
- Phosphoric acid fuel cell (PAFC)
- Alkaline fuel cell (AFC)

- Molten carbonate fuel cell (MCFC)
- Solid-oxide fuel cell (SOFC)

These fuel cells are named accordingly to the electrolyte used. Each of them is based in the same electrochemical principals but is distinguished by the characteristic operating regimens, system requirements and performance. In Table 1.1 are listed the characteristics of the five main types of fuel cells.

Table 1.1 – Description of the five main types of fuel cells [6, 17, 24].

	PEMFC		**PAFC**	**AFC**	**MCFC**	**SOFC**
	DMFC	**H_2 Fuel Cells**				
Operating Temperature / ºC	60 - 120	60 – 120	160 - 200	60 - 100	600 - 700	600 - 1000
Charge Carrier	H^+		H^+	OH^-	CO_3^{2-}	O^{2-}
Electrolyte	PEM		Liquid H_3PO_4 immobilized	Liquid KOH immobilized	Li_2CO_3/K_2CO_3 or Li_2CO_3/Na_2CO_3	Yttrium oxide-doped zirconia
Efficiency / %	30 - 35	35 - 40	35 - 40	55 - 60	40 – 55	35 - 45
Applications	Portable and Vehicles		Stationary (cogeneratio)	Military and spatial use	Stationary (cogeneration)	Stationary (housing and cogeneration)
Catalyst	Pt and Ru	Pt	Pt	Pt	Ni	Perovskites (Ceramic)
Range	1 W - kW	50 W - 150 kW	25 kW - 250 kW	< 12 kW	10 kW - MW	200 kW - MW

The technologies shown in Table 1.1 are thoroughly discussed in classical references [6, 17, 24] and besides the DMFC and PEMFC, the other technologies will not be subject of any further analysis.

1.1.2. Proton Exchange Membrane Fuel Cells

Along this work, the PEMFCs will be the subject of our interest and research. The PEMFC technology shows some advantages [17], such as a low working temperature (*cf.* Table 1.1) that, for transportation or small appliances, allows a quick start-up, but also compactness, flexibility, no corrosion problems and a considerable power density, namely when fuelled with hydrogen – H_2 fed PEMFC or DHFC (direct hydrogen fuel cell) [25, 26]. Indeed, hydrogen is the most known and used fuel due to its high electrochemical activity. However, hydrogen does not exist spontaneously in the nature and has to be produced from external processes, leading to more complex and expensive systems. Furthermore, hydrogen storage and transport is difficult. The typical ways to store hydrogen are as compressed gas, as liquid or in a metal or organic hydride [24]. The storage process related to the liquid and compressed hydrogen is very energy intensive and the option related to the metal or organic hydrides is considerably expensive [24, 27]. This set of problems led the researchers to use direct liquid fuels to feed the fuel cells devices, and in such manner avoid difficulties and hazards related with the handle, storage and distribution of hydrogen.

Among all possible fuels that can be used for feeding directly a fuel cell, methanol is the most studied due to its high electrochemical activity when compared with other liquid fuels such as ethanol or formic acid [28]. Simultaneously, methanol is liquid at room temperature, has high energy density and is not expensive. Furthermore, methanol production is not dependent on hydrogen generation processes because it can be obtained by steam reformation of natural gas or by wood distillation [29].

There is however a number of challenging problems to be solved before successful commercialization of DMFCs; among them the low methanol oxidation kinetics and the excessive methanol crossover [30]. In fact, the sluggish kinetics of the methanol electro-

oxidation is one of the major drawbacks for the commercial implementation of the DMFC technology. The use of pure Pt anodes shows a poor performance [31] because one of the intermediates (CO) that results from the methanol oxidation occupy catalyst active sites, slowing the reaction. In order to obtain increased performances, different binary catalysts are being studied [30 - 34]. Some of the elements added to Pt to produce catalytic composites with higher electro-oxidation activity are Os [32], Sn [33], Mo [34] or Ru [30, 31]. Up to now, the Pt-Ru composite catalyst seems to be the most effective one [30, 35]. On the other hand, the methanol crossover is responsible for the occurrence of a mixed potential at the cathode. Whenever the methanol crosses through the electrolyte, from the anode to the cathode, it leads to unavoidable parasitic reactions that tend to lower the equilibrium electrode potential [30]. Also, methanol reacting on the platinum surface occupies sites that should be available for the oxygen reduction, and thus increases the overpotential losses. The effect of the methanol crossover is more notorious at the open circuit condition because the driving force for permeation is increased.

Other fuels that are becoming more important to feed directly a fuel cell are ethanol (direct ethanol fuel cells – DEFC) [28, 36] and formic acid (direct formic acid fuel cells – DFAFC) [37]. Ethanol is considered to be attractive [28] due to its low toxicity, natural availability, renewability and minimal pollutants emission. However, under similar operating conditions, the direct ethanol fuel cells performance is still much inferior to that of fuel cells fed with hydrogen or methanol. This happens essentially due to the slow reaction kinetics of the ethanol electro-oxidation [28].

The DFAFCs present some interesting characteristics, such as a low crossover through Nafion membranes when compared with DMFCs [38] and a higher electromotive force than either hydrogen or direct methanol fuel cells [38]. The main disadvantage related to the use of DFAFCs is that the formic acid has a low volumetric energy density,

2104 $Wh \cdot L^{-1}$, considerably smaller than the methanol energy density. Some improvements are still therefore needed in the DFAFC technology considering the electrocatalytic reaction and the power density output.

1.1.2.1. Basics of a PEMFC

The experimental work performed in the framework of this thesis is related to the PEMFC technology with foccus in DMFCs and DHFC.

A short description of the DMFC operation is given below and depicted in Figure 1.1. Basically, a methanol aqueous solution, typically in the range of 0.5 M – 2 M, is fed to an electrode (anode) and converted to carbon dioxide, protons and electrons. This reaction occurs in general on a Pt - Ru catalyst, with a 1:1 molar ratio and with a load of about 2 $mg \cdot cm^{-2}$, releasing 6 electrons per methanol molecule, according to the following reaction (electrode potentials at standard conditions, P = 1 atm and T = 298.15 K):

$$CH_3OH + H_2O \xrightarrow{Pt/Ru} CO_2 + 6\,H^+ + 6e^- \qquad E^o = -0.23\ V \qquad (1.1)$$

The electrons are conducted through an external circuit (which includes a load), while protons cross through the solid electrolyte (PEM – proton exchange membrane), which is sandwiched between two electrodes, the anode and the cathode. At the cathode, air or oxygen streams are fed; the oxygen reacts with the electrons taken from the anode and with protons on a Pt catalyst (**~** 0.5 $mg \cdot cm^{-2}$**)**, to form water, according to the following reaction:

$$\tfrac{3}{2} O_2 + 6\,H^+ + 6\,e^- \xrightarrow{Pt} 3\,H_2O \qquad E^o = 1.43\ V \qquad (1.2)$$

These two half reactions lead to the production of water, carbon dioxide, work and wasted heat, as follows:

$$CH_3OH + \tfrac{3}{2} O_2 \longrightarrow CO_2 + 2\,H_2O + work + heat \qquad E^o = 1.20\ V \qquad (1.3)$$

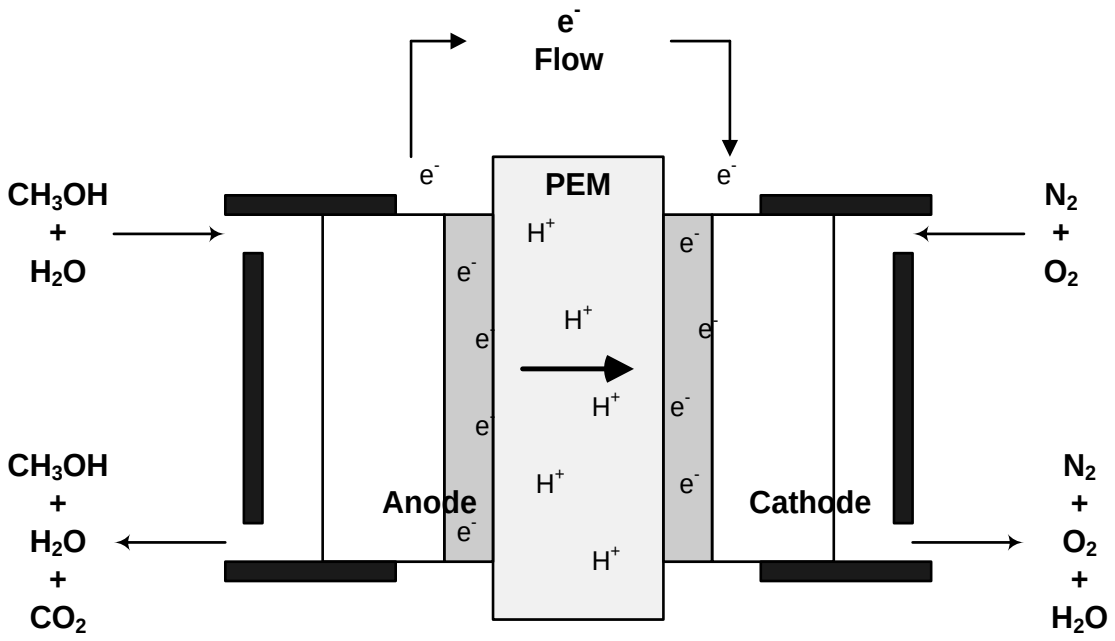

Figure 1.1 - Sketch of a DMFC illustrating the different species involved in the electrochemical reactions.

The operating process is similar for the direct hydrogen fuel cells. However, the anode is fed with a gaseous hydrogen stream instead of a methanol aqueous solution. The anode and cathode reactions proceed as follows (electrode potentials at standard conditions, P = 1 atm and T = 298.15 K):

$$H_2 \xrightarrow{Pt} 2\,H^+ + 2e^- \qquad E^o = 0\ V \qquad (1.4)$$

$$\tfrac{1}{2}O_2 + 2\,H^+ + 2e^- \xrightarrow{Pt} H_2O \qquad E^o = 1.23\ V \qquad (1.5)$$

These reactions occur, in general, on a Pt catalyst with a load of about 0.1 mg·cm^{-2}.

1.1.2.2. Polarization Behaviour

The reversible cell voltage of a DMFC always differs from the open circuit voltage, because of the overpotentials resulting from the electrochemical activation energy and the mixed potential at the cathode (fuel crossover losses), which result from unavoidable parasitic reactions that decrease the equilibrium electrode potential.

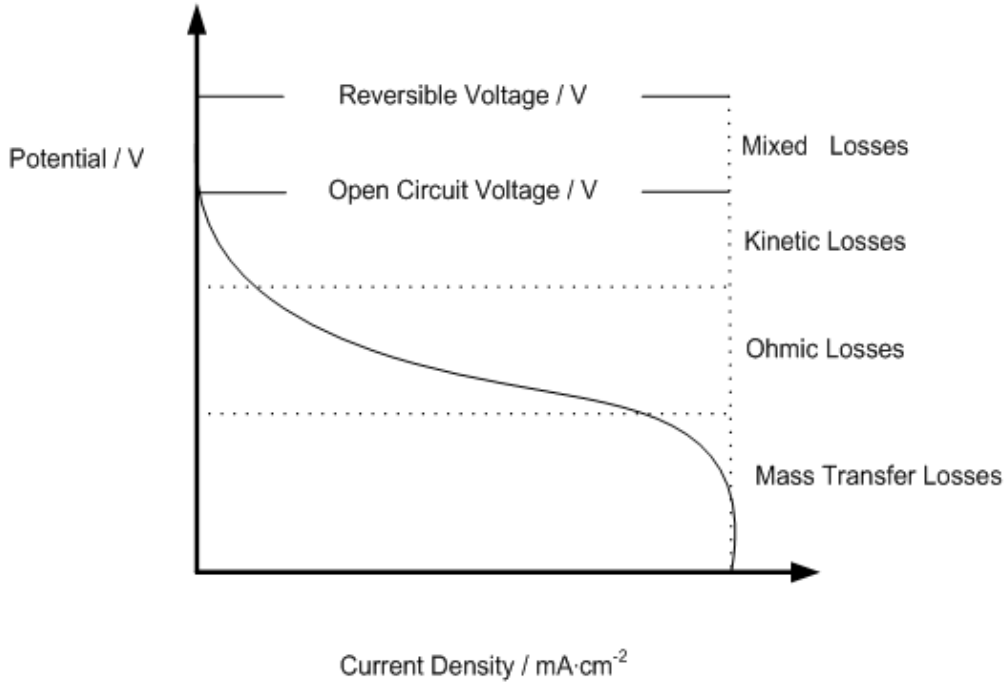

Figure 1.2 – Typical current density – potential behaviour of a DMFC.

At low current densities, the kinetic effects are more pronounced, due to the sluggish methanol oxidation kinetics at the anode, where the transference of six electrons and the formation of several intermediate compounds could be expected [30, 31]. The deviation from the equilibrium potential at low current densities is known as activation losses.

At intermediate current densities, ohmic losses arise from the proton transport

across the electrolyte, from electrons transport across the electrodes and from resistances related with the bipolar plates, current collectors and contact between them. However, the great source of overpotential for these current ranges is associated to the ionic transport between the anode and the cathode through the electrolyte.

Finally, at high current densities the sources of overpotentials are essentially related to the depletion of reactants in the electrode layers. In the limit, the voltage fells to zero and no more energy is produced; this current is defined as the limiting current density.

The polarization behaviour is also similar for the DHFCs; however at low current densities, the kinetic effects are more pronounced essentially due to the oxygen reduction kinetics at the cathode.

1.1.2.3. PEMFC Components

A PEMFC comprises a set of different components: a proton exchange membrane, a pair of catalyst and diffusion layers, a pair of gaskets, a pair of bipolar plates and a pair of current collectors – Figure 1.3. When the proton exchange membrane is assembled with the catalyst layers, it forms the so-called membrane electrode assembly (MEA). The PEM is the main component of this assembly, enabling the proton transport between the anode and the cathode and barring the transport of electricity and reactants.

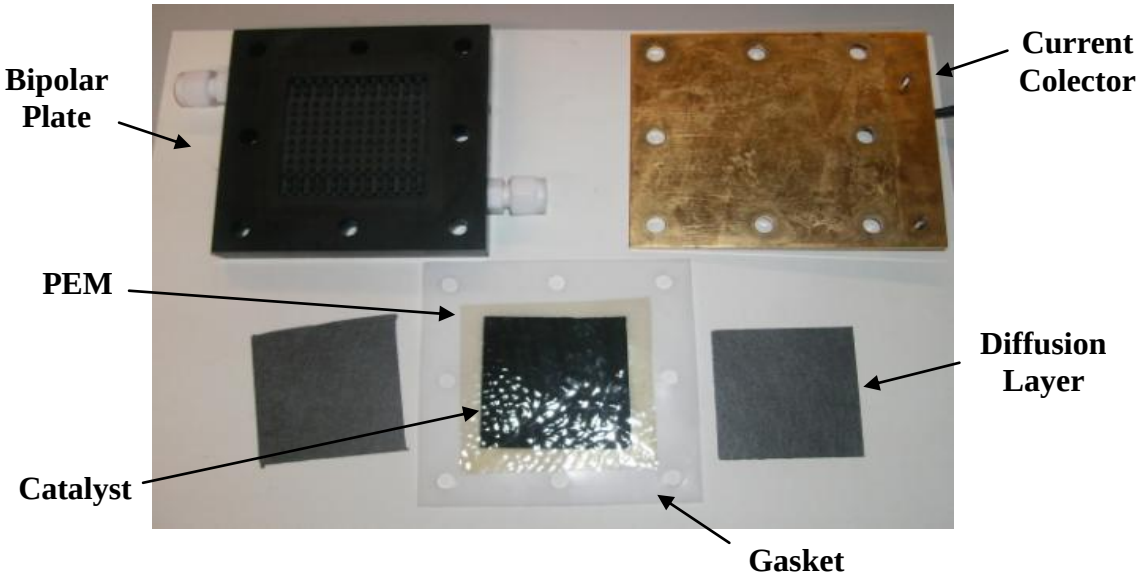

Figure 1.3 – Fuel cell components.

The main function of the catalyst layers is to promote the electrochemical reactions. The reaction occurs on metal sites (typically Pt - Ru at the anode and Pt at the cathode for DMFCs, and Pt at the anode and cathode for the DHFCs) and, in general, these catalyst particles are supported in carbon black particles that allow electrical conductance. The supported catalyst particles are involved by an ionomer to promote proton transport to the electrolyte, and by PTFE to hold the carbon particles and to avoid water flooding. Attached to the catalyst layers, the diffusion layers are used to provide mechanical stability to the MEA, electrical current conductance and to homogenise the distribution of reactants over the catalyst layer [24, 30].

A sealing gasket is placed between the bipolar plates to prevent reactants leakage. Typical sealing materials for fuel cell are made of silicone or EPDM (ethylene propylene diene M-class rubber) [39]. The degradation of the seals can lead to compression losses, external leaks, reactants crossover or plate electrical shorting. On the other hand, residues from the sealing materials can influence negatively the hydrophobic nature of the electrodes and poison the catalysts or even reduce the PEM proton conductivity or mechanical integrity.

The bipolar plates play a set of important roles in a fuel cell, namely collecting the current generated by the electrochemical reactions and guiding it to the current collectors, distributing the reactants and the products but also ensuring mechanical support to the MEA components.

1.1.3. Activation Procedures

Both DMFCs and DHFCs do not show the maximum power and energy performance after the start-up or after resting periods [40, 41]. In fact, their performances increase gradually with the operation time, i.e. the fuel cell needs to be activated.

Activation procedures can be understood as all the actions that can bring the MEA to its highest and stabilized performance. An activation procedure is divided in: pre-treatment and *in situ* activation. Pre-treatment procedures include all actions carried over a fresh MEA, including the PEM and electrodes, while the *in situ* activation procedures are actions used to improve the performance of a MEA when the fuel cell is on a working state.

In the literature some studies describing methodologies to activate a fuel cell are reported [42 - 46]. Despite all these studies show effective methods to improve the cell's performance, scarce information is provided in the literature about the mechanisms behind them and that justifies the observed performance improvement. Furthermore, electrochemical techniques are not employed to identify and quantify the various overpotentials that occur during the applied activation procedures. This challenging question has been receiving scarce attention from the research community and little information is available in the open literature [47]. To obtain a better knowledge concerning MEA's activation it is necessary to select an activation protocol (meaning that the PEM and catalyst should be activated simultaneously) and apply *in situ*

characterization techniques to follow the induced activation changes. At these circumstances, *in situ* electrochemical experiments and techniques, such as Linear Sweep Voltammetry (LSV), Cyclic Voltammetry (CV), polarization curves and Electrochemical Impedance Spectroscopy (EIS) can be looked as valuable tools to proceed to a quantitative and qualitative analysis about the performance of the fuel cell.

The LSV experiments allow determining the fuel crossover through the proton exchange membrane – hydrogen for the DHFCs and methanol for the DMFCs. Fuel crossover data are especially important for the DMFCs because the methanol crossover is one of the most important phenomena affecting the power performance and energy efficiency of these cells. The LSV technique can be combined with EIS experiments to quantify the overpotentials caused by the fuel crossover and by the mixed potential.

The CV technique allows evaluating the effective catalyst area available to promote the electrochemical reactions.

The overall performance of a fuel cell can be obtained from the polarization curve [24]. In general, a polarization curve exhibits an S-shaped that can be delimited in 3 different regions, each one corresponds to one controlling mechanism (Figure 1.2). From the polarization curve, it can also be computed the power curve, power density as a function of the current density. Additionally, the energy overall efficiency values can be computed from the polarization curves, in the case of the DHFCs and from the the polarization curves and methanol crossover, in de case of the DMFCs.

EIS experiments can discriminate the contributions of the different overpotential sources that affect the performance of a fuel cell. In general, the obtained spectra are fitted to a model and important parameters as PEM proton resistance and electrodes charge transport resistances can be obtained separately.

The study of a PEMFC activation procedure will be the main subject of the present dissertation and will be discussed in detail in the next chapters.

1.1.4 Outline of the Thesis

The present dissertation is organized as follows.

Part I (also Chapter 1) considers a general introduction and review of the state of the art concerning the fuel cells, addressing particular attention to the proton exchange membrane fuel cells technology.

In Part II, the changes experienced by a MEA (inserted in a DHFC) along an activation procedure are studied. The MEA was fully characterized along the activation procedure performing polarization curves, LSV, CV and EIS (Chapter 2).

Part III reports the characterization and optimization of an activation procedure applied to a DMFC. The MEA behaviour along an activation procedure was followed applying a set of loading cycles interrupted by *in situ* electrochemical tests, such as polarization curves, methanol crossover, cyclic voltammetry and impedance spectroscopy experiments (Chapter 3). The effect of the *in situ* loading cycles in the maximum power density is mainly determined by the fuel cell operating conditions. To minimize the number of runs needed to obtain the optimum conditions, a Design of Experiments methodology was adopted. Simultaneously, several pre-treatments were also tested to find the best activation protocol (Chapter 4). The effect of the activation procedure was also studied considering MEAs equipped with membranes of different natures, namely sulfonated poly(ether ether ketone) (sPEEK) (sulfonation degree of 42 %) plain and loaded with zirconium oxide (2.5 wt.% and 5.0 wt.%) and membranes of Nafion® 112, 1135 and 117 (Chapter 5).

In Part IV, the effect of the temperature, methanol concentration, air flow rate, methanol flow rate and air relative humidity in the power density of a DMFC is studied using a Design of Experiments methodology (Chapter 6).

Finally, in Part V, the main conclusions are summarized and suggestions for future work presented (Chapter 7).

1.1.5. References

1. V. Ramanathan and Y. Feng, *Atmospheric Environment*, 43, 37 (2009).
2. G. A. Florides and P. Christodoulides, *Environment International*, 35, 390 (2009).
3. M. Asif and T. Muneer, *Renewable and Sustainable Energy Reviews*, 11, 1388 (2007).
4. http://www.eia.doe.gov/oiaf/ieo/world.html, last access, 23/07/2009.
5. S. Shafiee and E. Topal, *Energy Police*, 37, 181 (2009).
6. C. S. Spiegel, *Designing & Building Fuel Cells*, Mc Graw Hill, New York (2007).
7. C. P. Barros, *Energy Economics*, 30, 59 (2008).
8. F. C. Menz, *Energy Policy*, 33, 2398 (2005).
9. A. L. Cowie and W. D. Garner, *Biomass and Bioenergy*, 31, 601 (2007).
10. Varun, R. Prakash and I. K. Bhat, *Renewable and Sustainable Energy Reviews*, (2009).

11. D. L. Gallup, *Geothermics*, (2009).

12. A. Demirbas, *Energy Conversion and Management*, 50, 2239 (2009).

13. A. Murugesan, C. Umarani, R. Subramanian and N. Nedunchezhian, *Renewable and Sustainable Energy Reviews*, 13, 653 (2009).

14. M. Balat and H. Balat, *Energy Conversion and Management*, 49, 2727 (2008).

15. M. Balat and H. Balat, *Applied Energy*, 86, 2273 (2009).

16. K. Vogt, D. Vogt, T. Patel, R. Upadhye, D. Edlund, R. Edmonds, J. Gordon, A. Suntana, R. Sigurdardottir, M. Miller, A. Roads and M. Andreu, *Renewable Energy*, 34, 233 (2009).

17. J. Larminie and A. Dicks, *Fuel Cell Systems Explained*, John Wiley & Sons, Chichester (2003).

18. J. Salgado and M. Aguilar, *Journal of Power Sources*, 186, 455 (2009).

19. P. Agnolucci, *International Journal of Hydrogen Energy*, 32, 4319 (2007).

20. R. Ahluwalia and X. Wang, *Journal of Power Sources*, 117, 167 (2008).

21. S. Varigonda and M. Kamat, *Computers & Chemical Engineering*, 30, 1735 (2006).

22. K. R. Cooper, V. Ramani, J. M. Fenton and H. R. Kunz, *Experimental Methods and Data Analysis for Polymer Electrolyte Fuel Cells*, Scribner Associates, North Carolina (2005).

23. C. Karger and R. Bongartz, *Energy Policy*, 36, 798 (2008).

24. R. O'Hyare, S. Cha, W. Colella and F. Prinz, *Fuel Cell Fundamentals*, John Wiley & Sons, New York (2006).

25. L. Quingfeng, H. A. Hjuler, C. Hasiotis, J. K. Kallitsis, C. G. Kontoyannis and N. J. Bjerrum, *Electrochemical and Solid-State Letters*, 5, A125 (2002).

26. R. Moore, S. Gottesfeld and P. Zelenay, *A Comparison Between Direct Methanol and Direct Hydrogen Fuel Cell Vehicles*, Institute of Transportation Studies (1999).

27. B. Sakintuna, F. Darkim and M. Hirscher, *International Journal of Hydrogen Energy*, 32, 1121 (2007).

28. S. Song and P. Tsiakaras, *Applied Catalysis B: Environmental*, 63, 187 (2006).

29. P. J. A. Tijm, F. J. Waller and D. M. Brown, *Applied Catalysis A: General*, 221, 275 (2001).

30. R. Dillon, S. Srinivasan, A. S. Aricò and V. Antonucci, *Journal of Power Sources*, 127, 112 (2004).

31. A. Hamnett, *Catalysis Today*, 38, 445 (1997).

32. A. Hamnett and B. J. Kennedy, *Electrochimica Acta*, 33, 1613 (1988).

33. D.M. Han, Z.P. Guo, R. Zeng, C.J. Kim, Y.Z. Meng and H.K. Liu, *International Journal of Hydrogen Energy*, 34, 2426 (2009).

34. H. Nakajima, *Journal of Chemical Technology*, 50, 555 (1991).

35. S. Wasmus and A. Kuver, *Journal of Electroanalytical Chemistry*, 461, 14 (1999).

36. E. Antolini, *Journal of Power Sources*, 170, 1 (2007).

37. X. Yu and P. Pickup, *Journal of Power Sources*, 182, 124 (2008).

38. U. B. Demirci, *Journal of Power Sources*, 169, 239 (2007).

39. M. Sculze, T. Knori, A. Schneider and E. Gulzow, *Journal of Power Sources*, 127, 222 (2004).

40. F. Liu and C. Y. Wang, *Electrochimica Acta*, 50, 1413 (2005).

41. Z. Qi and A. Kaufman, *Journal of Power Sources*, 111, 181 (2002).

42. C. He, Z. Qi, M. Hollet and A. Kaufman, *Electrochemical Solid-State Letters*, 5, A181 (2002).

43. Z. Qi and A. Kaufman, J*ournal of. Power Sources*, 114, 21 (2003).

44. Z. Xu, Z. Qi and A. Kaufman, J*ournal of. Power Sources*, 156, 281 (2006).

45. Y. Kiang, PhD Thesis, Spontaneous Hydrogen Evolution in Direct Methanol Fuel Cells, Hong Kong, 2005.

46. C. Rice, X. Ren, S. Gottesfeld, Methods of Conditioning DMFCs, United States Patent, 2005.

47. J. H. Kim, H. I. Lee, S. A. Hong and H. Y. Ha, *Journal of Electrochemical Society*, 152, A2345 (2005).

Part II

2. *In situ* Electrochemical Characterization Techniques Applied to a Hydrogen-Fed PEMFC along its Activation Process*

Abstract

The present study aims at obtaining a better understanding on the changes that the membrane electrode assembly (MEA) of a H_2-fed fuel cell experiences along an activation procedure. An activation protocol was set-up considering six loading cycles performed at 25 ºC. After each loading cycle, the electrochemical characterization was performed using polarization curves, Linear Sweep Voltammetry (LSV), Cyclic Voltammetry (CV) and Electrochemical Impedance Spectroscopy (EIS). Polarization curves showed an effective increase of the MEA performance along the activation procedure, with the maximum power density increasing from 116.1 $mW \cdot cm^{-2}$ to 229.9 $mW \cdot cm^{-2}$ and the overall efficiency increasing from 9.3 % to 19.7 %. Simultaneously, it was observed a decrease on the Tafel slope and an increase on the exchange current density, indicating improved catalyst characteristics. From the LSV experiments it was concluded that hydrogen crossover at open circuit increases along the activation procedure, however the open circuit voltage (OCV) also increases, mainly due to an overvoltage decrease caused by mixed potential. CV experiments showed that the available catalyst area also increases. From the impedance experiments it was observed that the proton exchange membrane (PEM) and the anode and cathode charge transfer resistances decrease along the activation cycles. The opposite trend was verified for the anode and cathode double layer capacitances.

*V. B. Silva, V. S. Silva, L. M. Madeira, A. Mendes, submitted

2.1. Introduction

After being manufactured, a polymer electrolyte membrane fuel cell (PEMFC) needs to be activated for showing a maximum energy performance [1, 2]. This performance increase is related with the hydration of the proton exchange membrane (PEM) and the catalyst area available to promote the electrochemical reactions. The PEM proton conductivity increases with the hydration of the membrane and the overall catalytic activity increases with the catalyst area. Furthermore, it is widely accepted that the performance of a PEMFC is largely influenced not only by the fabrication procedure of the membrane electrode assembly (MEA), but also by the employed pre-treatment [3, 4] or by the applied *in situ* activation procedure [5].

An activation process can be defined as all procedures intended to bring the MEA to a stable and improved energy performance and include pre-treatment and *in situ* activation procedures. It is considered that the pre-treatment comprises all the procedures carried on the PEM and electrodes and that are made over a fresh MEA, while the *in situ* activation procedures are the actions used to improve the performance of a MEA when the fuel cell is under operation.

In the open literature are reported several procedures to improve the MEA performance [4, 6-9]. He et al. [6], for instance, presented the so-called hydrogen evolution method. In this approach, air at the cathode side is replaced by nitrogen, while the anode side is fed with pure hydrogen. Basically, to activate the cathode, hydrogen passes across the membrane with the help of an external power source, which is applied to the fuel cell, with the cathode side having a lower voltage than the anode. The protons resulting from the hydrogen oxidation in the anode cross the membrane and are reduced in the cathode forming hydrogen. Structural changes may occur in the catalyst layers, namely involving porosity and tortuosity [6].

Another activation process suggested considers exposing the MEA to elevated temperature and pressure [7]. It seems that this procedure is able to reduce the ionic resistance, including membrane and catalyst layer resistances. It is proposed by these authors that the catalyst utilization is increased by opening many "dead" regions. The effect is claimed to be long-lasting.

Co-oxidative stripping is also described as an activation method [8]. CO strongly adsorbs onto the catalyst surface, poisoning it, but it can be removed by applying a positive potential to oxidize it to CO_2. It was found that in such way the catalyst could be activated.

The combination of all these methods in the correct sequence could provide even better PEM performance [9]. Among the previous methods, the most effective one considers exposing the MEA at elevated temperature and pressure, but applying hydrogen evolution or CO oxidative stripping afterwards could further increase the final performance.

Steaming or boiling an electrode can also enhance the MEA's performance [4]. It is suggested that the improved performance was due to the increased catalyst utilization and namely by the opening of regions which were blocked.

Despite all these studies show effective methods to improve the cell's performance, scarce information is provided in the literature about the mechanisms behind them and that justifies the observed performance improvement. Furthermore, electrochemical techniques are not exploited to identify and quantify the various overpotentials that occur during the applied activation procedures. To obtain a better knowledge concerning MEA's activation it is necessary to choose an activation protocol (meaning that the PEM and catalyst should be activated simultaneously) and apply *in situ* techniques to follow the induced activation changes. At these circumstances, *in situ* electrochemical techniques

can be looked as valuable tools to proceed to a quantitative and qualitative analysis. *In situ* electrochemical experiments and techniques, such as Cyclic Voltammetry (CV), Linear Sweep Voltammetry (LSV), polarization curves and Electrochemical Impedance Spectroscopy (EIS) can provide the ability to measure these modifications, identifying not only the overpotential sources but also their values [10]. This is the main goal of the present work, i.e., to use these techniques to better understand the hydrogen-fed PEMFC behaviour during its activation.

A fuel cell never attains its reversible potential due to internal leakages (fuel crossover) [11] and to mixed potential [12, 13]. The open circuit voltage behaviour is then related with the hydrogen crossover that should be determined as a function of the activation process. This can be performed carrying out LSV experiments. Combining this technique with EIS analysis at open circuit allows quantifying the overpotential caused by the fuel crossover and consequently the mixed potential losses [14].

It has been verified experimentally that the current drawn from the cell along the activation procedure increases [5], making then important to evaluate the history of the effective active catalyst area. This can be achieved performing CV experiments [10, 15]. EIS experiments are also needed in this study because they can discriminate the contributions of the different overpotential sources along the activation procedure [10, 16]. EIS can be carried out at different current densities along the activation cycles. Furthermore, PEM proton resistance and electrodes charge transport resistances can be evaluated separately.

Finally, polarization curves allow evaluating the history of the potential and power density as a function of the current. Energy overall efficiency values can be computed from the polarization curves.

2.2. Experimental

2.2.1. MEA Pre-treatment

In this work a PEM made of Nafion 112 was used. This membrane was boiled in distilled water during one hour before being assembled and used in the fuel cell, as suggested by Silva et al. [3], in order to improve its protonic conductivity. The backing and catalyst layers were also boiled during one hour for improving the catalyst performance [4].

2.2.2. MEA Activation Protocol

The loading procedure was performed submitting the MEA, inside the fuel cell, to a set of sequential cycles, each one composed by open circuit (OC) and loading periods. At the first cycle, the MEA was operated at the OC condition during 30 minutes. Subsequently, the cell was loaded during one hour (30 minutes at 600 mV and 30 minutes at 400 mV). These voltages were selected because are within the optimal operating conditions of the fuel cell, concerning the power density. Then, the MEA was fully characterised regarding the polarization curve, impedance at different voltages, LSV and CV experiments. Between each analysis the MEA was allowed to rest for 30 minutes under the OC condition. At the end of this characterisation sequence, the first cycle was considered concluded. The procedure was then repeated for a new cycle until almost steady state PEMFC performance was reached.

It should be pointed out that during the electrochemical experiments, the cell was gradually activated. However, the obtained values from each experimental electrochemical technique give us a good idea about the performance history along the activation procedure.

2.2.3. Characterization Methods

2.2.3.1. *In situ* Cyclic Voltammetry (CV)

In situ cyclic voltammetry was carried out with the PEMFC in operation. The cathode was fed with nitrogen, acting as working electrode, while hydrogen was fed to the anode acting as counter-electrode. Because of the negligible overpotential at the counter electrode (hydrogen oxidation), this also serves as reference electrode [10]. The working electrode was swept up to potentials that allow hydrogen molecules that cross the electrolyte to oxidize. Additionally, the reverse potential sweep was performed. During this reverse scan, the electrochemical reduction of protons occurs, as described by the following equation:

$$Pt + H^+ + e^- \Leftrightarrow Pt - H_{ads} \tag{2.1}$$

The electrochemical area associated to the hydrogen adsorption can be evaluated by the following relation:

$$ECA = \frac{Q}{\mu_{Pt} \times L} \tag{2.2}$$

where ECA is the electrochemical active area, Q is the charge density of the atomic hydrogen adsorption, μ_{Pt} is the charge required to reduce a monolayer of protons on a polycrystalline Pt surface of 1 cm^2 (210 $mC \cdot cm^{-2}$ Pt) and L is the Pt load (0.5 $mg \cdot cm^{-2}$).

The charge density was obtained from the hydrogen adsorption area obtained from the CV scans between 0.06 V and 0.4 V. Double layer charging was subtracted for not overestimating the electrocatalytic activity.

The CV scans were performed at a scan rate of 40 $mV \cdot s^{-1}$, with hydrogen (200 $ml_N \cdot min^{-1}$ feed flowrate at 25 ºC, 100 % relative humidity and 1.5 bar backpressure) on the anode side and nitrogen (200 $ml_N \cdot min^{-1}$ feed flowrate at 25 ºC, 100 % relative humidity and 1.5 bar backpressure) on the cathode side.

2.2.3.2. Linear Sweep Voltammetry (LSV)

Similarly to the CV experiments, nitrogen was fed to the fuel cell cathode (working electrode) while hydrogen was passed through the anode compartment (which acts as counter/reference electrode). Then, the potential was linearly swept with time leading to the hydrogen oxidation.

The amount of hydrogen that crosses the electrolyte is related with the diffusion limiting current attained at the electrodes potential and can be computed using the Faraday's law:

$$N_{H_2} = \frac{I_{\lim}}{n \times F} \tag{2.3}$$

where N_{H_2} is the hydrogen molar flowrate that crosses the electrolyte, $I_{\lim}$ is the limiting current, n is the number of electrons involved on the hydrogen oxidation ($n = 2$) and F is the Faraday's constant.

The LSV scans were performed at a scan rate of 2 $mV \cdot s^{-1}$ between 0 and 0.8 V, with hydrogen (200 $ml_N \cdot min^{-1}$ feed flowrate at 25 ºC, 100 % relative humidity and 1.5 bar backpressure) on the anode side and nitrogen (200 $ml_N \cdot min^{-1}$ feed flowrate at 25 ºC, 100 % relative humidity and 1.5 bar backpressure) on the cathode side.

2.2.3.3. Electrochemical Impedance Spectroscopy (EIS)

The electrochemical impedance measurements were performed using a Zahner IM6e workstation coupled with a potentiostat (PP-240, Zahner). Spectra were obtained at OC, 800 mV, 600 mV, 400 mV and 300 mV (for each loading cycle), in the potentiostatic mode. Impedance spectra were also recorded at ten points per decade by superimposing a 5 mV ac signal over the frequency range from 100 kHz to 10 mHz.

Impedance experiments are only meaningful when the system behaves linearly. A sinusoidal voltage perturbation of 5 mV was then applied, which is considerable smaller than the thermal voltage at 25 ºC (26 mV) [10].

2.2.3.4. PEMFC Tests

The studied MEA was prepared by hot pressing the membrane sample, Nafion 112, between two Quintech electrodes at 90 ºC and 150 bar for 150 seconds. The noble metal (Pt) loading on both anode and cathode sides was 0.5 $mg \cdot cm^{-2}$.

Single cell measurements were carried out in a 25 cm^2 active area fuel cell. Each polarization curve was obtained starting at OC and decreasing the potential until near limiting current densities, waiting 3 minutes at each step (i.e., to obtain each data point in the potential vs. current density plots). The PEMFC was operated with humidified hydrogen (1.5 bar of backpressure, 100 $ml_N \cdot min^{-1}$ feed flowrate and 100 % relative humidity) on the anode and with humidified air (1.5 bar of backpressure, 1000 $ml_N \cdot min^{-1}$ feed flowrate and 100 % relative humidity) on the cathode side. The PEMFC bench test is described elsewhere [17]. The cell temperature was maintained at 25 ºC.

2.2.3.5. Efficiency Tests

There are several approaches to obtain the fuel cell efficiency. In this study it was considered that the overall energy efficiency is the product of the current and voltage efficiencies, defined as follows [10]:

1. The current efficiency can be defined as the ratio between the current produced and the current that should be produced from the stoichiometry (considering the feed conditions).

2. The voltage efficiency can be defined as the ratio between the cell voltage and the thermodynamic maximum cell voltage for the tested conditions.

2.3. Results and Discussion

When a fresh MEA is assembled to be operated, its performance is appreciably low. The MEA's performance undergoes a considerable increase along time until reaching a stabilized steady-state performance. The use of several *in situ* electrochemical techniques will be discussed along this text to better understand the underpinning mechanisms that are behind an activation procedure. Polarization curves, LSV, CV and EIS experiments will be the subject of the different discussion sections.

2.3.1. Polarization Curves

2.3.1.1. Low, Medium and High Current Densities

Polarization curves provide a good insight about the evolution and quantification of the fuel cell performance. Figure 2.1 plots the potential (a) and power density (b) as a function of the current density along different activation cycles, both evidencing a clear performance increase. The activation procedure at these operating conditions was stopped after 6 cycles because changes in the polarization curves became negligible.

In general, a current-potential curve, Figure 2.1a, can be divided into 3 distinct zones, which are related with the limiting phenomena occurring in a MEA. The activation zone (low current densities) is related with reaction kinetic limitations. It can be seen from Figure 2.1a that at low current densities the curves practically superimpose after the third cycle, confirming the idea that the catalyst activation is preferentially done during the first cycles. However, straightforward information can be obtained when Tafel slopes and exchange current densities are extracted from low current densities (up to 100 $mA \cdot cm^{-2}$).

Tafel slopes were obtained from the following equation, which results from the simplification of the Butler-Volmer equation [18]:

$$\eta_{act} = -\frac{R \times T}{\alpha \times n \times F} \times \ln i_0 + \frac{R \times T}{\alpha \times n \times F} \times \ln i \qquad (2.4)$$

where R is the universal gas constant, T is the absolute temperature, α is the charge transfer coefficient, n is the number of electrons involved in the electrochemical reaction, F is the Faraday constant, i_0 is the exchange current density, i is the current density and η_{act} is the activation overpotential. The term $\frac{R \times T}{\alpha \times n \times F}$ is the Tafel Slope.

From Table 2.1 it can be seen that Tafel slopes, obtained from the linear regression of the iR-compensated polarization curves (the slope obtained from Eq. (2.4) gives us the Tafel slope while the exchange current density is extracted from the yy axis intercept), decrease along the conditioning period, particularly for the first 3-4 cycles.

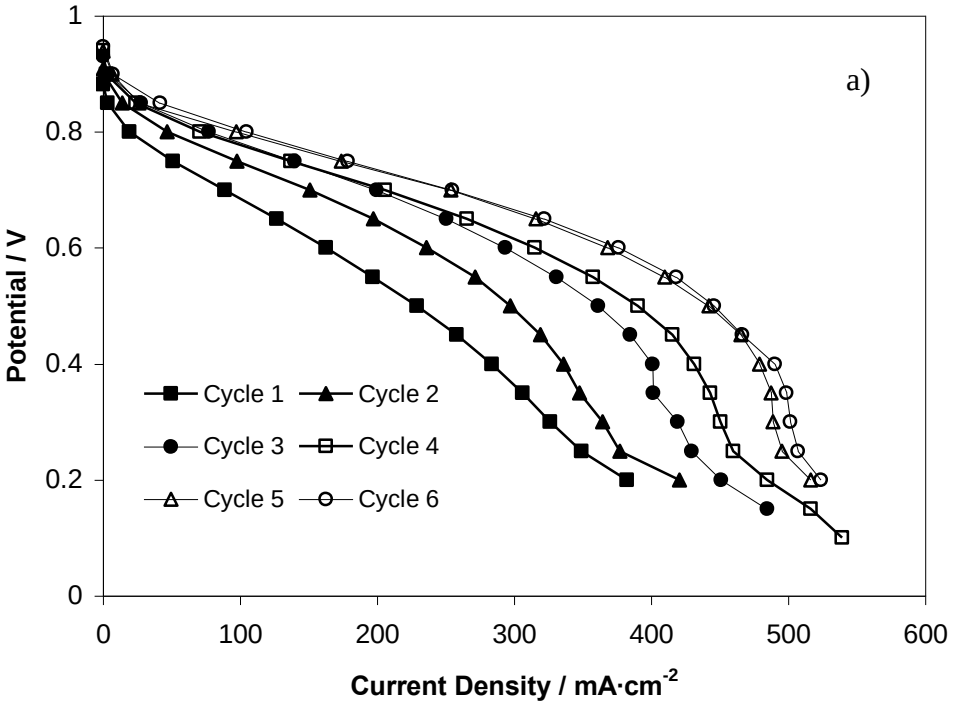

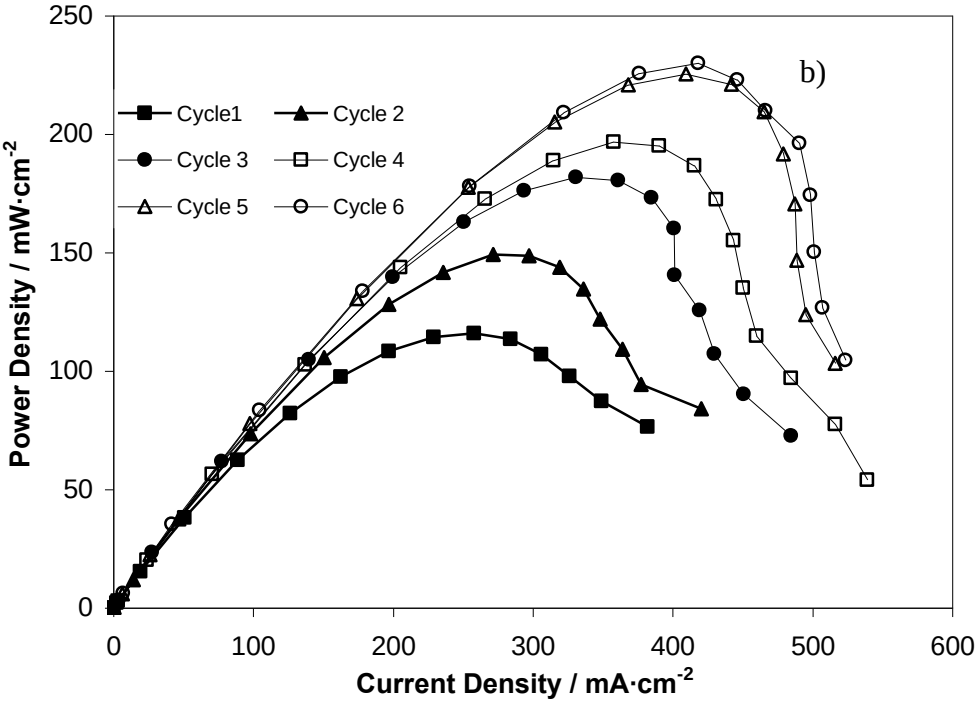

Fig. 2.1 - Potential - current density (a) and power density - current density (b) plots of the PEMFC during the activation process.

Table 2.1 – Tafel slopes, exchange current densities (i_o) and exchange current densities ratio between consecutive cycles along the activation.

Cycles	Tafel Slope / mV	$i_0 \times 10^3$ / A	$\frac{i_{0,n+1}}{i_{0,n}}$
1	66	1.05	------
2	63	1.39	1.32
3	60	1.68	1.21
4	58	1.81	1.08
5	57	1.86	1.03
6	57	1.87	1.01

A Tafel slope of 57 mV was obtained for the activated MEA. This value is in agreement with the open literature, where the typical Tafel slope at 25 ºC for an oxygen reduction reaction in platinum surface is 59 mV [19]. This confirms an improvement on the catalyst activity. As expected, an opposite trend was verified for the exchange current densities, with a total increase along the 6 cycles of 78 % (cf. Table 2.1). The ratio between the exchange current densities between two consecutive cycles can be accepted as very similar to the ratio between the electrode catalyst areas [18]. From these data, it is then inferred that the catalyst area available to promote electrochemical reactions increases along the conditioning period and that increase is more significant for the first cycles. We will come back to this issue in section 2.3.3.

The pseudo-linear portion of the current density-potential curves (middle current densities) is intimately related with ohmic losses, the main portion results from the resistance to the H^+ transport through the PEM. The increase on the MEA performance can be ascribed, up to a certain extent, to the higher degree of hydration attained by the PEM when submitted to the activation process. This improved performance can be observed from Figure 2.1a, due to the successive slope reduction (in terms of absolute value) associated to the ohmic zone. Additionally, a decrease on the PEM resistance will be also confirmed by the impedance experiments (section 2.3.4.).

At high current densities, it can be observed that the potential starts to fall more abruptly along the activation protocol, indicating where the mass transfer limitations begin to prevail. On the other hand, these potential drops shift to higher current densities along the activation procedure. From Figure 2.1b it can be verified that a significant power density increase occurs, from 116.1 $mW \cdot cm^{-2}$ in the first cycle up to 229.9 $mW \cdot cm^{-2}$ in the last one. This large improvement results from an increased catalyst activity and area, as confirmed by the Tafel slope decrease, but also from a higher PEM

ability to conduct the protons from the anode to the cathode, as discussed below – section 2.3.4.

2.3.1.2. Open Circuit Voltage

Figure 2.2 shows the OCV variation during this cyclic process. It can be observed that the OCV increases, but this effect is more pronounced for the first three cycles, in agreement with the behaviour found in the polarization curves for low current densities.

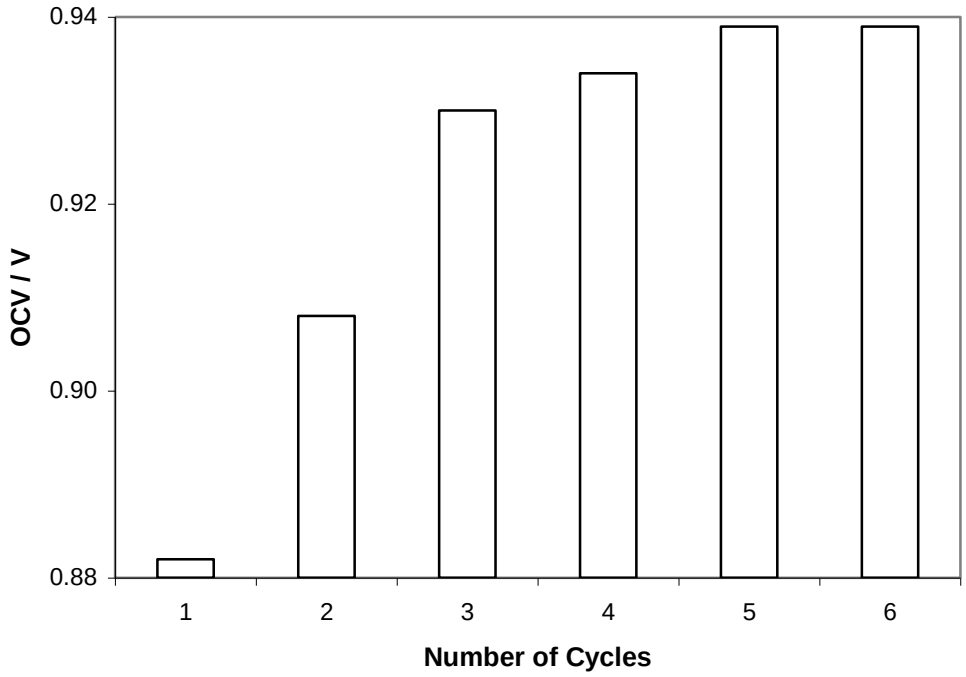

Figure 2.2 – Open circuit voltage as function of the number of cycles, during the activation process, until obtaining a steady performance.

2.3.2. Linear Sweep Voltammetry Applied to Measure the OC Overpotential

Additional experiments using the LSV and EIS techniques were then employed to explain the trend shown in Figure 2.2. It is well known that the OCV is always lower than the thermodynamic value. This happens due to: i) leakage currents associated with the

hydrogen that crosses the PEM ($\Delta E^{OCV}_{H_{2-xover}}$) and ii) a mixed potential mainly due to the cathode electrochemical reactions, ΔE^{OCV}_{mixed}.

The OCV thermodynamic value can be computed using the Nernst equation [10]:

$$E_{rev} = E^{\circ}_{rev} + \left(\frac{R \times T}{n \times F}\right) \ln\left[P_{H_2} \times P_{O_2}{}^{2} \right] \quad (2.5)$$

where E_{rev} is the reversible cell voltage at non-standard conditions regarding concentrations and temperatures, E°_{rev} is the reversible cell voltage at standard conditions, and P_{H_2} and P_{O_2} are the partial pressures of hydrogen and oxygen, respectively. From this equation at the adopted operating conditions the reversible OC value (E_{rev}) is 1.23 V.

The experimental OC values for each activation cycle were obtained using the polarization data. On the other hand, assuming that the only losses at OC are the above-mentioned, i.e., $\Delta E^{OCV}_{H_{2-xover}}$ and ΔE^{OCV}_{mixed}, the difference between the reversible OC value and the measured one should equal the sum of these two contributions, in agreement with the following equation:

$$E_{rev} - E^{OCV}_{measured} = \Delta E^{OCV}_{H_{2-xover}} + \Delta E^{OCV}_{mixed} \quad (2.6)$$

The first term of the right hand side of Eq. (2.6) ($\Delta E^{OCV}_{H_{2-xover}}$) can be obtained from the parasitic current density due to the hydrogen crossover, as explained below. In its turn, the hydrogen that crosses the PEM can be quantified by performing LSV experiments, as described in section 2.2.3.2.

The parasitic current density resulting from the hydrogen crossover (I_{lim} or $I_{H2\text{-}xover}$) as a function of the number of activation cycles is depicted in Figure 2.3.

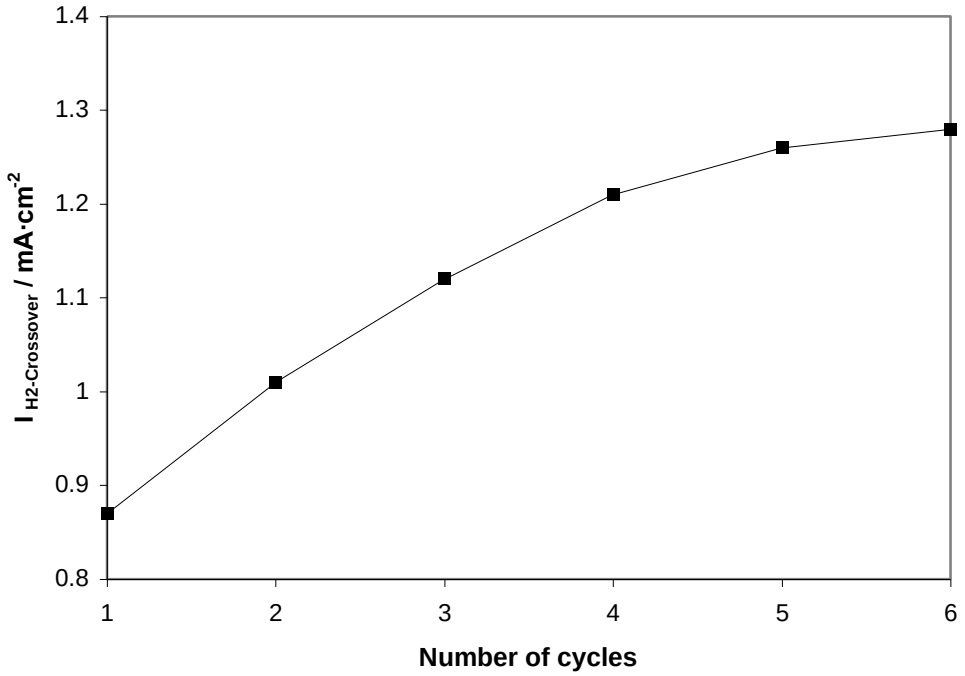

Figure 2.3 – Parasitic current density due to hydrogen crossover at OC as a function of the number of cycles, during the activation process.

It can be seen that hydrogen crossover increases slightly along the activation procedure and consequently the parasitic current density. This behaviour was expectable because it is known that the hydrogen permeability coefficient increases with the water content, mainly due to the increase in the diffusion coefficient [20]. Gierke et al. [21] also claimed that hydrogen permeates mainly through the water contained in the ion clusters of the membrane. The above-mentioned consecutive slope reduction, at middle current densities (Figure 2.1a), confirms the proton resistance decrease and the consequently increased PEM water contents.

A parasitic current density of 1.28 mA·cm^{-2} was obtained for the last cycle, a value that is in agreement with the open literature [14].

The overpotential due to the hydrogen that crosses the PEM, $\Delta E_{H_{2-xover}}^{OCV}$, can be obtained employing the following equation:

$$\Delta E_{H_{2-xover}}^{OCV} = \frac{R \times T}{n \times F \times i_{O_2}^0} I_{H_{2-xover}} \quad (2.7)$$

where $I_{H_{2-xover}}$ is the parasitic current density due to the hydrogen crossover (obtained by LSV experiments – Fig. 2.3) and $i_{O_2}^0$ is the exchange current density obtained by EIS experiments, which can be computed from the following equation:

$$R_{O_{2-ct}}^{OCV} = \frac{R \times T}{n_{\alpha O} \times F \times i_{O_2}^0} \quad (2.8)$$

where $R_{O_{2-ct}}^{OCV}$ is the charge transfer resistance at OC for the oxygen reduction reaction. The charge transfer resistance is extracted from the impedance measurements at OC (shown below), assuming that the cathode charge transfer resistance is significantly higher than the anode one. This assumption is acceptable when small ac sinusoidal perturbations (< 5 mV) are used.

Applying this methodology, also described elsewhere [14], one can obtain the overpotential due to hydrogen crossover ($\Delta E_{H_{2-xover}}^{OCV}$) and also quantify the deviations from the reversible cell voltage along the activation procedure at the open circuit condition. Employing Eq. (2.6) ΔE_{mixed}^{OCV} is then determined. In Table 2.2 are shown the $\Delta E_{H_{2-xover}}^{OCV}$ and the ΔE_{mixed}^{OCV} values obtained for each activation cycle.

Table 2.2 – Open circuit, fuel crossover and mixed overpotentials along the activation cycles.

Cycles	$\Delta E^{OCV} = E_{rev} - E_{measured}^{OCV} / mV$	$\Delta E_{H_{2-xover}}^{OCV}$ / mV from Eqs. (2.7)-(2.8)	ΔE_{mixed}^{OCV} / mV from Eq. (2.6)
1	346.0	7.0	339.0
2	320.0	8.1	311.9
3	298.0	9.0	289.0
4	294.0	9.7	284.3
5	289.0	10.1	278.9
6	289.0	10.2	278.8

It was found that the open circuit overpotential decreases about 16 % during the conditioning period, leading therefore to an increased OC value, in agreement with the polarization curves experiments (cf. Fig. 2.2). It was also observed that the two overpotentials responsible for an OC value different from the reversible one present opposite trends along the activation protocol. The mixed overpotential decreases along the cycles, being however always the main factor that induces the OC response (contribution to the overall overpotential at OC always above 96.4 %.). The mixed overpotential is intimately related with the fact that the Pt catalyst surface is covered partially by a PtO layer [14]. It can be concluded that during the activation process the available Pt surface to promote the electrochemical reactions increases, reducing the PtO surface coverage. The OCV analysis indicates that the catalyst is being activated and this fact can be confirmed and quantified by performing CV experiments during the fuel cell conditioning, as shown in the following section. The overpotential associated with the hydrogen crossover increases along the activation (Table 2.2), in line with the data shown in Fig. 2.3.

2.3.3. Cyclic Voltammetry Applied to Estimate the Electrochemical Catalyst Area

In Figure 2.4 is depicted the electrochemical catalyst area (ECA), estimated from Eq. (2.2), as a function of the number of activation cycles. From Figure 2.4 it was verified that ECA increases considerably on the first three cycles, in agreement with the Tafel slopes decrease and the increase of the exchange current densities (Table 2.1). In fact, from the different experimental approaches it can be concluded that the first load cycles determines large part of the catalyst activation, due to an increased catalyst area that promotes the electrochemical reactions. Furthermore, the ratio between the ECA's of the

last and first cycle (71 % increase) is very similar to the one obtained for the exchange current densities (78 %).

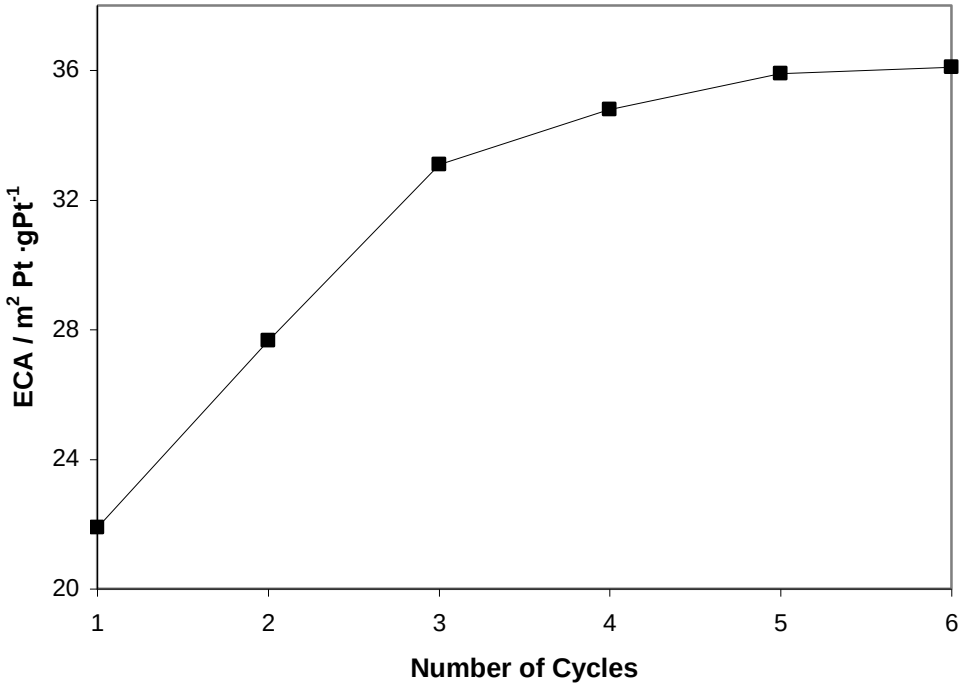

Figure 2.4 – Electrochemical cathode catalyst area as a function of the number of activation cycles.

Assuming that the Pt particles that adsorb the hydrogen molecules have a spherical shape [22], the relation between their mean particle size (d_m) and the ECA can be given by:

$$d_m = \frac{6000}{ECA \times \rho} \tag{2.9}$$

where d_m is the catalyst particles mean size given in nm and ρ is the Pt density. From this equation it can be inferred that at the end of the activation protocol the catalyst particles presented a mean size of 8.1 nm. This value is however higher than the optimum mean particle size of platinum for the oxidation-reduction reaction proposed by Peuckert et al. [23] and Stonehart [24], which lies between 3 nm and 5 nm.

The obtained results put into evidence the importance of finding reasons of the observed catalyst performance improvement, i.e., triple phase boundary, tortuosity, or mass transfer resistance, in addition to the decrease of the particle size and the decrease of the PtO surface coverage above identified. These questions will be discussed with the help of EIS experiments – section 2.3.4.

2.3.4. Electrochemical Impedance Spectroscopy

Several impedance spectra at different operating voltages were recorded for each activation cycle. This procedure allows evaluating the relevant impedance parameters that quantify the potential losses during the conditioning period at low and moderate current densities.

The impedance spectra of the fuel cell at low and moderate current densities can be simulated by the combination of two electrode-electrolyte interfaces, one for each electrode, in series with a PEM resistance [25]. Each electrode-electrolyte interface is composed by a charge transfer resistance, R , and a constant phase element, CPE , to describe the double layer capacitive behaviour. An inductance element, L, was added for obtaining a better fitting, therefore taking into account possible interferences due to the wires or other sources of disturbance. The corresponding electric analogue is given in Figure 2.5.

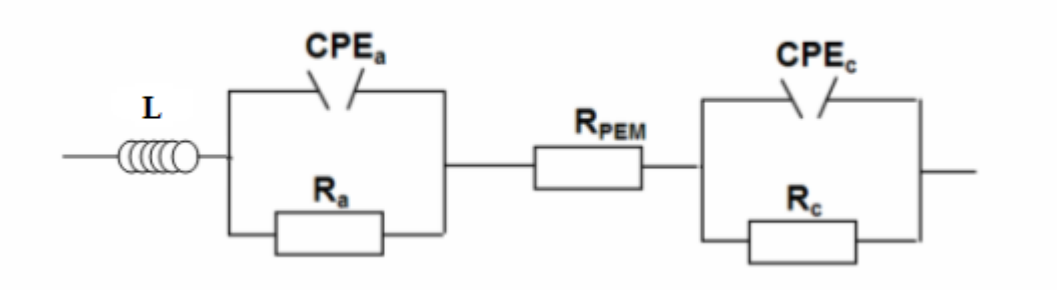

Figure 2.5 – Equivalent circuit of the fuel cell for low and moderate current densities.

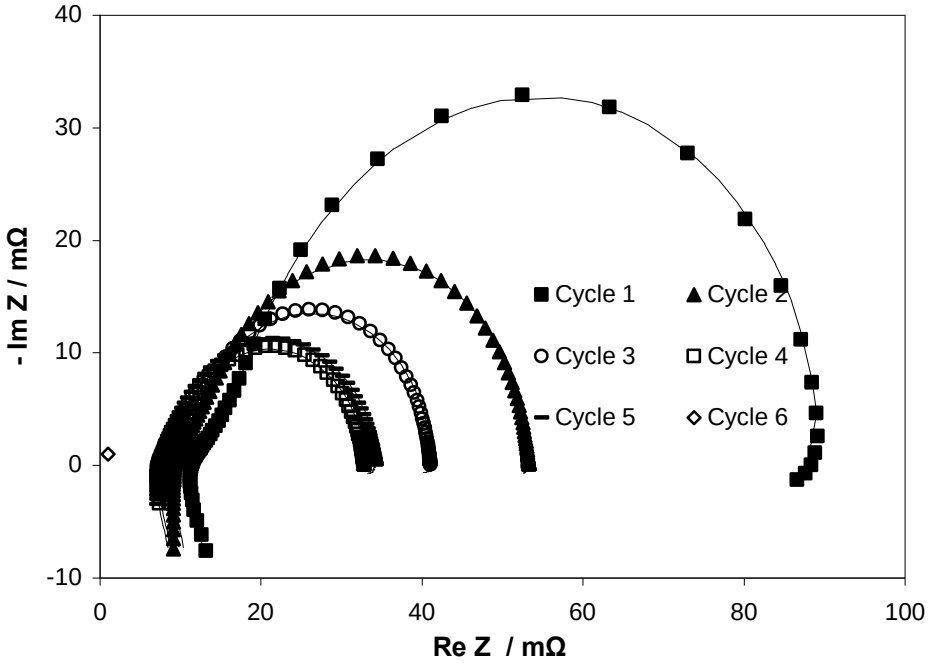

Figure 2.6 – Experimental (dots) and simulated (lines) impedance values of the PEMFC at 800 mV along the activation cycles.

The obtained impedance spectra at 800 mV for several activation cycles (Figure 2.6) were fitted to the previous model, minimizing the sum of the square residues using the Thales Software (Zahner Elektrik). The model fits well with the experimental results, which parameters are discussed below. From Figure 2.6 it can be seen that during the conditioning period, the Nyquist plots show only two arcs for cycles 2 to 6, which are associated to the dynamics of the charge transfer in two domains (anode and cathode). It can be concluded that there are no significant resistances due to the transport of oxygen in these conditions, otherwise a 3rd arc at low frequencies would be noticed. However, for the first cycle, it can be observed a very small low frequency arc, probably due to some mass transport resistances before the activation procedure.

Similar Nyquist plots were obtained (but not shown) in a range from OCV to 400 mV. However, it should be pointed out that as the current density increases, the radius of

cathode related semicircle decreases, reflecting the increasing driving force for the reduction reaction. The opposite trend occurs at 300 mV, presenting a large semicircle radius when compared with the 400 mV spectra. This means that at 300 mV some mass transfer resistances start to occur, in agreement with the polarization curves. It was also observed that the ohmic cell resistance changes slightly in a range between OCV and 300 mV. Furthermore, the slight differences occur in the first activation cycles and are completely negligible in the last ones. Pourcelly et al. [26] suggested that for lower water content the pores that connect the hydrophilic regions of the Nafion membrane become smaller, promoting the accumulation of protonic charges with an increase in the PEM relaxation time. At these circumstances, the PEM does not act anymore as a pure resistance and some discrepancies can be found for the PEM resistance values at different current densities for the first cycles while at the last ones it is nearly constant.

Table 2.3 – Impedance parameters extracted from Nyquist plots at 800 mV along the activation cycles.

Cycles / Parameters	**1**	**2**	**3**	**4**	**5**	**6**
L / nH	11.9	11.9	11.8	11.8	11.9	11.8
R_a /mΩ	5.5	3.9	2.6	2.5	2.5	2.5
C_a / mF	$101.3^{0.620}$	$144.0^{0.632}$	$171.0^{0.646}$	$239.4^{0.655}$	$274.6^{0.660}$	$282.7^{0.665}$
R_{PEM} / mΩ	11.5	9.1	8.4	7.5	7.0	6.9
R_c /mΩ	73.4	40.3	30.8	25.6	24.7	23.5
C_c / mF	$611.9^{0.950}$	$645.2^{0.956}$	$709.1^{0.964}$	$807.6^{0.969}$	$853.6^{0.973}$	$863.1^{0.980}$

In Table 2.3 are presented the model parameters that were extracted from the Nyquist plots. The inductance parameter, L, considers interferences that can possible arise from the wires or other external sources of disturbance [27]. As previously mentioned, part of the cell ohmic resistance is due to the proton transport resistance, PEM resistance. From Table 2.3 it can be seen that the PEM resistance decreases along the cycles. So, it can be inferred that H^+ species become much more easily transported across the PEM during the activation procedure. It is widely accepted that the Nafion proton conductivity and water content are strongly related, obeying to a linear relationship at room temperatures [28]. Activation cycles enable the PEM to increase its hydration level, favouring this way the protons transport and consequently the power output demands. On the other hand, it can be noticed that significant changes in the PEM resistance occur up to the fourth/fifth cycle, indicating that the PEM proton conductivity needs a slightly longer period to stabilize than the catalyst, in agreement with the trends observed in the polarization curves. The PEM cell resistance obtained with the MEA completely activated was 172.5 $m\Omega \cdot cm^2$.

From Table 2.3 it also can be seen that, as expected, the cathode charge transfer resistance is higher than the anode one and both also decrease along the activation. The charge transfer resistance is intimately related with the electrochemical reactions that occur at the interface of the PEM and the catalyst. This decrease can be related to a catalyst roughness surface increase as found by other authors [29, 30]. However, the charge transfer resistance is not only related with the area associated to the triple phase boundary but also with mass transfer resistances [31], reinforcing the idea that changes in the porosity and tortuosity of the diffusion and catalytic layers probably occur. Furthermore, based one the history of these parameters (anode and cathode resistances), one could infer that porosity and tortuosity changes occur mostly on the first cycles.

However, the catalyst performance is the result not only of the charge transfer resistance but also of the double layer capacitance.

It is known that the capacitance is related with the level of the double layer formation at the interface between the electrolyte and the catalyst [16, 32]. The capacitance increases with the area of the double layer. In other words, the capacitance is an indicator of the triple phase boundary area available for promoting the catalytic reactions. It can be observed from Table 2.3 that the capacitance parameters for both the anode and cathode (C_a and C_c, respectively) increase, not only at the first three cycles, as in the case of the charge transfer resistances, but along the first five activation cycles. Furthermore, the increase of the anode and cathode capacitances may be related with the PEM swelling, which occurs more significantly up to the fourth cycle. When the PEM swells, it is probably that a better connection between the three different phases occurs. This fact can explain part of the ECA increase after the first three cycles (Figure 2.4). Finally, it was also observed that the capacitance values present the same trend in the studied voltage range.

It is important to notice that the PEM has a significant role not only on the proton conductivity improvement but also on the overall performance due to its ability to facilitate the conduction of the protons from the anode catalyst to the PEM and then to the cathode catalyst. On the other hand, it is also important to notice that the catalyst improvement is the result of several factors, such as, particle size decrease, decrease of mass transfer resistance (tortuosity and porosity changes on the first cycles), increase of available catalyst area, and finally triple phase boundary increase.

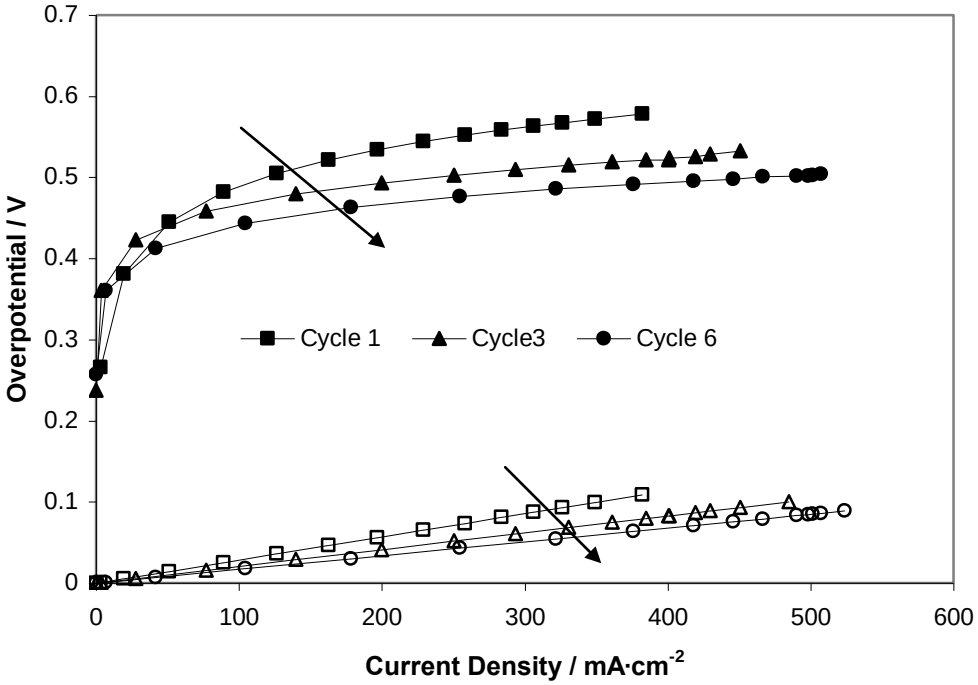

Figure 2.7 – Activation/catalyst (filled dots) and PEM (empty dots) overpotential as a function of the current density at the first, third and last cycle of the activation protocol.

In Figure 2.7 are shown the activation and PEM (ohmic) overpotentials as a function of the current density along the activation protocol (first, third and last cycles). The PEM overpotential was obtained from the impedance values at high frequency and the activation overpotential (catalyst) was obtained from Eq. (2.4). It can be concluded that the overpotentials related with the catalyst performance are responsible for most of the overpotential in the PEMFC. The activation procedure is effective on the PEMFC performance increase, considering not only the PEM but also the catalyst.

2.3.5. Overall Energy Efficiency

The overall energy efficiency was obtained as described in section 2.2.3.5. From Figure 2.8 it can be observed that the maximum overall efficiency (at 0.55 V) increases considerably along the activation, from 9.3 % on the first cycle to 19.7 % on the last one.

It can be concluded that the activation procedure enhances not only the fuel cell power but also its efficiency.

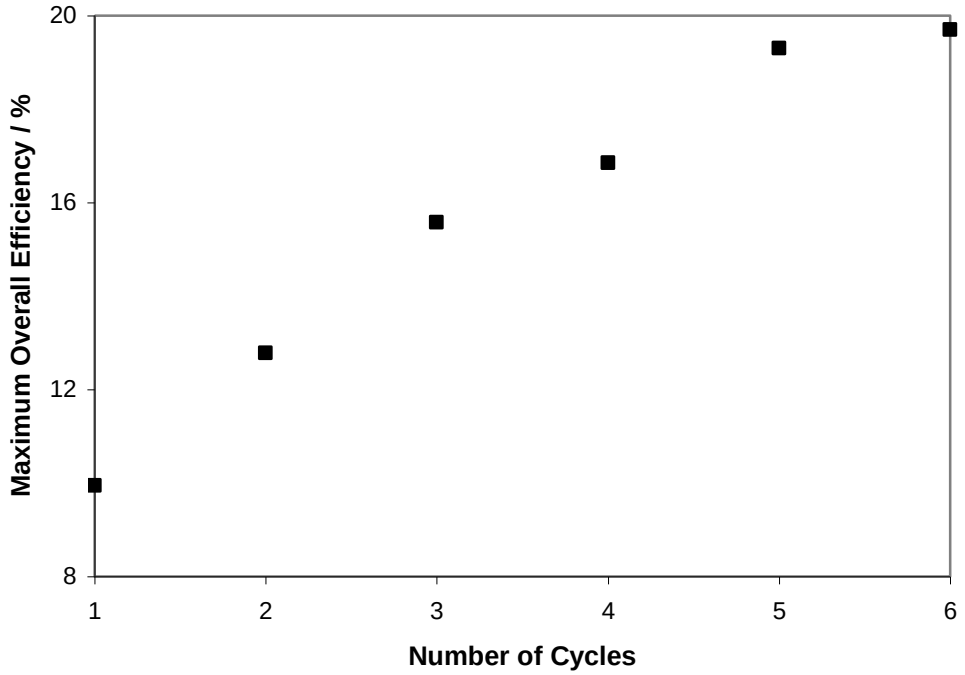

Figure 2.8 –Maximum overall efficiency (at 0.55 V) as a function of the activation cycles.

2.4. Conclusions

In situ electrochemical techniques were used to better understand the changes that a MEA experiences along an activation procedure.

The activation procedure was set-up considering six loading cycles (each loading cycle was composed by OC and loading periods) performed at 25 ºC. After each cycle, different electrochemical techniques were performed. From each technique it was possible to obtain valuable information about the changes experienced by the MEA, namely:

1 - Polarization curves showed an effective increase on the performance of a MEA. Indeed, the maximum power density increased from 116.1 $mW \cdot cm^{-2}$ in the 1^{st} cycle up to 229.9 $mW \cdot cm^{-2}$ in the last one.

2 - The analysis of the corresponding Tafel slopes and exchange current densities at each polarization curve showed an increase on the catalyst activity and area available to perform the electrochemical reactions.

3 - CV experiments confirmed a similar trend with an ECA increase of 71 % along the activation protocol (1^{st} cycle to 6^{th} cycle).

4 - The combination of LSV with EIS showed that the main reason responsible for the OC increase is the reduction of the mixed potential effect.

5 - Resistance and capacitance parameters were extracted from the fitting of the impedance experiments to a modified Randles electrical circuit. In this concern, it was shown that the PEM resistance decreased along the activation, what can be ascribed to the attainment of higher water contents that provide higher proton conductivities. The same trend was observed considering the anode and cathode charge transfer resistances. The history of these parameters indicated that diffusion and catalyst layers possible experience porosity and tortuosity changes, which occurred mainly on the first three cycles. The catalyst activity was also improved on the last cycles, mainly due to the enlargement of the triple phase boundary. This was confirmed by the double layer capacitance increase.

6 - The increase of the MEA performance along the activation procedure had the higher contribution due to the improvement of the catalyst activity. However, the PEM also played an important role on the increase of the triple phase boundary at the electrode/electrolyte interface.

7 - Finally, it can be concluded that the activation procedure enhances not only the fuel cell power but also its efficiency, which maximum increased from 9.3 % to 19.7 % (1^{st} cycle to 6^{th} cycle).

2.5. References

1. B. K. Kho, I. H. Oh, S.A. Hong and H.Y. Ha, *Electrochimica Acta*, 50, 781 (2004).

2. Z. Qi and A. Kaufman, *Journal of Power Sources*, 111, 181 (2002).

3. V.S. Silva, V.B. Silva, A. Mendes, L.M. Madeira, H. Silva, J. Michaelmann, B.Ruffmann and S.P. Nunes, *Separation Science Technology*, 42, 2909 (2007).

4. Z. Qi and A. Kaufman, *Journal of Power Sources*, 109, 227 (2002).

5. C.A. Rice, X. Ren and S. Gottesfeld, Methods of Conditioning Direct Methanol Fuel Cells, United States Patent (2005).

6. C. He, Z. Qi, M. Hollet and A. Kaufman, *Electrochemical Solid-State Letters*, 5, A181 (2002).

7. Z. Qi and A. Kaufman, *Journal of Power Sources*, 114, 21 (2003).

8. Z. Xu, Z. Qi and A. Kaufman, *Journal of Power Sources*, 156, 281 (2006).

9. Z. Xu, Z. Qi and A. Kaufman, *Journal of Power Sources*, 156, 315 (2006).

10. K. R. Cooper, V. Ramani, J. M. Fenton and H. R. Kunz, *Experimental Methods and Data Analysis for Polymer Electrolyte Fuel Cells*, Scribner Associates, North Carolina (2005).

11. J. Larminie and A. Dicks, *Fuel Cell Systems Explained*, John Wiley & Sons, Chichester (2003).

12. A. J. Appleby, *Journal of Electrochemical Society*, 117, 328 (1970).

13. J. P. Hoare, *Journal of Electrochemical Society*, 109, 858 (1962).

14. J. Zhang, Y. Tang, C. Song, J. Zhang and H. Wang, *Journal of Power Sources*, 163, 532 (2006).

15. A. Pozio, M. Francesco, A. Cemmi, F. Cardellini and L. Giorgi, *Journal of Power Sources*, 105, 13 (2002).

16. J. H. Kim, H. I. Lee, S. A. Hong and H. Y. Ha, *Journal of Electrochemical Society*, 152, A2345 (2005).

17. E. Gulzow, S. Weibhaar, R. Reissner and W. Schroder, *Journal of Power Sources*, 118, 405 (2003).

18. R. O`Hayre, S. W. Cha, W. Colella and F. B. Prinz, *Fuel Cell Fundamentals*, John Wiley & Sons, New Jersey (2006).

19. Y. W. Rho, O. A. Velev, S. Srinivasan and Y. T. Kho, *Journal of Electrochemical Society*, 141, 2084 (1994).

20. S. S. Kocha, J. D. Yang and J. S. Yi, *American Institute of Chemical Engineers*, 52, 1916 (2006).

21. T.D. Gierke, G. E. Munn and F. C. Wilson, *Journal of Polymer Science*, 19, 1687 (2003).

22. J. A. Stoyanova, V. Naidenov, K. Petrov, I. Nikolov, T. Vitanov and E. Budevski, *Journal of Applied Electrochemistry*, 29, 1197 (1986).

23. M. Peuckert, T. Yoneda, R. Betta and M. Boudart, *Journal of Electrochemical Society*, 133, 944 (1986).

24. P. Stonehart, *Journal of Applied Electrochemistry*, 22, 995 (1992).

25. N. Wagner, *Journal of Applied Electrochemistry*, 32, 859 (2002).

26. G. Pourcelly, A. Oikonomou, C. Gavach and H.D. Hurwitz, *Journal of Electroanalytical Chemistry*, 287, 43 (1990).

27. E. Barsoukov, J. Macdonald, Impedance Spectroscopy: Theory, *Experiment, and Applications*, John Wiley & Sons, New Jersey (2005).

28. T. E. Springer, T. A. Zawodzinski and S. Gottesfeld, *Journal of Electrochemical Society*, 138, 2334 (1991).

29. H. Varela and K. Krischer, *Journal of Physical Chemistry B.*, 106, 12258 (2002).

30. X. Ren and S. Gottesfeld, *Journal of Electrochemical Society*, 148, A87 (2001).

31. T. E. Springer, T. A. Zawodzinski, M. S. Wilson and S. Gottesfeld, *Journal of Electrochemical Society*, 143, 587 (1996).

32. Z. Siroma, *Journal of Electroanalytical Chemistry*, 546, 73 (2003).

Part III

3. DMFC Behavior During an Activation Process*

Abstract

A direct methanol fuel cell (DMFC) needs to be activated to achieve its maximum performance. The activation procedure includes a pre-treatment and an *in situ* activation procedure. The *in situ* activation procedure, performed at various temperatures and loadings, consisted of loading cycles applied to a DMFC equipped with a proton exchange membrane (PEM) of Nafion 112. A pre-screening study indicated that the best *in situ* activation conditions were at 55 °C and 200 mV of loading; these conditions were then used for the characterization work. Along the activation procedure the membrane electrode assembly (MEA) experiments significant changes that are studied by electrochemical impedance spectroscopy (EIS), cyclic voltammetry (CV) and from polarization curves, methanol crossover and electro-osmotic drag measurements. It is shown that the activation procedure makes the proton conductivity of the PEM to increase, which can be ascribed to a hydration increase. A resistance decrease of the charge transfer at the catalytic layer interface with the PEM was also observed. The adsorption/dehydrogenation related resistances at the catalyst are the main source of overvoltage; this overvoltage decreased about 45 % along the activation procedure. Indeed, it was verified that the anode electrocatalytic area increases along the activation cycles. On the other hand, it is also shown that the DMFC power density increases from 8.8 $mW \cdot cm^{-2}$ to 22.4 $mW \cdot cm^{-2}$ at 55 °C along the activation procedure and the overall efficiency increases only for high current densities. Finally, it was concluded that both temperature and loading cycles play an important role on the activation procedure.

*V. B. Silva, L. M. Madeira, A. Mendes, submitted

3.1. Introduction

Due to their near zero pollutants emission and potentially high energy efficiencies, polymer electrolyte fuel cells (PEFCs) are growing of interest, assuming a crucial role on the research and development of new energy production systems [1]. In particular, direct methanol fuel cells (DMFCs) are promising candidates for portable power applications because they do not require fuel processing and allow simple and compact designs [2]. Although, DMFCs are being deeply studied, challenging issues still to overcome, such as the most effective procedures for starting-up or restarting DMFCs – the so-called activation procedures.

Whenever a membrane electrode assembly (MEA) is inserted in a DMFC, it does not reach the best performance immediately after starting up. It is well known that DMFCs undergo a gradual increase in performance before reaching a stabilized power density output [3]; the MEA needs to be activated. Activation procedures can be understood as all the actions that can bring the MEA to its highest and stabilized performance. In this study we distinguish between pre-treatment and *in situ* activation procedures. Pre-treatment procedures include all actions carried over a fresh MEA, including the proton exchange membrane (PEM) and electrodes, while *in situ* activation procedures are actions used to improve the performance of a MEA when the fuel cell is on a working state.

Activation procedures can be applied during the start-up or after resting periods (restarting) and are common to both hydrogen and methanol fuel cells [4-5]. Regarding pre-treatment procedures, several approaches are discussed in the literature [3, 6-9]; Kho et al. [3] proposed that the MEA should either be immersed in water or methanol aqueous solution for hours prior to use. These authors claim that a significant increase on the DMFC performance is observed due to the attainment of higher levels of hydration, both

in the membrane and in the electrodes. Silva et al. [6] observed a considerable increase on the PEM proton conductivity and DMFC performance when the PEM is boiled in water during one hour. Other studies indicate that higher levels of hydration are achieved when immersing the MEA in ethanol, ethanol aqueous solutions or even in aqueous solutions of diluted sulfuric acid at elevated temperatures [7-9].

In situ conditioning procedures are also reported, namely the so-called hydrogen evolution [10], where the air feed to the cathode is replaced by nitrogen, while pure hydrogen is fed to the anode. It seems that forcing hydrogen to cross the membrane with the help of an external power source leads to possible structural changes in the catalyst layer, namely in porosity and tortuosity. The same authors reported other two procedures to enhance and accelerate the PEMFC start-up. One method refers the exposing of the MEA to elevated conditions of temperature and pressure. It is claimed that the resistances of both membrane and catalyst are reduced and that the effect is long-lasting [9]. Another approach considers submitting the catalyst surface to a CO poisoning and subsequence CO oxidation. It seems that this procedure increases the electrode active surface area [11]. Sometimes, DMFC anodes are activated running the cell under H_2/O_2 prior to the use. It is believed that this activation procedure is speeded up due to the high current densities obtained [12]. Indeed, the easiest way to activate a MEA should be based on the application of loading periods [12-13], using either hydrogen or methanol as a fuel. Ren et al. [14] presented a different approach named current conditioning. The current conditioning procedure considers the operation of the MEA with a current of polarity opposite to the normal use. This leads to an electrochemical generation of hydrogen at the PtRu electrocatalyst, reducing the surface oxides that might exist there.

As described in the last paragraphs, there are several reports studying different approaches to obtain better performances at the start-up of a fresh PEMFC (namely

DMFC) device. However, only few studies provide phenomenological support for the observed increase of performance during the activation process [4, 15].

This paper analyzes the behaviour of a MEA (DMFC) along an activation procedure aiming to understand how this activation affects the PEM and the catalyst. The activation procedure comprehends six *in situ* loading cycles. The polarization curve, the impedance spectrum and the methanol crossover were obtained along the activation loading cycles, while the cyclic voltammogram and the open circuit voltage (OCV) response after a load cut were performed before the activation procedure, after the third loading cycle and after the last loading cycle; the water electro-osmotic drag coefficient was obtained before the first activation cycle and after the last one. These results gave the complete picture of how the activation changed the MEA towards a higher performance.

3.2. Experimental

3.2.1. MEA Pre-treatment

In this work it was used a PEM of Nafion 112. This membrane was boiled during one hour before being assembled and used in the fuel cell, in order to improve its protonic conductivity [6]. The backing and catalyst layers were also boiled during one hour for improving the catalyst performance [8].

3.2.2. MEA Activation Protocol

The MEA activation protocol consists in submitting it to six loading cycles at 55 ºC, interrupted by a set of electrochemical measurements. These measurements are the polarization curve, impedance vs dynamic hydrogen electrode (DHE) at 300 mV, cyclic voltammetry (CV), methanol crossover, electro-osmotic drag and the OCV after a load cut. The CV and the OCV response after a load cut were measured before the activation procedure and after the, third and sixth loading cycle and the electro-osmotic drag coefficient was obtained before and after the activation procedure. It was allowed the MEA to rest at OC for 30 min before applying a new characterization technique.

Each loading cycle lasted 180 min at 200 mV. The activation procedure, including the open circuit periods, load periods and different electrochemical tests had lasted of ca. 30 h. It should be pointed out that also during the electrochemical measurements the cell was gradually activated.

3.2.3. Characterization Methods

3.2.3.1. Methanol Crossover Measurements

The current density that results from the methanol that crosses the electrolyte, $I_{crossover}$, is intimately related with the anode mass-transport limiting current density, $I_{\lim}$, by the following equation [16]:

$$I_{crossover} = I_{OCV,crossover} \times \left(1 - \frac{I}{I_{\lim}}\right) \quad (3.1)$$

where $I_{OCV,crossover}$ is the methanol crossover current density at the OCV and I is the operation current density. As shown by this equation, that assumes a direct relation between the actual current and the methanol crossover, the parasitic current density due to the methanol crossover at any current value is obtained evaluating the parasitic current density at open circuit voltage and the limiting current density. To evaluate the parasitic current density at open circuit, the DMFC cell was operated with a methanol aqueous solution (12 $mL \cdot min^{-1}$ at 55 °C, 1.5 M and 2.5 bar) at the anode side and with hydrogen on the cathode chamber (200 $mL_N \cdot min^{-1}$ at 55 °C and 2.5 bar). Scans were performed at a scan rate of 3 $mA \cdot s^{-1}$ between 0 and 0.8 V *vs* the reference electrode, in the galvanostatic mode. Finally, the limiting current density was obtained measuring the polarization curves to 0 V.

3.2.3.2. *In situ* Cyclic Voltammetry (CV)

In situ cyclic voltammetry was carried out with the DMFC in operation. The anode evaluation was accomplished feeding a hydrogen stream (200 $ml_N \cdot min^{-1}$ at 55 °C, 100 % relative humidity and 2.5 bar) to the cathode compartment, which serves as reference/counter electrode, while a nitrogen stream (200 $mL_N \cdot min^{-1}$ at 55 °C, 100 % relative humidity and 2.5 bar) was fed to the anode compartment which serves as working electrode. The working electrode was swept at 50 $mV \cdot s^{-1}$ between -0.4 V and 1.3 V versus the cathode (counter/reference electrode).

Relative anode electrochemical active areas (rECA) were obtained by calculating the areas of the hydrogen oxidation peaks from the cyclic voltammograms [17] using the following equation:

$$rECA = \frac{Q}{\mu_{Pt} \times L} \tag{3.2}$$

where $rECA$ is the relative anode electrochemical active area, Q is the charge density of the atomic hydrogen adsorption, μ_{Pt} is the charge needed to reduce a monolayer of protons at the polycrystalline Pt surface of 1 cm^2 (μ_{Pt} = 210 $mC \cdot cm^{-2}$ Pt) and L is the Pt load (1 $mg \cdot cm^{-2}$). Despite the absolute ECAs could not be obtained due to the Ru interference, it is possible to compare the relative surface areas [17] along the activation procedure. These experiments were performed before the activation and after the third and the sixth cycles at 55 ºC.

3.2.3.3. Electrochemical Impedance Spectroscopy

Impedance spectra were obtained operating the DMFC cell with a methanol aqueous solution (12 $mL \cdot min^{-1}$ at 55 °C, 1.5 M and 2.5 bar) at the anode side and a dry hydrogen stream (200 $mL_N \cdot min^{-1}$ at 55 °C and 2.5 bar) on the cathode chamber. The cathode side worked as a dynamic hydrogen electrode (DHE) and the applied voltage was 300 mV between the anode and the cathode. In this way, only the anode impedance behavior was studied. The electrochemical impedance measurements were performed using a Zahner IM6e workstation coupled with a potentiostat (PP-240, Zahner). Impedance spectra were also recorded at ten points per decade by superimposing a 5 mV ac signal over the frequency range from 100 kHz to 10 mHz.

Impedance experiments are only meaningful when the system behaves linearly. It was then applied a sinusoidal voltage perturbation of 5 mV, which is considerable smaller than the thermal voltage at 55 ºC [18].

3.2.3.4. Evaluation of the Electro-osmotic Drag Water Coefficient

The electro-osmotic drag coefficients of water were evaluated as suggested by Ren et al. [19].

When a DMFC is operated with aqueous methanol solutions (approximately 1 M) at the anode and dry oxygen at the cathode, the water flux across the PEM (at sufficiently high current densities) is driven only by protonic drag. The cell was operated at constant current with a 1.5 M methanol aqueous solution feed to the anode at 12 $mL \cdot min^{-1}$ and dry oxygen feed to the cathode at 300 $mL_N \cdot min^{-1}$. To eliminate any water transport by hydraulic pressure difference across the PEM, the backpressures at the anode and at the cathode were kept equal at 2.5 bar. Water vapour emerging with the cathode effluent was condensed in a U-shaped tube immersed in glycolated water kept at -10 °C. The experiments were run for approximately 1.5 h. Previous experiments were performed to ensure that the volume of water collected represents the steady state condition.

3.2.3.5. Swelling Measurements

Swelling studies were performed by drying the membrane samples in a vacuum reservoir at 80 °C for 5 hours. After drying, four samples of Nafion 112 (at each temperature) were weighted and immersed in 1.5 M aqueous methanol solution and equilibrated for 3 days at 25 ºC, 40 ºC, 55 ºC, 70 ºC and 90 ºC. This ensured that the equilibrium was attained. The weights of the swollen membranes were measured after carefully removing the solution from both surfaces. Membrane swelling (wt. %) was obtained from the ratio between the difference of the wet and dry weight and the dry weight. The average error obtained using this procedure was 5.5 % (t distribution for 95% confidence interval).

3.2.3.6. DMFC Tests

The studied MEA was prepared by hot pressing the membrane sample, Nafion 112 from GEFC, between two ElectroChem electrodes at 90 ºC and 150 bar for 150 s. Supported PtRu (1 $mg \cdot cm^{-2}$ and 1:1 molar ratio) and Pt (0.5 $mg \cdot cm^{-2}$) were used on the anode and cathode, respectively. Single cell measurements were performed in a 25 cm^2 effective area cell. The DMFC was operated with a methanol aqueous solution (backpressure of 2.5 bar, 12 $mL \cdot min^{-1}$, 1.5 M) at the anode side and with humidified air (backpressure of 2.5 bar, 1000 $mL_N \cdot min^{-1}$, 100 % relative humidity) at the cathode side. The DMFC set-up is described elsewhere [20]. The cell temperature was maintained at 55ºC.

From the methanol crossover measurements and from the polarization curves, it was computed the DMFC Faraday and potential efficiencies and then the global efficiency. Basically, the Faraday efficiency is defined as the ratio between the converted fuel into electricity (anode) and the total amount of converted fuel (anode and cathode) and the potential efficiency is defined as the DMFC voltage divided by the standard cell voltage, while the global efficiency is the product of both efficiencies.

3.3. Discussion and Results

3.3.1. Selection of Temperature and Loading Conditions

The activation procedure previously described was applied at five different temperatures, 25 ºC, 40 ºC, 55 ºC, 70 ºC and 90 ºC. Figure 3.1 depicts the power density (obtained with the MEA activated) as a function of the current density performed at 55 ºC for the above-mentioned five activation temperatures.

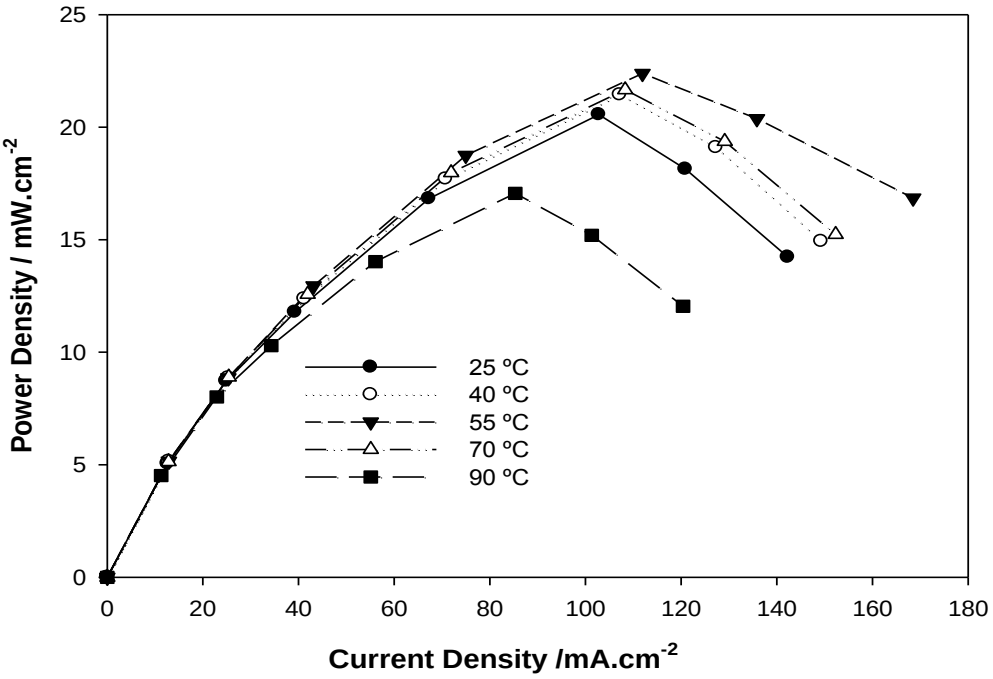

Figure 3.1 - Power density as a function of the current density at 55 ºC (MEA activated) for MEAs activated at different temperatures.

From Figure 3.1, it can be observed that the increase of the temperature helps the activation up to 55 ºC; the worst performance was obtained when the MEA was activated at 90 ºC. A similar trend was found by Kim et al. [15], which claim that an activation procedure is considerable more effective at 25 ºC than at 90 ºC. This happens essentially because at 25 ºC the level of the ionomer in contact with the catalyst layer will undergo

considerable but not excessive swelling, leading to a strong increase on the interfacial triple phase area [15].

In Figure 3.2 is shown the PEM swelling in a 1.5 M methanol aqueous solution as a function of the temperature; it can be seen that the membrane swelling increases with the temperature. This suggests that the low performance obtained with a MEA activated at 90 ºC is probably related with an excessive swelling experienced by the PEM that on one hand allows a higher crossover of methanol and on the other reduces both the ionic conductance and the area of the triple phase boundary [15]. This was also confirmed by impedance experiments that showed decreased capacitance of the double layers and increased charge transfer resistances at 90 ºC, this probably due to the decrease of proton conductivity between the catalyst surface and the proton exchange membrane (results not shown).

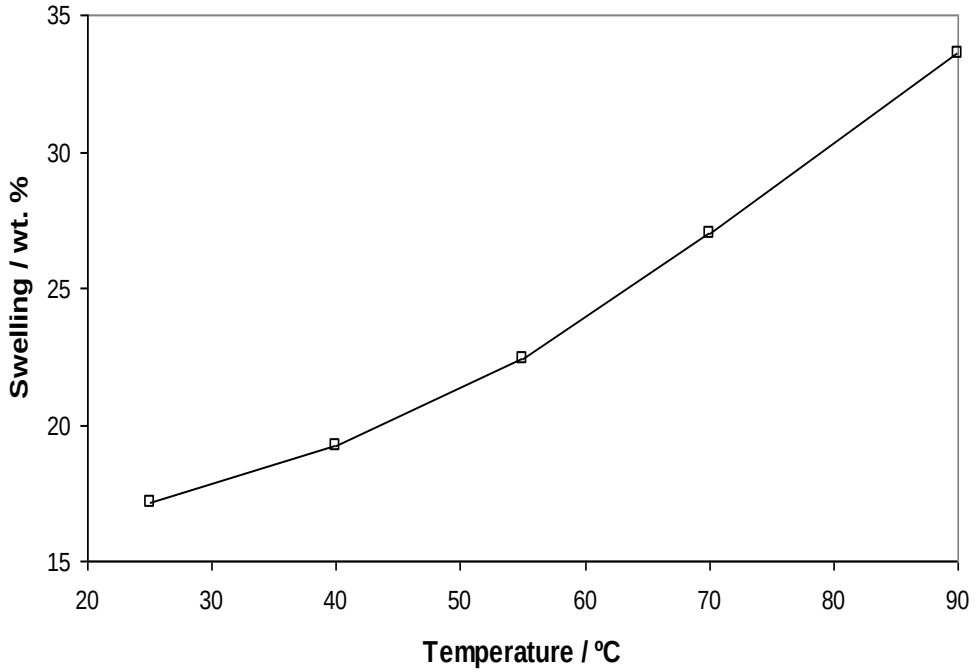

Figure 3.2 – Methanol solution uptake (1.5 M) on Nafion 112 as function of the temperature.

Four MEAs were then submitted to a set of six loading cycles at 55 ºC: OCV, 350 mV, 200 mV and 50 mV. Figure 3.3 shows the power density as a function of the current density for the different loading cycles. It can be verified that the MEA's performance increases with the load applied. However, below 200 mV the performance increase becomes marginal; on the other hand and for stack fuel cells, there is also the danger of polarity inversion for these high loads [7].

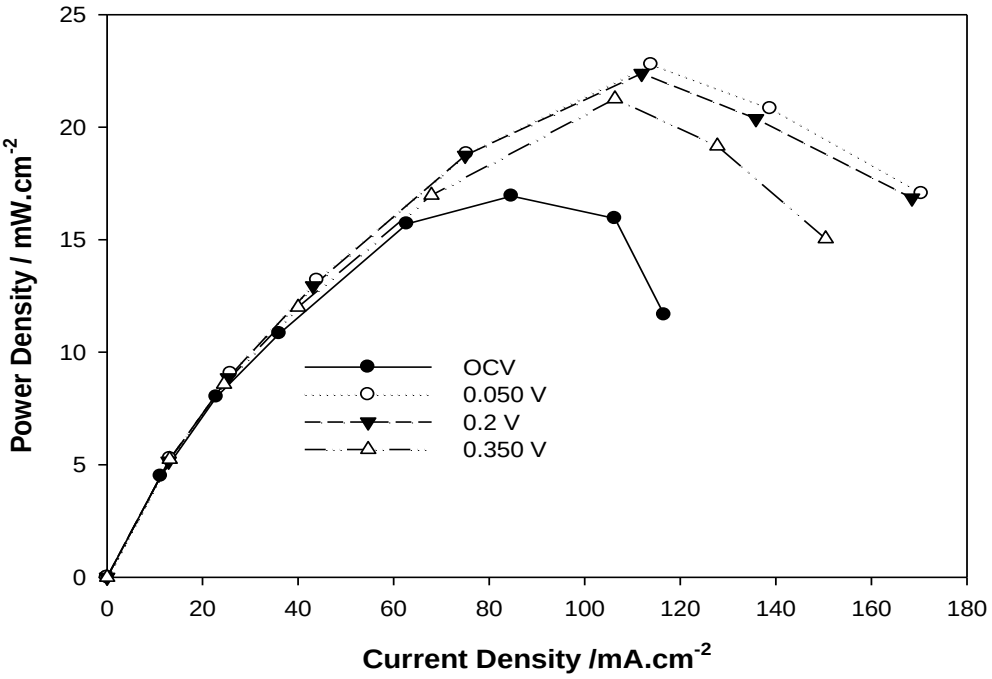

Figure 3.3 - Power density as a function of the current density at 55 ºC after six loading cycles performed at different loadings.

3.3.2. Polarization Curves

From the results of the previous experiments it was decided to use an activation protocol at 55 °C comprehending a set of six loading cycles performed at 200 mV. Figure 3.4 plots the potential (a) and power density (b) as a function of the current density and the activation cycle. It can be seen that the performance of the MEA levels off after the sixth cycle of activation.

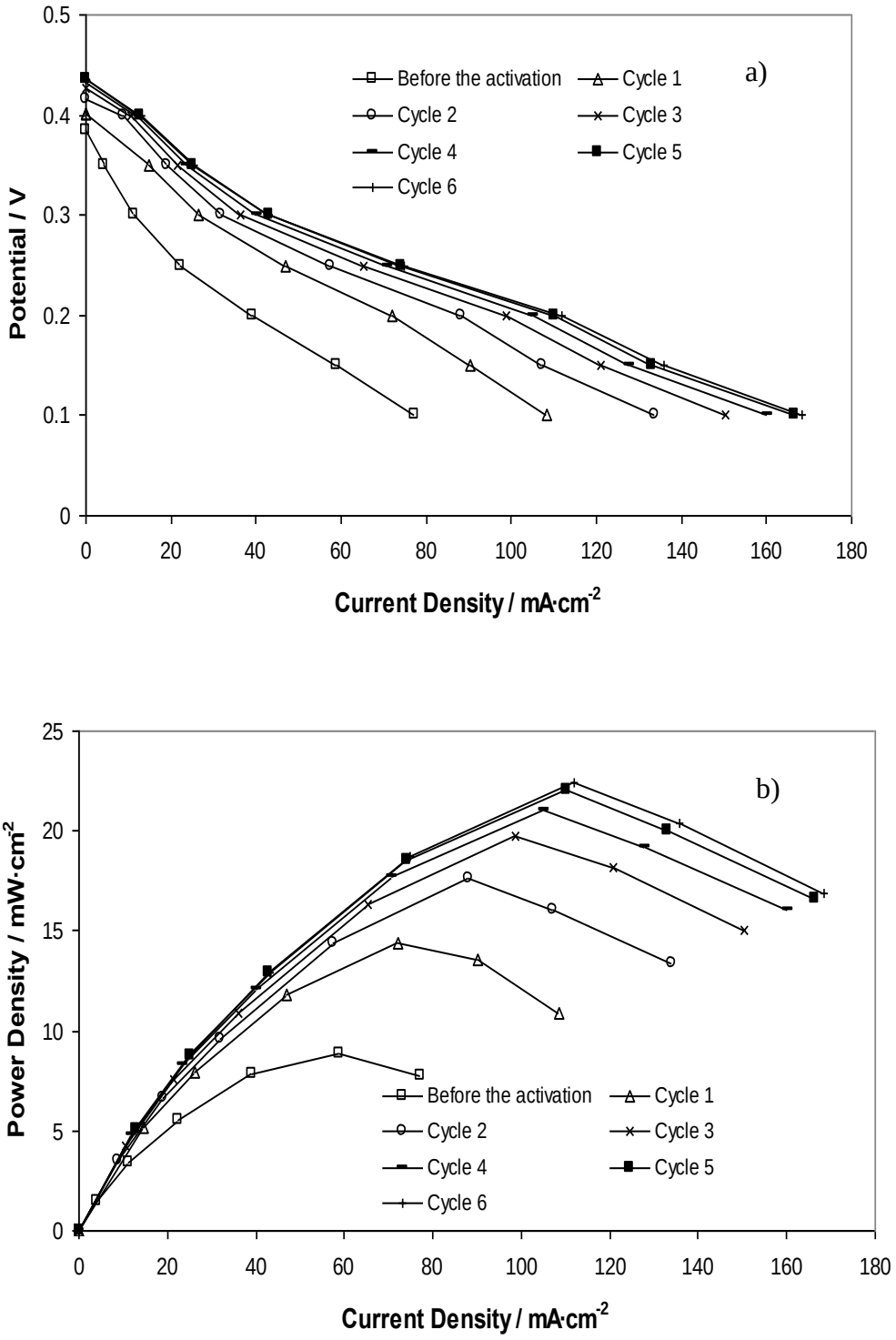

Figure 3.4 - Potential (a) and power density (b) as a function of the current density and activation cycle.

In general, a current-potential curve, Figure 3.4a, can be divided into 3 distinct zones, which are related with the limiting phenomena occurring in a MEA. At low current densities, the kinetic effects are more pronounced, due to the sluggish methanol oxidation kinetics at the anode. Figure 3.4a shows that the major differences at low current densities occur up to the third cycle indicating that the performance of the catalyst is mainly improved during this period.

At intermediate current densities, the potential losses are associated to the ionic transport between the anode and the cathode through the electrolyte, known as ohmic losses. From Figure 3.4a it can be observed a consecutive slope reduction (in terms of absolute value) associated to the ohmic zone confirming an improvement on the ionic transport across the PEM.

Table 3.1 – Limiting current densities obtained from the potential-current density curves for each activation cycle.

Number of Cycles	**Limiting Current Density / mA·cm^{-2}**
0	108.3
1	129.4
2	155.1
3	175.3
4	190.4
5	199.2
6	203.7

Finally, at high current densities the sources of potential losses (concentration losses) are essentially due to the mass transfer limitations of reactants in the diffusion and catalyst layers. It also can be seen that along the activation high current densities can be drawn from the fuel cell. Table 3.1 gives the limiting current densities as a function of the activation cycle. From this Table it can be observed that the limiting current density

almost doubles along the activation cycles. The mass transfer coefficient is proportional to the limiting current density, so, it can be concluded that the activation procedure leads to an improved mass transfer of methanol.

From Figure 3.4b, it is noteworthy that the activation was concluded after a 15-18 hours (6 cycles) period. It can be seen that the maximum power density increases substantially along the activation cycles, even though this increase is more pronounced during the first cycles; the maximum power density increases about 2.5 times, from 8.8 to 22.4 $mW \cdot cm^{-2}$.

In Figure 3.5 is given the open circuit voltage as a function of the activation cycles. It can be observed that the OCV increases 51 mV during the activation procedure.

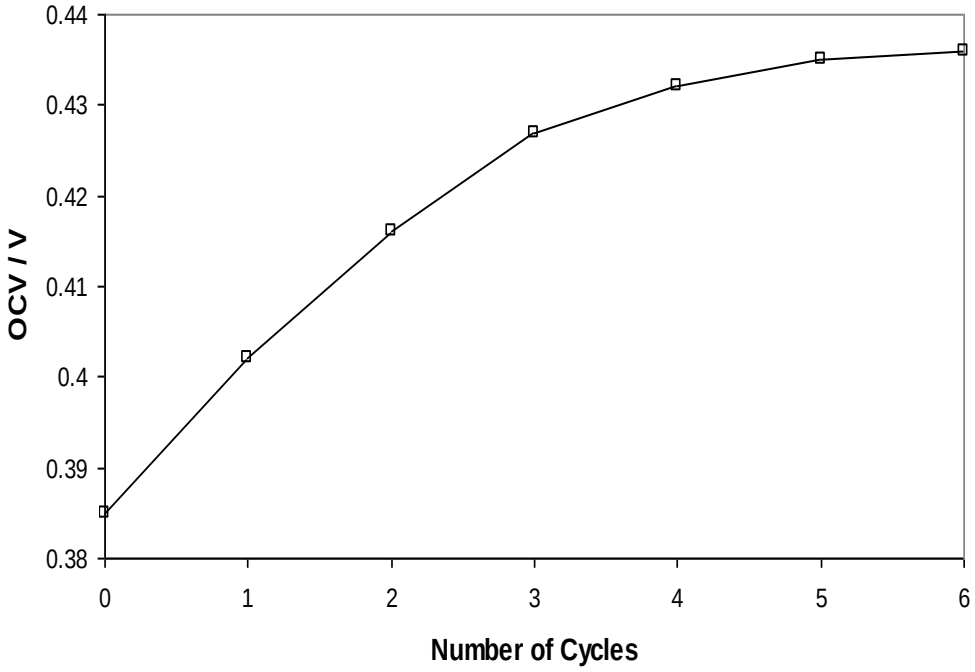

Figure 3.5 - Open circuit potential as function of the activation cycles.

3.3.3. Methanol Crossover Measurements

The experimental open circuit voltages are considerable smaller when compared with the thermodynamical value, $OCV_{Exp} \approx 0.43$ V vs $OC_{therm} \approx 1.20$ V [21]. This should happen essentially because of the strong adsorption of intermediates on the catalyst sites available to promote the electrochemical reactions at the anode [22]. Along the activation procedure, the MEA was submitted to loading cycles that helped to reduce the resistances caused by the adsorption and dehydrogenation of methanol oxidation on the catalyst – section 3.3.5. The methanol crossover also contributes significantly for the observed low OCV. In fact, the parasitic current resulting from the methanol crossover increases considerable along the activation procedure as shown in Figure 3.6.

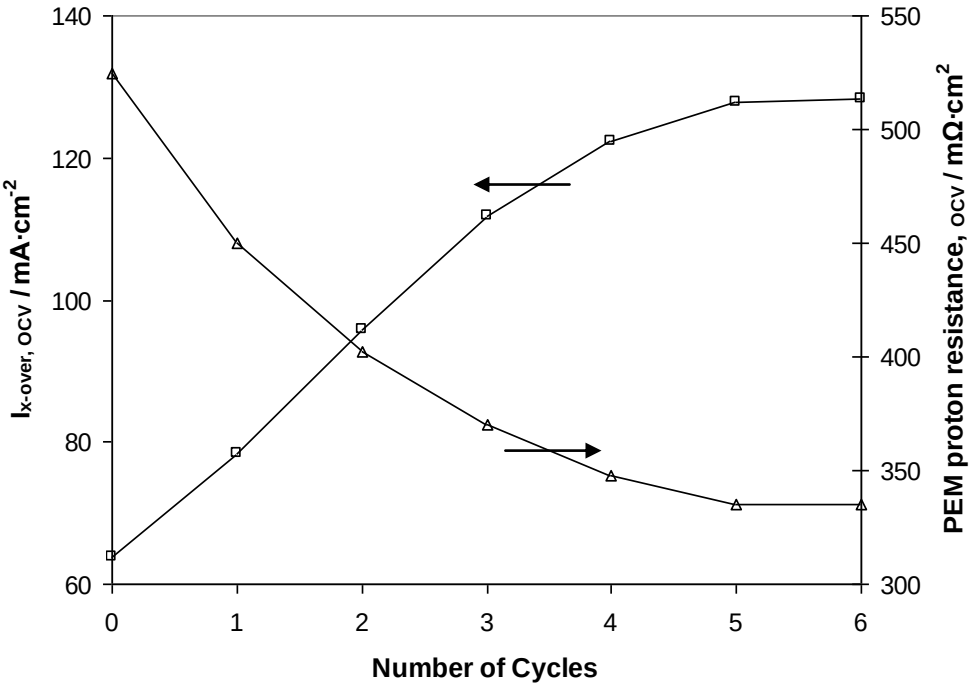

Figure 3.6 – Parasitic current density due to the methanol crossover and PEM proton resistance at OC as a function of the activation cycles.

Figure 3.6 also shows that the PEM proton resistance measured at open circuit decreases, indicating a higher hydration state of the PEM. It is known that when more

hydrated, Nafion exhibits higher permeability towards water and methanol. Despite the methanol crossover effect on the OCV being considerably higher than the PEM proton conductivity, the OCV value increases along the activation process. This indicates that the overpotential related with the adsorption of intermediate species has the main role on the OCV increase during the activation.

3.3.4. Cyclic Voltammetry

In Table 3.2 is given the relative anode ECA as a function of the activation cycle. The ECA values show that after the third activation cycle the electrocatalyst area is 95 % of after completing the activation procedure. This is in agreement with Figure 3.4a, where it can be seen that the major catalyst performance improvement occurs up to the second cycle

Table 3.2 – Relative ECAs as a function of the activation cycles. The obtained results are normalized considering the value obtained on the 6^{th} cycle (last cycle).

Number of Cycles	Relative anode catalyst area
0	0.65
3	0.95
6	1.00

3.3.5. Electrochemical Impedance Spectroscopy

An impedance spectrum was obtained at 300 mV vs DHE and recorded at the end of each activation cycle. This technique allows obtaining several impedance parameters that can help to understand the changes that both the anode catalyst and the PEM experiment during the activation process.

The electric analogue shown in Figure 3.7 [22] was found to be suitable to fit the data along the conditioning procedure. The inductance L takes into account the magnetic

disturbance caused by spurious sources on the connection of the wires and on the metal plates; resistance R_{PEM} can be assigned to the proton transport resistance across the PEM; R_{ct} is the resistance of the charge transfer process; C_{dl} is the double layer capacitance; the $C_{ad}\,R_{ad}$ analogue can be assigned to the methanol oxidation reaction including the adsorption and dehydrogenation process; finally the $C_{ox}\,R_{ox}$ analogue can be associated to the surface bound residue oxidation process.

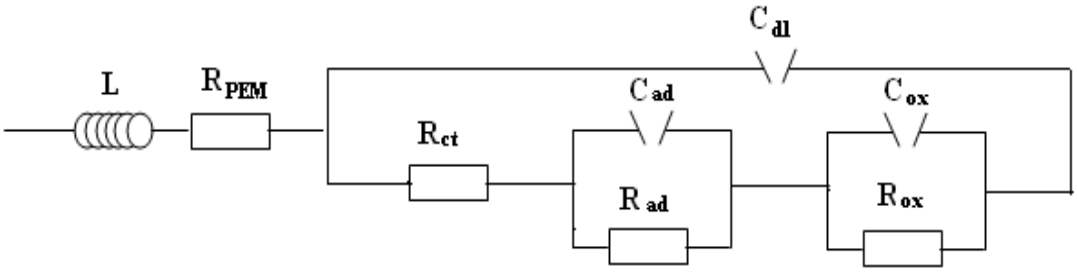

Figure 3.7 – DMFC equivalent circuit.

In Figure 3.8 is depicted the impedance data which was fitted to the previous analogue circuit, minimizing the sum of the squares residues using a commercial software (Thales Software from Zahner-Elektrik). From Figure 3.8, it can be seen that during the conditioning period there are three main time constants. At low frequencies, the impedance spectrum shows pseudo-inductive behaviour, indicating the presence of adsorbed intermediates [23-25]. At medium-high frequencies, there are two slightly overlapped semicircles representing the charge transfer contribution and the adsorption/dehydrogenation contribution. The adsorption/dehydrogenation contribution occurs at a lower frequency what can be confirmed by computing the time constants collected from the impedance data. From Figure 3.8, it also can be seen that all the semicircles diameters are decreasing along the conditioning procedure suggesting a decrease on the several cell resistances. Additionally, the spectrum experiences the larger

changes up to the second cycle. On the other hand, it is also shown that the intersection of the imaginary impedance with the real impedance at high frequencies shifts to the left with the activation cycles, indicating a decrease on the PEM resistance. Finally, the inductance contribution seems to be similar along all the activation procedure.

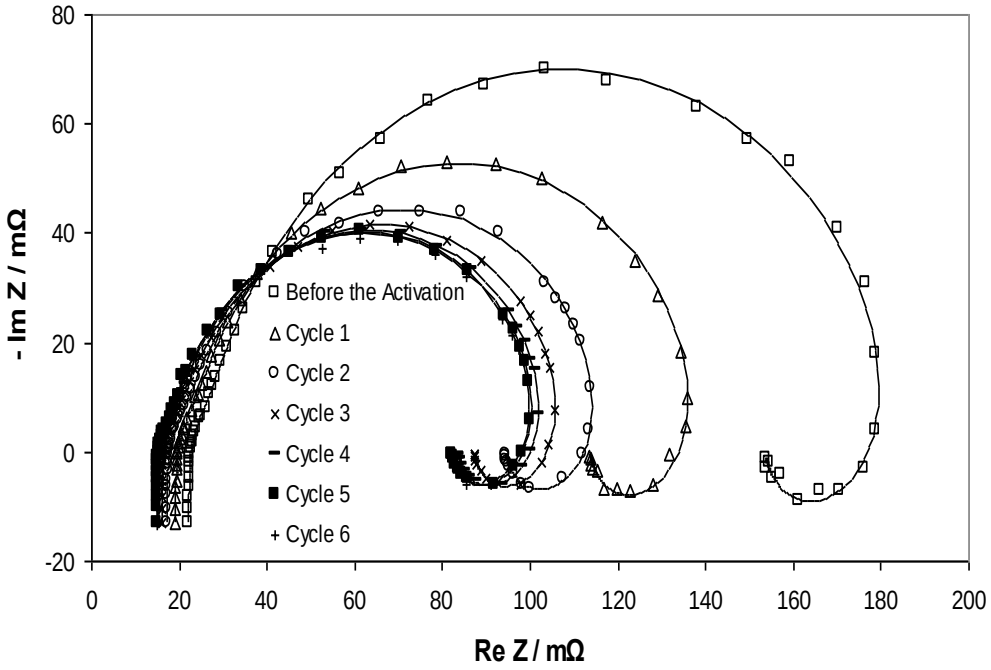

Figure 3.8 – Experimental (dots) and simulated (lines) impedance values of the DMFC at 300 mV versus DHE along the activation cycles.

In Table 3.3 are presented the model parameters extracted from fitting to the proposed model. From Table 3.3, it can be seen that the inductance value, L, remains unchanged along the entire procedure indicating that all the impedance spectra are affected in a similar way by the interference caused by other sources. As mentioned before, the PEM resistance decreases along the activation process, in agreement with the current-potential experiments (Figure 3.4a). Therefore, one can conclude that along the activation process the PEM is hydrating, enhancing the ability to transport H^+ ions supplied from the methanol oxidation reaction at the anode. To confirm this it was

obtained the number of water molecules that are accompanying the movement of each proton, i.e., the electro-osmotic drag coefficient of the water ($n_{drag} = \frac{n_{H2O}}{H^+}$), before and after the activation procedure. The experimental electro-osmotic drag coefficient of the water increased from 1.62 to 2.12, an increase of 30 % along the activation procedure that is very similar to the decrease of the PEM proton transport resistance, which was about 33 % (cf. Figure 3.6).

Table 3.3 – Impedance parameters extracted from the Nyquist plots at 300 mV versus DHE along the activation cycles.

Cycles	L / nH	R_{PEM} / mΩ	R_{ct} / mΩ	C_{dl} / mF	R_{ad} / mΩ	C_{ad} / mF	R_{ox} / mΩ	C_{ox} / mF
0	21.3	22.1	24.3	5.8	147.3	5.8	-40.3	-613
1	21.3	19.1	20.8	6.8	108.9	7.0	-35.3	-470
2	21.3	17.2	18.7	7.6	90.5	8.0	-32.1	-390
3	21.3	16.0	17.8	8.2	84.2	8.3	-30.9	-342
4	21.3	15.1	16.6	8.4	82.3	8.4	-30.5	-329
5	21.3	14.8	16.1	8.5	81.5	8.5	-30.3	-315
6	21.3	14.8	15.9	8.5	81.3	8.5	-30.2	-312

From Table 3.3, it can be realised that the charge transfer resistance, R_{ct}, decreases along the activation procedure. It is known that the charge transfer resistance is intrinsically related with mass transfer limitations associated to the electrode's reactions (in this case to the methanol oxidation) [15]. So, it can be concluded that there is probably a porosity and tortuosity change on the diffusion and catalyst layers leading to an easier access of the reactants to the catalyst active sites; the charge transfer resistance is also related to the area of the triple phase boundary [15].

The double layer capacitance, C_{dl}, is an indicator of the extension of the interconnection of the PEM, the catalyst and the reactants [26]. Its value is usually

proportional to the electrochemical catalyst active area [26]. Table 3.4 shows the relative ECA and the double layer capacitance for activation cycles 0, 3 and 6. From this Table, it can be seen that the ratio of the relative anode ECA between different cycles is closer to the corresponding ratio between the double layer capacitance. It also should be noticed that the PEM proton resistance, the charge transfer resistance decrease while the double layer capacitance increases. This should indicate that the PEM water load plays an important role in the catalyst active area improvement, namely at the interconnection between the electrode/electrolyte.

Table 3.4 – Relative ECAs, the ratio of relative ECAs between different cycles, double layer capacitances and the ratio of double layer capacitance between different cycles.

Number of Cycles	**Relative ECA**	$\frac{\mathrm{Re}\,lativeECA,_n}{\mathrm{Re}\,lativeECA,_{n-}}$	C_{dl}	$\frac{C_{dl,n}}{C_{dl,n-3}}$
0	0.65	---	5.84	---
3	0.95	1.46	8.20	1.40
6	1.00	1.05	8.51	1.04

From Table 3.3, it can be seen that the highest resistance is related with the methanol adsorption, R_{ad}; an effective activation procedure should make the methanol oxidation resistance to decrease significantly. In this activation protocol, the methanol adsorption resistance decreases about 45 %. Also from Table 3.3, it can be verified that the analogue $C_{ad}\,R_{ad}$, which represents the time constant associated to the adsorption and dehydrogenation of methanol on the catalyst, decreases along the activation procedure indicating improved reaction kinetics.

When a pseudoinductive behaviour is verified at low frequencies, it means that the working potential is above the onset. Chakraborty et al. [22] showed that the occurrence of the pseudoinductive loop coincides with the onset potential for methanol oxidation on PtRu. Before the onset, the catalyst surface is covered with adsorbed hydrogen and reaction intermediates from methanol dehydrogenation and so, there are no available free sites available for methanol oxidation. After the onset potential, holes are created in the adsorbed layer by the oxidation of the intermediates. The $C_{ox}R_{ox}$ analogue is intrinsically related to the ability to oxidize these intermediates creating new free catalyst sites available to promote the methanol oxidation. The negative signal of both parameters is related to inductive loop of this analogue. The absolute values of these parameters also decrease with the activation cycles. From these results, it can be expected that the MEA response becomes quicker with the activation procedure.

3.3.6. Voltage Step Perturbations

Figure 3.9 plots the OCV history of the DMFC after a load step perturbation at instant 10 s, from 50 mV to open circuit, along the activation procedure. When changing from 50 mV to open circuit, the OCV increases rapidly and reaches a peak. A similar response is obtained for all cycles considered (0, 3 and 6). This behaviour is intimately related to the ohmic losses of the fuel cell. On the other hand, the maximum peak value is not the real OCV value, in fact the real value is only reached after a certain time. The voltage decay is associated to the methanol oxidation reactions and mass transport kinetics [27]. It can be observed that the steady-state potential is reached sooner as the activation proceeds, indicating that the fuel cell responds more quickly to loads changes. When the cell is being operated at 50 mV and suddenly experiences a load cut, there is an increase on methanol concentration at the anode that leads to an increase in methanol crossover causing a potential decrease. For cycle 6 (Figure 3.9), the potential decrease up

to the steady state is larger due to a large methanol crossover; this indicates a more permeable membrane.

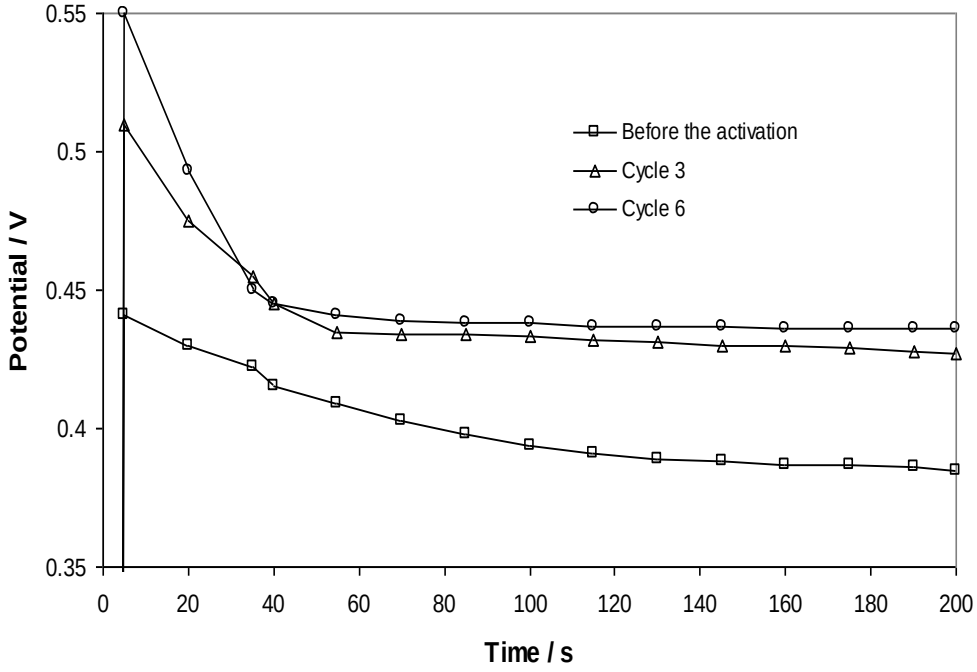

Figure 3.9 - Open circuit voltage as a function of time – response to a step perturbation from 50 mV to open circuit, at 55 °C. Lines are there for easy reading.

3.3.7. Potential, Faraday and Overall Energy Efficiency

Besides the power density analysis, the energy efficiency is critical on characterizing a DMFC system. The DMFC global efficiency is obtained from the product of two different contributions, the potential and the Faraday efficiencies. The potential efficiency is directly related with the overpotentials – difference between the thermodynamic and the actual potential. On the other hand, the Faraday efficiency is related to the methanol crossover from the anode to the cathode, decreasing with the methanol crossover increase.

Figures 3.10a and 3.10b show the potential and Faraday efficiencies along the activation cycles, respectively. From Figure 3.10a, it can be verified that the potential efficiency increases during the whole process and that this increase is for the entire

polarization curve. Figure 3.10b shows that higher Faraday efficiencies (for the same current densities) are obtained before the MEA activation process, decreasing along the activation process. During this process, the PEM is hydrated and its proton conductivity increases – the potential efficiency improves – but the methanol crossover increases – and the Faraday efficiency decreases. This effect is easily perceived from Table 3.1 where it is shown the parasitic methanol current density along the activation cycles. At this point it is important to establish which of the contributions is more important and for that the DMFC global efficiency should be computed.

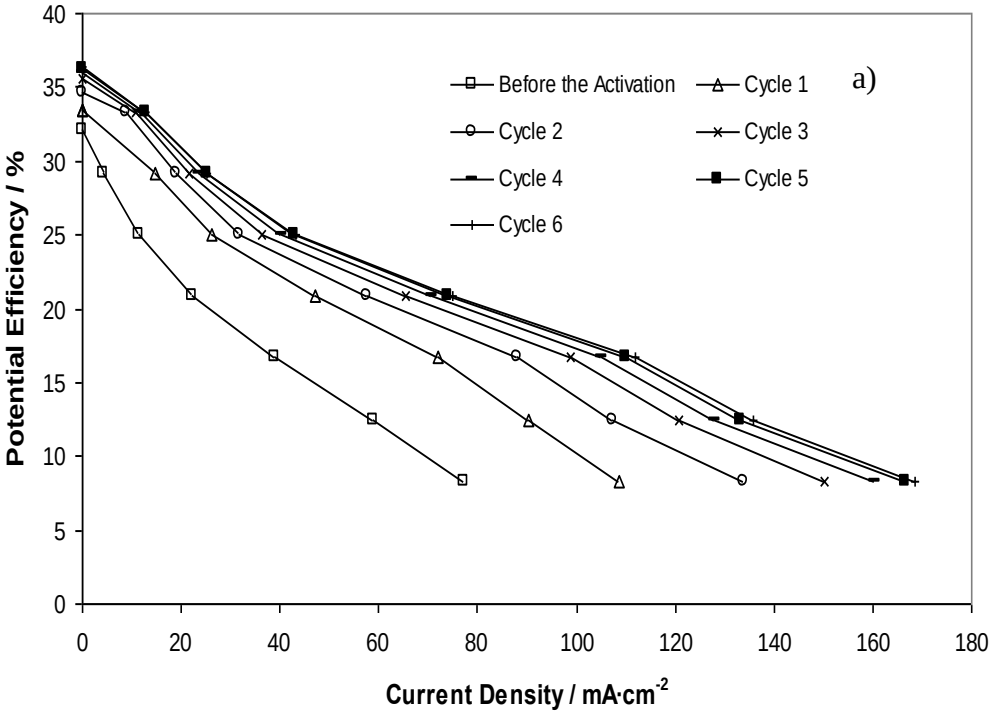

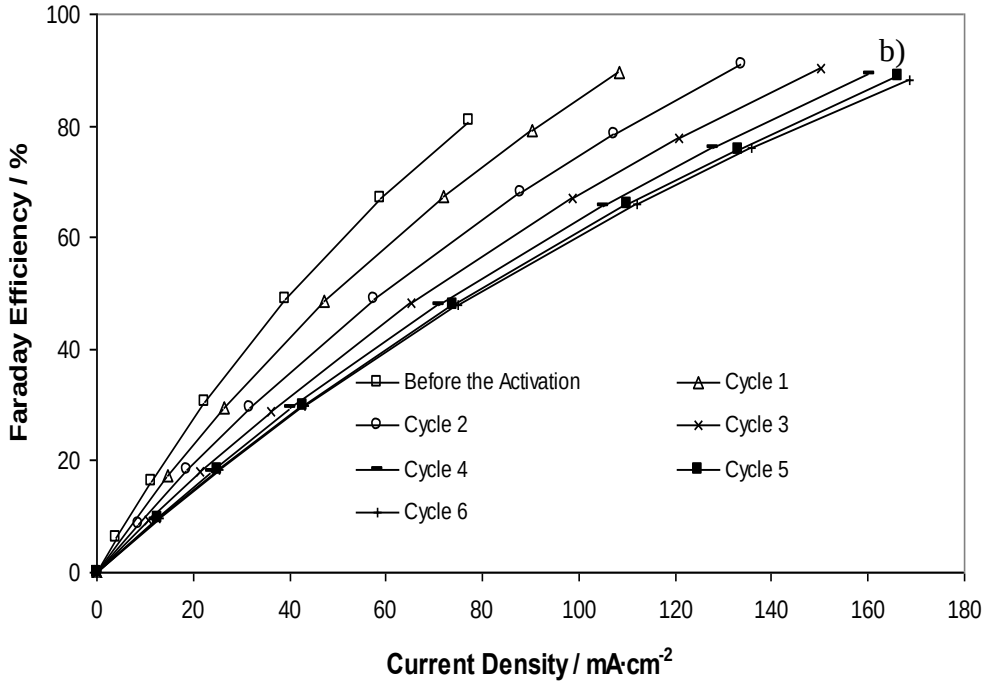

Figure 3.10 - Potential efficiency (a) and Faraday efficiency (b) as function of the current density and activation cycle.

Figure 3.11 shows the global efficiency as a function of the activation cycle. It is observed that very similar efficiency patterns are obtained for the last three activation cycles, which maximum is around 11 % global efficiency. It is also observed that at low current densities the controlling efficiency phenomenon is the methanol crossover. This is confirmed by the higher energy efficiency obtained for the first cycle where a reduced methanol crossover is observed. For high current densities, it can be seen that the methanol crossover starts playing a secondary role, being now more important the PEM proton conductivity and the catalyst activity. At this stage the best performance is obtained after the activation of the MEA.

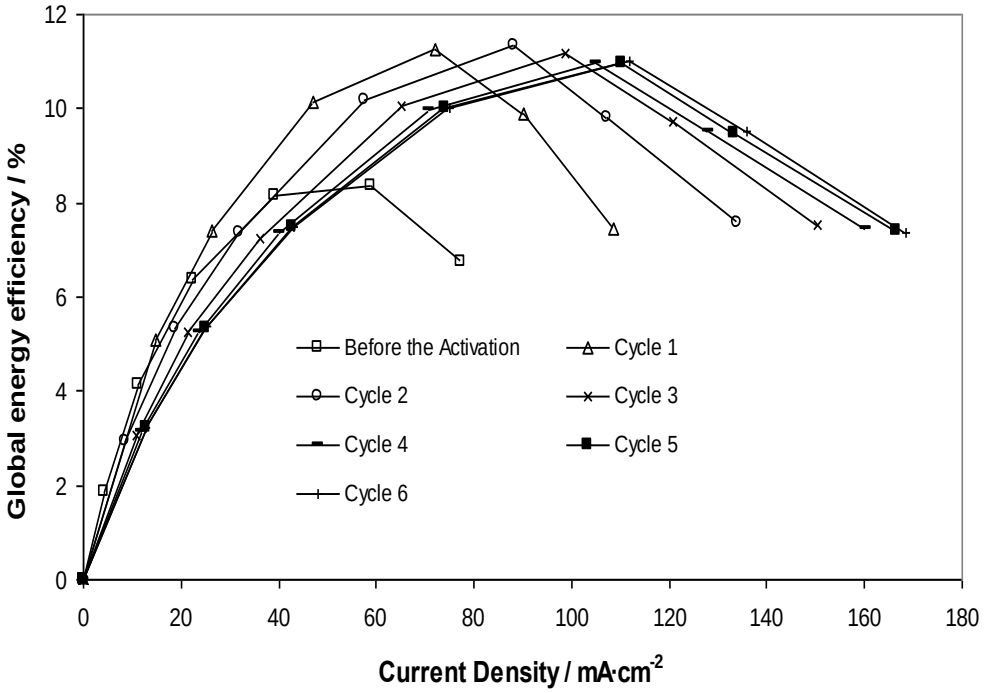

Figure 3.11 – Global energy efficiency as function of the current density and activation cycle.

3.4. Conclusions

An activation protocol was set-up comprehending six loading cycles performed at different temperatures and voltages. It was observed that the increase of the temperature favours the MEA activation up to 55 ºC. Furthermore, the MEA performance is detrimentally affected when the activation procedure is performed at 90 ºC probably due to an excessive swelling on the ionomer that involves the catalyst. When the activation procedure is carried out at the OCV condition the final performance of the MEA is considerably lower. Indeed, the MEA should be always submitted to load cycles for higher energy outputs.

In order to study the changes that the MEA experiences along the activation procedure, it was followed a set of loading cycles at 55 ºC and 200 mV. These changes

were followed performing polarization curves, linear sweep voltammetry, cyclic voltammetry and electrochemical impedance spectroscopy.

Along the activation procedure, the maximum power density increased about 2.5 times, from 8.8 to 22.4 $mW \cdot cm^{-2}$ due to improved PEM and catalyst performances. It was also concluded from cyclic voltammetry experiments that the anode catalyst available area to promote the electrochemical reactions increased along the activation procedure. Despite the methanol crossover increase along the conditioning procedure, the OCV increased 51 mV mostly because the decrease of the PEM resistance and the improvement of the catalyst activity.

The increase of the PEM hydration along the activation cycles, as confirmed by the electro-osmotic drag experiments, led to higher PEM proton conductivities. Furthermore, improvements on the ionomer proton conductivity that involves the catalyst layers allowed the enlargement of the triple phase boundary, confirmed by the increase of the double layer capacitance as shown by the impedance data. From the charge transfer resistance decrease, it was inferred that the diffusion and catalyst layers experienced structural changes, probably on the porosity and tortuosity. However, the major performance improvements experienced by the MEA along the activation procedure were due to the decrease of the anode resistances related to the adsorption and dehydrogenation phenomena associated to the methanol oxidation. It was also observed that the activation procedure decreases the MEA response time to changes on DMFC load from 50 mV to open circuit. It was also verified improvements concerning the DMFC global energy efficiency, especially at higher current densities; it was observed a maximum global energy efficiency increase of about 11 %.

3.5. References

1. J. Larminie, A. Dicks, *Fuel Cell Systems Explained*, John Wiley & Sons, Chichester, (2003).

2. R. Dillon, S. Srinivasan, A. S. Aricò and V. Antonucci, *Journal of Power Sources*, 127, 112 (2004).

3. B. K. Kho, I. H. Oh, S. A. Hong and H. Y. Ha, *Electrochimica Acta*, 50, 781 (2004).

4. F. Liu and C. Y. Wang, *Electrochimica Acta*, 50, 1413 (2005).

5. Z. Qi and A. Kaufman, *Journal of Power Sources*, 111, 181 (2002).

6. V. S. Silva, V. B. Silva, A. Mendes, L. M. Madeira, H. Silva, J. Michaelmann, B. Ruffmann and S. P. Nunes, *Separation Science. Technology*, 42, 2909 (2007).

7. E. Yasumoto, H. Gyoten, K. Nishida and T. Kanbara, Method for Activating a Fuel Cell, United States Patent, (2001).

8. Z. Qi and A. Kaufman, *Journal of Power Sources*, 109, 227 (2002).

9. Z. Qi and A. Kaufman, *Journal of Power Sources*, 114, 21 (2003).

10. C. He, Z. Qi, M. Hollett and A. Kaufman, *Electrochemical Solid-State Letters*, 5, A181 (2002).

11. Z. Xu, Z. Qi and A. Kaufman, *Journal of Power Sources*, 156, 281 (2006).

12. H. N. Dinh, X. Ren, F. H. Garzon, P. Zelenay and S. Gottesfeld, *Journal of Electroanalytical Chemistry*, 491, 222 (2000).

13. Y. Kiang, PhD Thesis, *Spontaneous Hydrogen Evolution in Direct Methanol Fuel Cells*, Hong Kong, 2005.

14. C. Rice, X. Ren and S. Gottesfeld, Methods of Conditioning DMFCs, United States Patent, 2005.

15. J. H. Kim, H. I. Lee, S. A. Hong and H. Y. Ha, *Journal of Electrochemical Society*,152, A2345 (2005).

16. B. Sunden and M. Faghri, *Transport Phenomena in Fuel Cells*, WIT Press, United Kingdom, (2005).

17. J. H. Kim, H. Y. Ha, I. H. Oh, S. A. Hong, H. N. Kim and H. I. Lee, *Electrochimica Acta*, 50, 801 (2004).

18. K. R. Cooper, V. Ramani, J. M. Fenton and H. Kunz, *Experimental Methods and Data Analyses for Polymer Electrolyte Fuel Cells*, Scribner Associates, North Carolina, (2005).

19. X. Ren, W. Henderson and S. Gottesfeld, *Journal of Electrochemical Society*, 144, L267 (1997).

20. E. Gülzow, S. Weißhaar, R. Reissner and W. Schröder, *Journal of Power Sources*, 118, 405 (2003).

21. V. Silva, PhD Thesis, *Direct Methanol Fuel Cell: Analysis Based on Experimentation and Modeling*, Porto, 2005.

22. D. Chakraborty, I. Chorkendorff and T. Johannessen, *Journal of Power Sources*, 162, 1010 (2006).

23. L. Bai and B. E. Conway, *Journal of Electrochemical Society*, 138, 2897 (1991).

24. R. D. Armstrong and M. Henderson, *Journal of Electroanalytical Chemistry*, 39, 81 (1972).

25. D. Chakraborty, I. Chorkendorff and T. Johannessen, *Journal of Power Sources*, 173, 110 (2007).

26. Z. Siroma, T. Sasakura, K. Yasuda, M. Azuma and Y. Miyazaki, *Journal of Electroanalytical Chemistry*, 546, 73 (2003).

27. P. Argyropoulos, K. Scott and W. M. Taama, *Electrochimica Acta*, 45, 1983 (2000).

4. Targeting an Improved DMFC Performance Using an Optimized Activation Procedure*

Abstract

An activation procedure considers all the actions done to improve the performance of a direct methanol fuel cell (DMFC). It includes the pre-treatment of the proton exchange membrane (PEM) and catalyst and the *in situ* activation procedure. The Design of Experiments (DoE) methodology was applied to optimize the *in situ* activation, where loading cycles were employed. The factors considered for the experimental design were the temperature, the potential (defined as constant) and the cathode air pressure. These factors were previous selected after a few screening experiments. The maximum power density response was optimized using a central composite design (CCD). It was observed a good agreement between the experimental and predicted power density responses. It was also verified that the potential was the most significant factor. After, the MEAs were submitted to the optimized *in situ* activation procedure based in membranes submitted to different pre-treatments. Considering the pre-treatment, it was observed that the pre-treated membrane electrode assemblies (MEAs) showed higher proton conductivity but also increased methanol permeability towards the cathode. Furthermore, it was observed that boiling the PEM and the catalyst in water was the pre-treatment procedure that led to the highest maximum power density. Finally, the *in situ* loading cycles procedure was critically compared with other *in situ* activation procedures reported in the literature. It was concluded that the hydrogen conditioning and the *in situ* loading cycles procedure led to the best performance of the DMFC.

---

*V. B. Silva, V. S. Silva, L. M. Madeira, A. Mendes, submitted

4.1. Introduction

An intensive research effort has been devoted to the development of Direct Methanol Fuel Cells (DMFCs) [1, 2]. It is believed that DMFCs will be able to revolutionize the performance and use of a large set of portable electronic equipments, namely notebook computers, mobile phones, video cameras, among others [3]. Before being widely commercialized, it is crucial to overcome some drawbacks such as low catalyst activity [1, 4] and high methanol crossover [1, 4], but also to provide effective activation procedures that could ensure a DMFC to give its best performance immediately upon the start-up. Furthermore, the activation procedure should originate DMFCs uniform start-ups. In fact, much of the scatter in the published DMFC results reflects the effect of the handling and pre-treatment of the proton exchange membrane (PEM) [5, 6] and catalyst [7, 8], but also the influence of the employed *in situ* activation procedure [9, 10].

In this study we distinguish between pre-treatment methods and *in situ* activation procedures. Pre-treatment methods include all the procedures carried on a PEM and catalyst, before assembling them in a membrane electrode assembly (MEA), while *in situ* conditioning procedures are actions used to improve the performance of a MEA when the fuel cell is on a working state.

In the open literature there are several approaches to prepare the MEA for obtaining the best and stabilized performance at the start-up [5 - 12]. One of the most well-known activation procedures includes the anode pre-conditioning with hydrogen. It is believed that this procedure speeds up the activation procedure due to high discharge currents [11]. Other traditional techniques are the hot methanol conditioning [12], where the fuel cell is previously fed with a methanol aqueous solution at medium to high temperatures, and the current conditioning [13], which considers the operation of the MEA with a current of polarity opposite when in normal use. Despite the generalized

implementation of methods to activate a MEA, there is no systematized data comparing the various procedures. Additionally, the characterization of the MEA using a set of electrochemical tests along the *in situ* activation procedure is rarely performed. In general, only the polarization curves and impedance spectra are taken, missing crucial data as the methanol crossover, the effective electrochemical catalyst area and the determination of the water electro-osmotic drag coefficient.

As mentioned previously, the activation process considers both pre-treatment and *in situ* activation procedures. Regarding the *in situ* activation procedure, it is crucial to select the best operating conditions to maximize the output performance [10]. So, a straightforward methodology to minimize the number of runs to select the optimal operating conditions is needed. Classical methods of experimentation involve the performance of several experimental runs following a one-factor-at-a-time approach, which are time consuming and ignore the interaction effects between factors [14]. In fact, these disadvantages lead to a poor optimization of the activation procedure. However, these limitations can be left behind using methods of design of experiments (DoE), where all the factors are varied inside the design space. These methods can be implemented with some advantage to semi-empirically select the optimal operating conditions to use during an *in situ* activation procedure. The DoE methodology was implemented after a pre-screening. The set of factors considered in this strategy (preliminary experiments) were the air flow rate, methanol flow rate, air pressure, methanol concentration, temperature and loading and were varied in a selected range with all other factors held constant. This allowed the selection of the relevant factors (loading, temperature and air pressure) and their ranges for subsequent application of the DoE.

As mentioned above, the pre-treatment of the PEM and catalyst plays a key role to target an improved DMFC performance. The Nafion proton exchange membrane has a

very hydrophobic and highly crystalline polymer matrix with ionic clusters attached to flexible side chains [15]. This allows the formation of large ionic clusters that make water, methanol or other alcohol solutions to be easily sorbed. Aware of this, several research groups tested different PEM pre-treatments, namely with methanol [5], water [6], and other alcoholic and acidic aqueous solutions in a large range of temperatures and concentrations. Several standard characterization techniques to evaluate the proton conductivity, methanol crossover or swelling were employed; however, each research group used his own characterization techniques leading to results that can not be easily compared. In fact, this problem can be extended to the pre-treatment of the catalyst, where different characterization methodologies were also employed for evaluating the catalyst performance evolution [7, 8]. So, it is important to analyse some of the most common pre-treatments and compare the results based in the same set of characterization methods.

In this paper several PEM and catalyst pre-treatments are tested and compared using standard characterization techniques such as proton conductivity, swelling degree and methanol crossover. The pre-treated MEAs were then conditioned using a previously optimized *in situ* activation procedure made of loading cycles. This *in situ* activation was characterized performing polarization curves, electrochemical impedance spectroscopy (EIS) and cyclic voltammetry (CV) analyses. In this way, it was possible to obtain the characterization of the pre-treated and activated MEAs to understand not only the effect of the pre-treatment on the final DMFC performance but also the most effective activation procedure.

Finally, the optimized pre-treatment and activation procedure based on loading cycles was compared with other known procedures, such as the anode hydrogen conditioning and the hot-methanol conditioning.

4.2. Experimental

4.2.1. MEA Pre-treatment

In this work, several PEM pre-treatments were performed, as listed in Table 4.1.

Table 4.1 – Proton exchange membrane pre-treatments.

	Name	Pre-treatment description
MEA	**A**	Immersed in water at room temperature during 3 days
	B	0.33 M H_2SO_4
	C	1 M H_2SO_4
	D	3 M H_2SO_4
	E	1 M methanol aqueous solution
	F	2 M methanol aqueous solution
	G	Boiled in water during 1 hour
	H	As received

PEMs B, C, D, E and F were immersed in water at room temperature during 3 days and then were also immersed in the above mentioned environments at 55.5 ºC during one hour previously to the measurements. All the backing and catalyst layers were submitted to the same pre-treatment than the corresponding PEM.

4.2.2. Design of Experiments Applied to the *In situ* Activation Procedure

To evaluate the DMFC response along the *in situ* activation procedure, it was followed a DoE approach and selected a simple central composite design with 3 factors with axial values in orthogonal positions. It was used a commercial software (JMP 7.0 from SAS) that indicated 17 experiments. Temperature, loading and cathode air pressure were selected as input factors and the maximum power density as the response. All other

operating conditions were kept constant (a methanol aqueous solution at 12 $mL \cdot min^{-1}$ and 1.5 M at the anode side and humidified air at 1000 $mL \cdot min^{-1}$ and 100 % relative humidity at the cathode side). Each parameter range was selected taking into account the normal operating conditions associated to low-medium temperature DMFC operation but also to previous screening experiments where only one parameter was varied (data not shown). The ranges of the parameters given are in Table 4.2.

Table 4.2 – Operating range conditions considered in the DoE for the MEA's activation.

Operating Condition	**Temperature / ºC**	**Loading / mV**	**Cathode Air Pressure / bar**
Range	40 - 70	50 - 350	1.5 – 2.5

4.2.3. MEA Activation Protocol

The fresh MEAs were characterized obtaining the polarization curves (after each loading cycle) and the impedance spectra, the cyclic voltammograms and the methanol crossover before and after the activation protocol. All pre-treated MEAs were activated submitting them to several loading cycles at the optimum operating conditions (found with the help of a central composite design). Each loading cycle lasted 180 minutes and was interrupted for obtaining a polarization curve. Between each experiment, it was allowed to the MEA to rest at open circuit for 30 min. The activation procedure was interrupted whenever the changes in the current density became smaller than 3 % between successive loading cycles for the complete voltage range. This was the criterion for considering the fuel cell at the steady-state, i.e., fully activated.

4.2.4. Characterization Methods

4.2.4.1. Methanol Crossover Measurements

The current density equivalent to the methanol that crosses the electrolyte ($I_{crossover}$) is related to the anode mass-transport limiting current density ($I_{\lim}$) by [16]:

$$I_{crossover} = I_{OCV,crossover} \times \left(1 - \frac{I}{I_{\lim}}\right) \quad (4.1)$$

where $I_{OCV,crossover}$ is the methanol crossover current density at the OCV and I is the operation current density.

As shown by the above equation, the parasitic current density due to the methanol crossover at any current value is obtained evaluating the parasitic current density at open circuit voltage and the limiting current density. To evaluate the parasitic current density at open circuit, the DMFC anode feed and operating conditions were the same employed for activation and the hydrogen feed flowrate was 200 $mL_N \cdot min^{-1}$. Scans were performed at a scan rate of 3 $mA \cdot s^{-1}$ between 0 and 0.8 V *vs* the reference electrode, in galvanostatic mode.

4.2.4.2. *In situ* Cyclic Voltammetry (CV)

In situ cyclic voltammetry was carried out with the DMFC in operation. The anode evaluation was accomplished feeding a dry hydrogen stream (200 $mL_N \cdot min^{-1}$) to the cathode compartment, which serves as reference/counter electrode, while a humidified nitrogen stream (200 $mL_N \cdot min^{-1}$) was fed to the anode compartment which serves as working electrode. The working electrode was swept at 50 $mV \cdot s^{-1}$ between -0.4 V and 1.3 V versus the cathode (counter/reference electrode).

Relative anode electrochemical active areas (ECA) were obtained by calculating the areas of the hydrogen oxidation peaks from the cyclic voltammograms [17] using the following equation:

$$rECA = \frac{Q}{\mu_{Pt} \times L} \quad (4.2)$$

where $rECA$ is the relative anode electrochemical active area, Q is the charge density of the atomic hydrogen adsorption, μ_{Pt} is the charge needed to reduce a monolayer of protons at the polycrystalline Pt surface of 1 cm^2 (μ_{Pt} = 210 $mC \cdot cm^{-2}$ Pt) and L is the Pt load (1 $mg \cdot cm^{-2}$). Despite the absolute ECAs could not be obtained due to the Ru interference, it is possible to compare the relative surface areas [17] along the activation procedure.

4.2.4.3. Electrochemical Impedance Spectroscopy

Impedance spectra were obtained operating the DMFC cell as follows: at the anode side different conditions were imposed as employed during the activation process and at the cathode side a dry hydrogen stream was fed (200 $mL_N \cdot min^{-1}$). The cathode side worked as a dynamic hydrogen electrode (DHE) under 300 mV between the anode and the cathode side. In this way, only the anode impedance behavior was studied. The electrochemical impedance measurements were performed using a Zahner IM6e workstation coupled with a potentiostat (PP-240, Zahner). Impedance spectra were also recorded at ten points per decade by superimposing a 5 mV ac signal over the frequency range from 100 kHz to 10 mHz.

4.2.4.4. Proton Conductivity

Proton conductivity measurements were performed at 55.5 ºC in an in-house made cell – Figure 4.1.

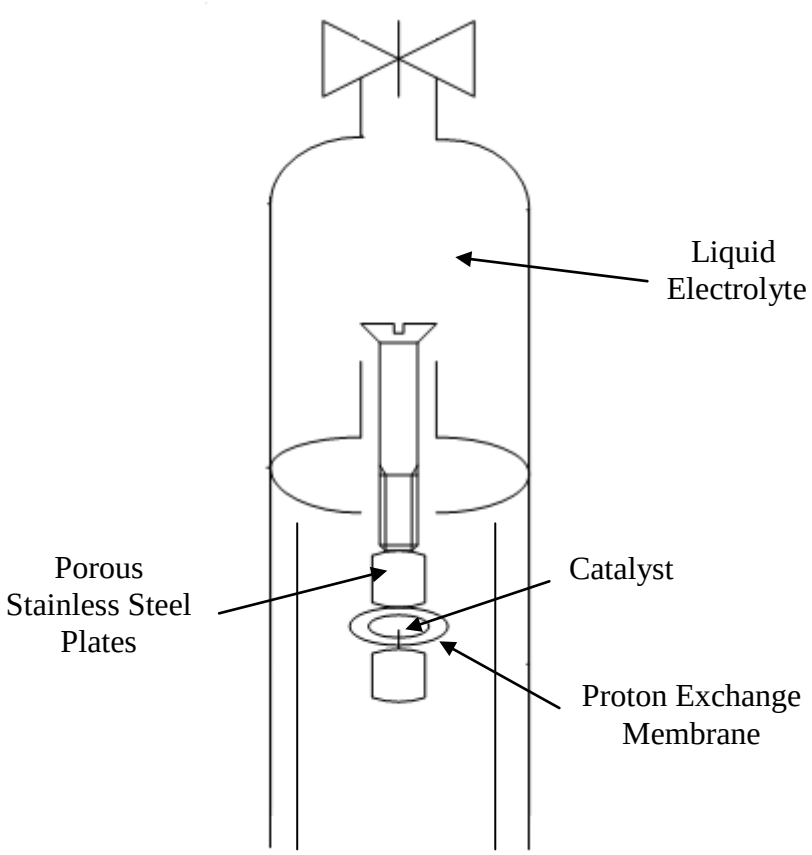

Figure 4.1 – Proton conductivity set-up.

In Figure 4.1 is shown the proton conductivity set-up. It consists of a compartment that can store the selected electrolyte and by two sintered stainless steel plates sandwiching the MEA (10 mm in diameter) with an applied torque of 1.5 N·m, obtained with the help of a dynamometric screwdriver.

The proton conductivity was obtained from the high frequency interception with the real axis of the Nyquist plot. When the resistance of a single membrane is close to the resistance at short-circuit condition, the measurement is applied on stacks containing several membranes. The membrane-membrane interface resistance is determined as described by Alberti et al. [18]. Before being inserted in the proton conductivity cell, samples were immersed in water at room temperature during 3 days to ensure total leaching. The samples were then pre-treated as described in Table 1. The impedance

spectrometer used was a Zahner IM6e workstation working in the frequency range between 0.1 and 10^5 Hz. The average error obtained using this procedure was 5.3 % (t distribution for 95 % confidence interval).

4.2.4.5. Swelling Measurements

Membrane samples were previously dried in a vacuum reservoir at 80 °C for 5 hours. After drying, samples of Nafion 112 were weighted and immersed in water, 1 M and 2 M methanol aqueous solutions, 0.33 M H_2SO_4, 1 M H_2SO_4 and 3 M H_2SO_4 at 55.5 ºC and for 90 h. This ensured that the equilibrium is attained. The weights of the swollen membranes were obtained after carefully removing the solution from both surfaces. Membrane swelling (wt.%) was computed from the ratio between the difference of the wet and dry weight and the dry weight. The average error obtained using this procedure was 5.5 % (t distribution for 95 % confidence interval).

4.2.4.6. DMFC Tests

The studied MEAs were prepared by hot pressing the membrane sample, Nafion 112 from GEFC, between two ElectroChem electrodes at 90 ºC and 150 bar for 150 s. Supported PtRu (1 $mg \cdot cm^{-2}$ and 1:1 molar ratio) and Pt (0.5 $mg \cdot cm^{-2}$) were used on the anode and cathode, respectively. Single cell measurements were performed in a 25 cm^2 active area cell. The DMFC was operated with a methanol aqueous solution (12 $mL_N \cdot min^{-1}$ and 1.5 M) at the anode side and with humidified air (1000 $mL_N \cdot min^{-1}$, 100 % relative humidity) at the cathode side. The DMFC set-up is described elsewhere [19].

4.2.4.6.1. Hot-Methanol Conditioning

The fuel cell was fed with a 1.5 M methanol solution at 80 ºC during 24 h through the anode compartment [12]. The DMFC was operated with a methanol aqueous solution (backpressure at 2.5 bar, 12 $mL_N \cdot min^{-1}$) at the anode side and with humidified air (backpressure at 2.5 bar, 1000 $mL_N \cdot min^{-1}$, 100 % relative humidity) at the cathode side.

4.2.4.6.2. Hydrogen Conditioning

The anode side was fed with hydrogen (15 h, backpressure 2.5 bar, 100 $mL_N \cdot min^{-1}$ and 200 mV) at the anode side and with humidified air (backpressure at 2.5 bar, 1000 $mL_N \cdot min^{-1}$ and 100 % relative humidity) at the cathode side.

4.3. Discussion and Results

4.3.1. Design of Experiments Applied to an Activation Procedure

The RSM is a set of mathematical and statistical techniques that are helpful for the analysis and modelling of problems that are determined by a set of variables [14]. The response surface method is a 3-level design that allows the fitting of a curved surface to continuous factors. Simultaneously, a response surface method allows determining if a minimum or maximum response exists inside the targeted region. The central composite design (CCD) is normally used with RSM. It is also usually applied when no more than six factors are considered simultaneously [20]. The CCD includes the two-level fractional factorial, usually coded as low (-1) and high (+1) values, the center points that can be replicated to estimate the experimental error variance, and the axial points that are located at the axis of each factor at a distance α from the center.

In this study the CCD was applied to obtain the maximum power response surface after an activation procedure; simultaneously, the optimal operating conditions were also determined. Previous screening experiments were performed to select the relevant DMFC operating variables: loading, temperature, cathode air pressure, methanol flowrate, air flow rate and methanol feed concentration. Loading, temperature and cathode air pressure are the variables that mostly determine the MEA power response along an activation procedure. The screening experiments were also helpful to select the relevant range of these variables (cf. Table 4.2), in order to find the optimal conditions. The DMFC response was later evaluated following a CCD as described in Table 4.3. The center point was replicated three times to assess the experimental error. In this set of runs, the PEMs and catalysts were pre-treated in boiling water during one hour.

Table 4.3 - DMFC's operating conditions given by the central composite design (α = 1.287) and the corresponding experimental maximum power densities after the *in situ* activation procedure.

Run Number	Temperature / ºC	Loading / mV	Cathode Air Pressure / bar	Maximum Power Density / $mW \cdot cm^{-2}$
1	40.0	350	1.50	17.1
2	55.0	200	2.00	21.6
3	35.7	200	2.00	21.2
4	55.0	6.9	2.00	21.5
5	74.3	200	2.00	19.9
6	40.0	50	1.50	20.3
7	70.0	50	2.50	22.5
8	55.0	393	2.00	16.9
9	55.0	200	2.00	21.5
10	55.0	200	1.36	20.8
11	55.0	200	2.64	22.6
12	70.0	50	1.50	20.6
13	70.0	350	2.50	18.9
14	40.0	350	2.50	18.1
15	40.0	50	2.50	21.7
16	70.0	350	1.50	17.3
17	55.0	200	2.00	21.6

In agreement with the experimental design, the parameters of a second order response model were obtained minimizing the sum of the residues square. The empirical model can be defined as:

$$Y = B_0 + \sum_{i=1}^{3} B_i \times X_i + \sum_{i=1}^{3} B_{i,i} \times X_i^2 + \sum_{j=2}^{3} \sum_{i<j}^{3} B_{i,j} \times X_i \times X_j \qquad (4.3)$$

where Y is the power density and the X_i terms are the main factors $-1 \leq X_i \leq 1$, temperature (1), loading (2) and cathode air pressure (3).

Table 4.4 shows the coefficients obtained and their significance determined by the Student t-test and by the p-values.

Table 4.4 – Empirical coefficients of Eq. (4.3) and their significance evaluated by the Student t test and by the p-values. The significant coefficients are in bold.

Regression Coefficient	**Estimate**	***t* ratio**	**Prob > |t|**
B_0	21.57	80.69	0.00
B_1	0.04	0.32	0.76
B_2	**-1.73**	**-12.63**	**0.00**
B_3	**0.75**	**5.44**	**0.00**
B_{11}	**-0.62**	**-3.13**	**0.02**
B_{22}	**-1.46**	**-7.39**	**0.00**
B_{33}	0.07	0.33	0.75
B_{12}	-0.03	-0.17	0.87
B_{13}	0.14	0.83	0.44
B_{23}	-0.09	-0.57	-0.59

The significance of the model parameters was assessed from the corresponding p-values. When the p-values are smaller than 0.05 indicates that the corresponding parameters have a significant effect on the response with a confidence level of more than 95 %; if the p-values are somewhere between 0.05 and 0.15, then the parameters have a marginal effect on the response and should be taken into account in a first approach. Whenever the p-values are above 0.15, the parameters should be neglected. From Table 4.4, it can be seen that the parameters show p-values smaller than 0.05 or higher than

0.15. This allowed reformulating the fitting model using only the parameters with p-values smaller than 0.05.

From Table 4.4, it can be concluded that loading is the most important variable affecting the maximum power density during an activation procedure (factor 2) followed by cathode air pressure (factor 3), what is evidenced by the Student *t*-test. The interactions parameters between different factors are also not significant; however the quadratic factors associated to the temperature and loading should be taken into account in the final polynomial fitting. The new fitting equation is as follows:

$$Y = B_0 - B_2 \times X_2 + B_3 \times X_3 - B_{11} \times X_1^2 - B_{22} \times X_2^2 \qquad (4.4)$$

and the corresponding parameters are given in Table 4.5:

Table 4.5 – Empirical coefficients of Eq. (4.4) and the corresponding p-values.

Parameters	**Estimate**	***t* ratio**	**Prob > |t|**
B_0	21.62	112.08	0.00
B_2	-1.73	-14.94	0.00
B_3	0.75	6.43	0.00
B_{11}	-0.62	-3.71	0.00
B_{22}	-1.46	-8.74	0.00

An analysis of variance (ANOVA) was performed to verify the significance of this second order model. The F ratio, model mean square divided by the error mean square, is considerable high (71.00) meaning that this model fits well the experimental data. The model coefficient of determination, R^2, is 0.97 meaning that most of variance can be described by the empirical model.

Using the empirical model, a maximum power density of 22.88 ± 0.47 $mW \cdot cm^2$ was computed for the following optimum operating conditions

The optimum operating conditions were:

- Temperature = 55.5 ºC
- Loading = 110.7 mV
- Cathode air pressure = 2.5 bar

Finally, Figure 4.2 shows the experimental and model responses for the 17 runs.

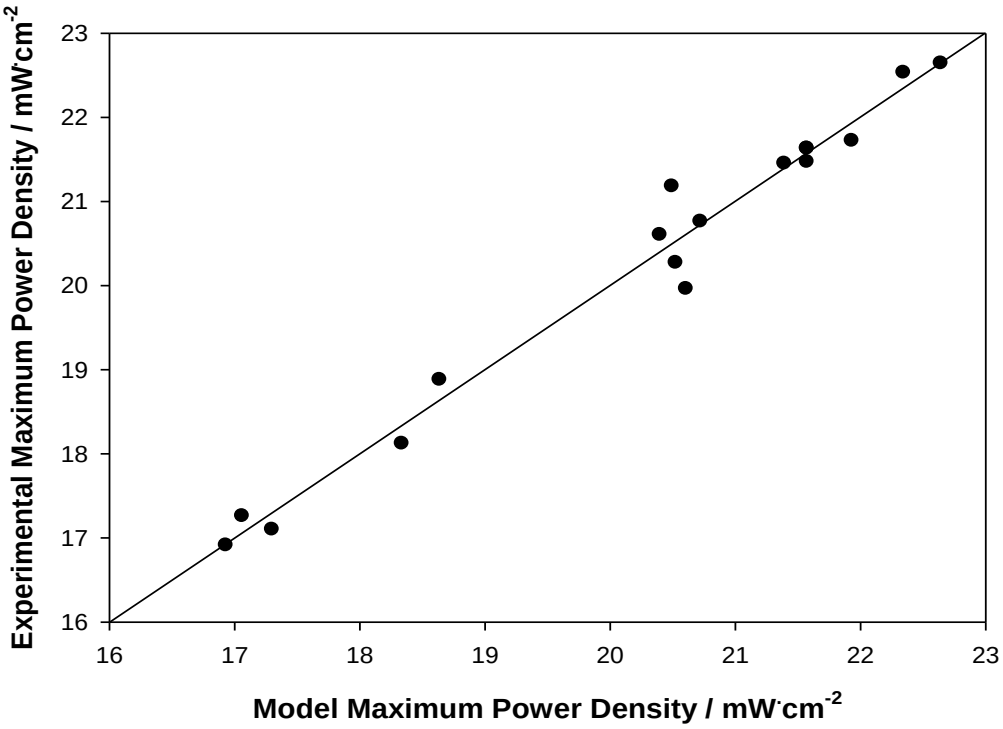

Figure 4.2 – Comparison of experimental and model maximum power density obtained from the central composite design.

It can be seen that both results are very similar, which is in agreement with the Anova analysis.

A new run was performed at the optimum operating conditions and a maximum average power density of 22.91 $mW \cdot cm^{-2}$ was obtained for 4 determinations. This value is in agreement with the value predicted by the model.

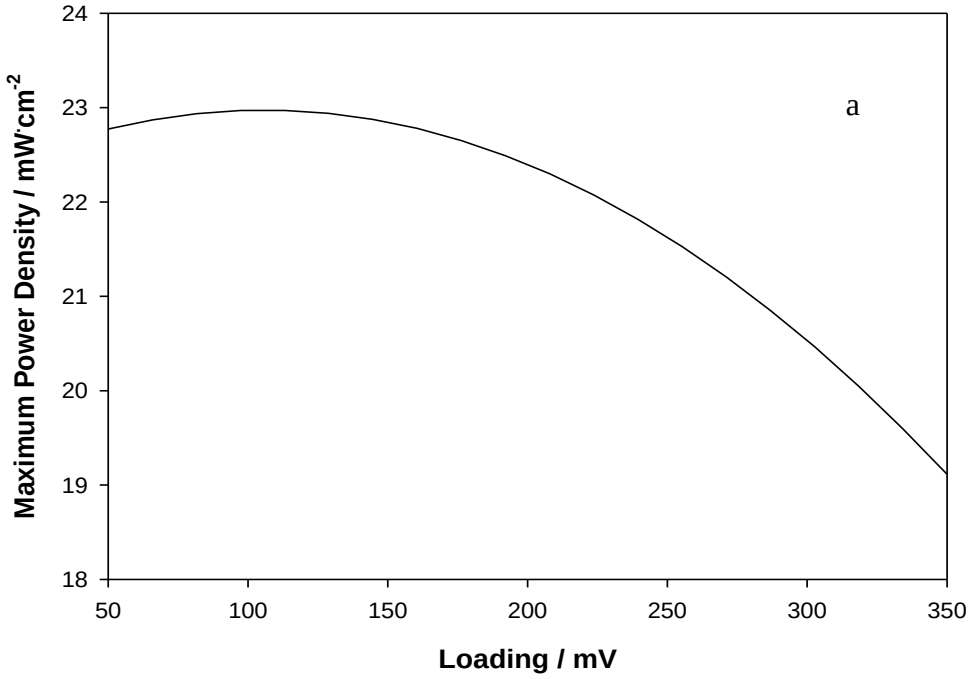
a
Maximum Power Density / mW'cm-2
Loading / mV
24
23
22
21
20
19
18
50
100
150
200
250
300
350

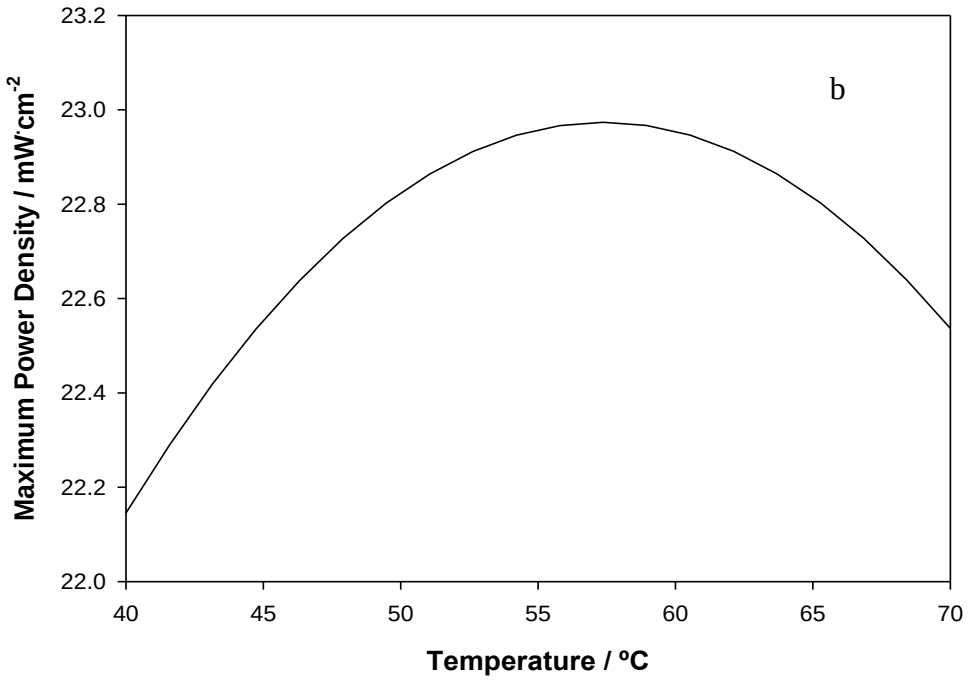
b
Maximum Power Density / mW'cm-2
Temperature / ºC
23.2
23.0
22.8
22.6
22.4
22.2
22.0
40
45
50
55
60
65
70

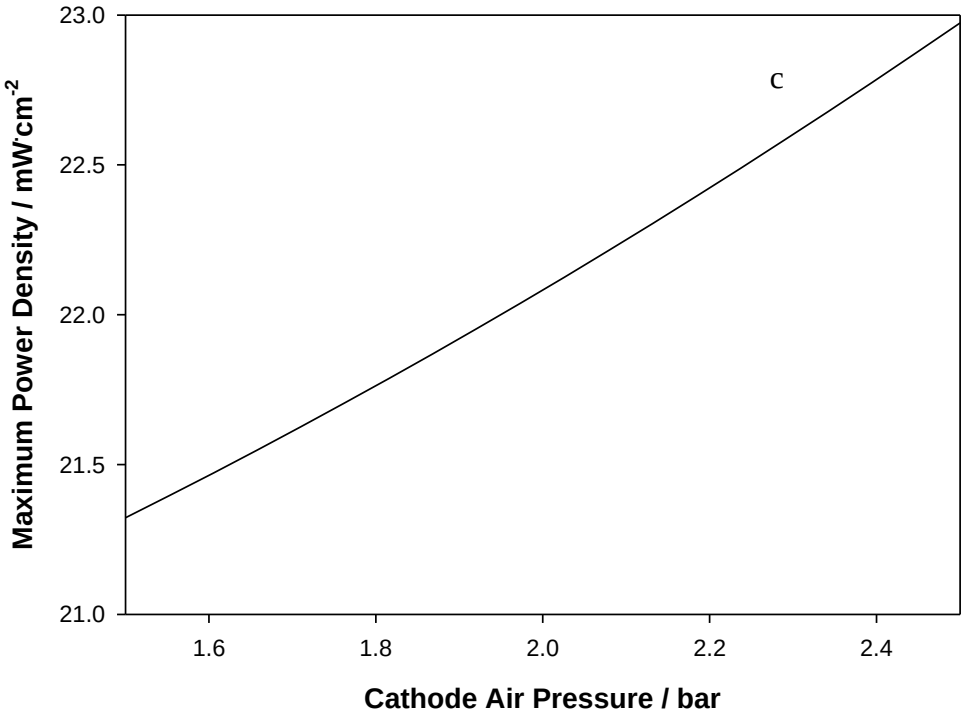

Figure 4.3 – Fitted maximum power density at the optimum operating conditions as a function of (a) loading (b) temperature and (c) pressure.

Figure 4.3 shows the predicted maximum power density response at the optimum operating conditions (temperature at 55.5 ºC, loading at 110.7 mV and cathode air pressure at 2.5 bar) as a function of the three factors. From Figure 4.3a, it can be seen that for the selected range, the loading influences significantly the power density response. On the other hand, it can be concluded that a MEA should be activated in a potential range not very different from 50 mV to 200 mV; in fact, the DMFC performance decreases considerably when the activation is made at high potentials. Furthermore, there are no considerable differences (< 1 $mW \cdot cm^{-2}$) on the final DMFC performance whenever the activation is performed at potentials between 50 mV and 200 mV. From Figure 4.3b, it can be observed that within the selected temperature range, the temperature leads to small variations on the power density, despite its crucial role on the activation procedure. It should be emphasised that above a certain activation temperature (55.5 ºC) the DMFC

performance starts to decreases. Elevated temperatures cause a detrimental effect in the DMFC activation procedure, because the triple phase boundary and the available electrochemical catalyst area decrease considerably [10]. Table 4.6 shows the normalized relative electrochemical catalyst area (rECA), the double layer capacitance, the charge resistance transfer and the swelling values for MEAs activated at the optimized conditions (temperature at 55.5 ºC, loading at 110.7 mV and cathode air pressure at 2.5 bar) and at 90 ºC (the other operating conditions were similar to the runs performed at 55.5 ºC).

Table 4.6 – Relative electrochemical catalyst area, double layer capacitance, charge transfer resistance and swelling values for MEAs activated at the optimized conditions and at 90 ºC.

Temperature / ºC	rECA	Swelling / wt.%	R_{ct} / mΩ	C_{dl} / mF
55.5	1	21.9	15.1	9.1
90.0	0.73	33.6	23.2	6.8

* PEMs pre-treated in boiled water

From Table 4.6 it can be seen that at the optimized conditions, the rECA and the double layer capacitance increase while the charge transfer resistance and the PEM swelling decrease. This behaviour can be explained by an excessive swelling (at 90 ºC) of the proton exchange membrane that is in contact with the catalyst particles [9, 10].

Figure 4.3c shows that increasing the cathode air pressure increases the DMFC performance. In this study, the maximum operating pressure employed was 2.5 bar; this value was selected to avoid possible leakages in the DMFC. From these experiments, it can be inferred that a MEA should be activated at high pressures. These results are in agreement with the conclusions obtained by Qi and Kaufman [21] concerning hydrogen fed PEMFC. These authors claim that increasing the feed pressure the access of the reactants to the catalyst sites also increases, allowing a faster and better activation.

4.3.2. Selection of the Best Pre-treatment

A complete activation procedure considers the pre-treatment of the MEA components, the proton exchange membrane and the diffusion and catalyst layers. The use of different pre-treatments can lead to a large scatter in the results [5, 6]. Indeed, even the same pre-treatments can lead to different results when evaluated by different characterization methods. So, it is almost impossible to state which is the best pre-treatment procedure. To minimize the variance of the results, the same characterization techniques were used to obtain the proton conductivity, swelling and methanol crossover. Similarly to the *in situ* activation procedure, all DMFC performance evaluations were performed at 55.5 ºC.

4.3.2.1. Proton Conductivity

Figure 4.4 shows the PEM proton conductivity evaluated at 55.5 ºC as a function of the pre-treatment procedure, as described in Table 4.1. From Figure 4.4 it can be seen that the PEM proton conductivity is sensitive to the pre-treatment employed. Indeed, significant differences were found concerning the proton conductivity: 51.8 $mS \cdot cm^{-1}$ with no pre-treatment (case H) and 140.1 $mS \cdot cm^{-1}$ for the best pre-treatment procedure (G). It was also observed that when a PEM is pre-treated with methanol solutions (in the range 1-2 M) the proton conductivity increases very slightly (E and F). Nafion has a very hydrophobic and highly crystalline polymer matrix with ionic clusters attached to flexible side chains. This structure favors the formation of relatively large ionic clusters, separated from the matrix, where water and methanol can sorb easily, improving the water-assisted proton transport. This leads to the formation of broader water channels enhancing the ability of the PEM to allow the transport of H^+ ions. When the PEM is immersed in sulfuric acid the proton conductivity values are similar to the ones obtained with the PEM pretreated in distilled water; low concentrated sulfuric acid solutions are used for

removing organic compounds from the membrane surface and for protonating the membrane. Concentrated sulfuric acid solutions dehydrate the membrane making it less proton conductive (case D). The proton conductivity of the PEM increases when boiled in water. In fact, this pre-treatment leads to the highest proton conductivity value. This essentially occurs due to a drastic structural reorganization in the PEM, increasing the water volume fraction [6].

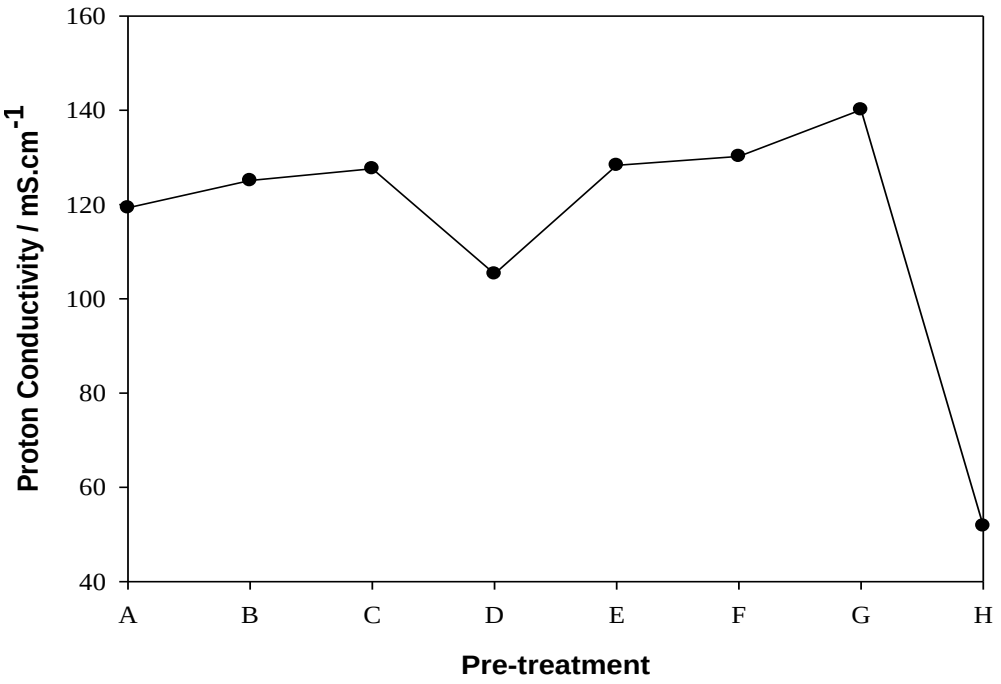

Figure 4.4 – PEM proton conductivity at 55.5 ºC as a function of the pre-treatment procedure.

4.3.2.2. Swelling

Figure 4.5 depicts the PEM swelling at 55.5 ºC as a function of the pre-treatment procedure.

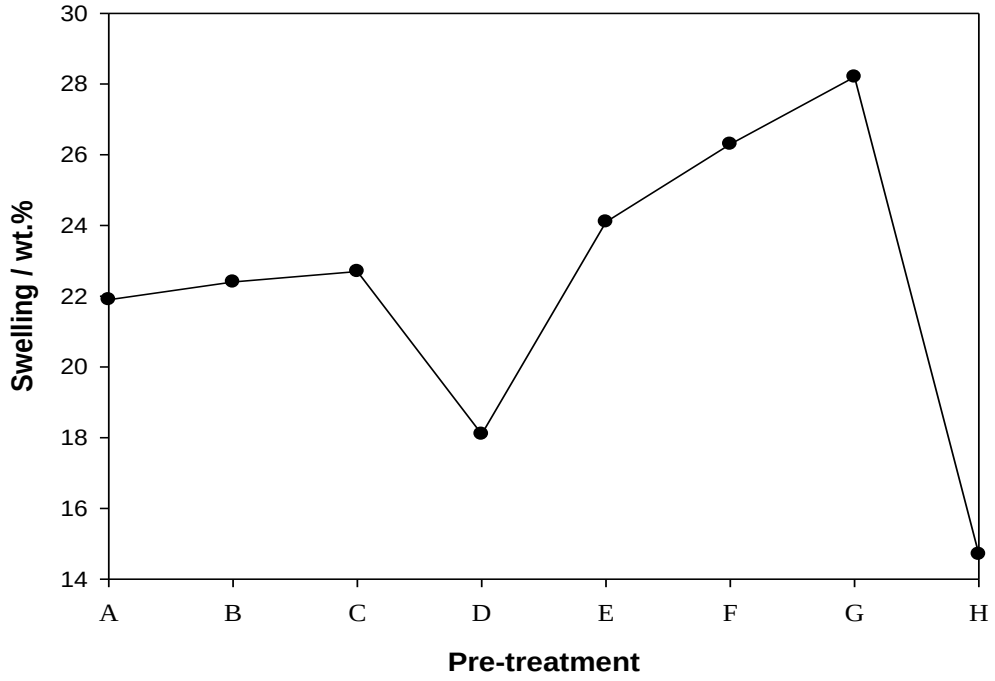

Figure 4.5 – PEM swelling at 55.5 ºC as a function of the pre-treatment procedure.

As expected, these results are in line with the corresponding proton conductivity ones (overall trends in Figs. 4.4 and 4.5 are similar).

4.3.2.3. Methanol Crossover

Figure 4.6 shows the parasitic current density at open circuit and 55.5 ºC as a function of the pre-treatment procedure (before the activation procedure).

From Figure 4.6 it can be seen that in all cases the pre-treatment leads to an increase of the methanol permeability as result of the broadening of the ionic channels of the membrane. On the other hand, increased PEM permeabilities towards methanol were obtained for the proton exchange membranes with higher proton conductivities and

swelling. To select the most advantageous pre-treatment procedure, it is important to find the best compromise between high proton conductivity and low methanol crossover. To find the most efficient pre-treatment procedure, all pre-treated MEAs were then submitted to the previously optimized *in situ* activation procedure. Thus, it can be expected that the differences in the final power density of the MEAs are related to the applied pre-treatment procedure.

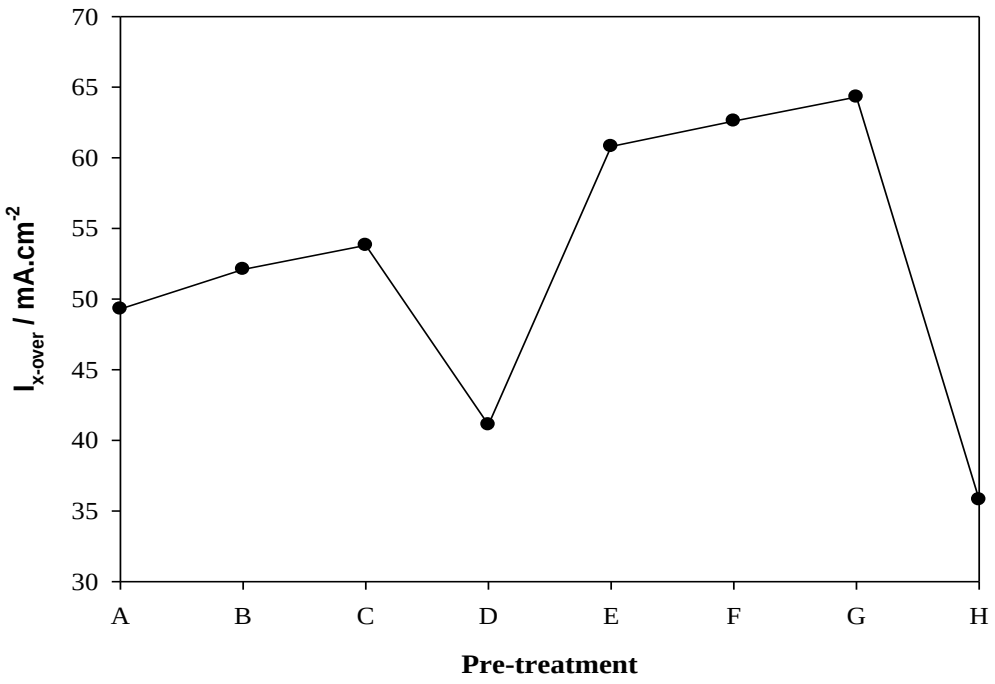

Figure 4.6 - Parasitic current density at open circuit due to methanol crossover at 55.5 ºC, as a function of the pre-treatment procedure.

4.3.2.4. DMFC Tests

Figure 4.7 shows the DMFC (a) potential and (b) power density as a function of the current density for the different pre-treatments procedures.

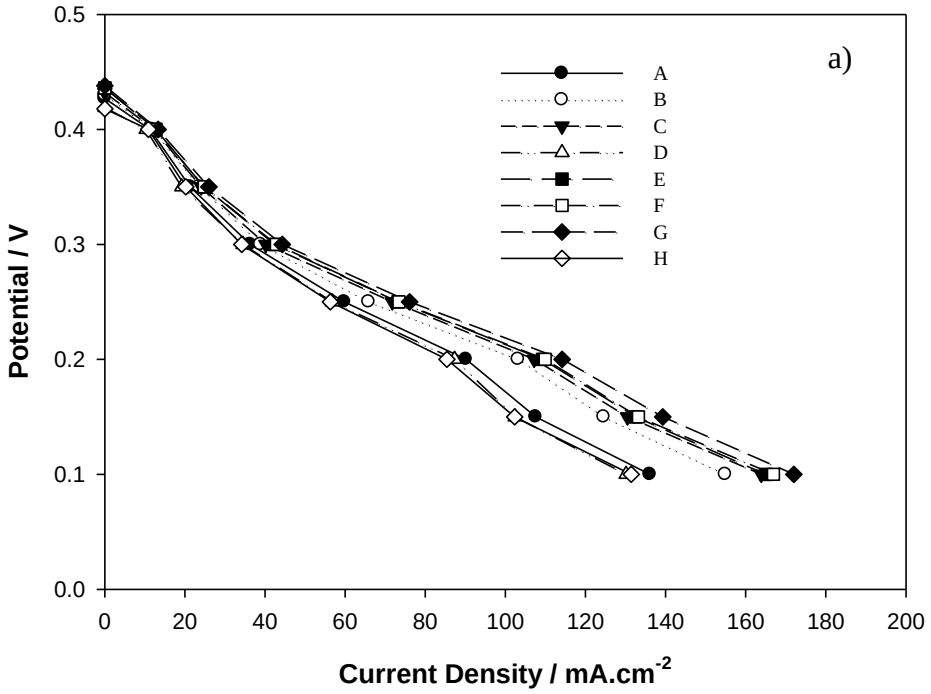

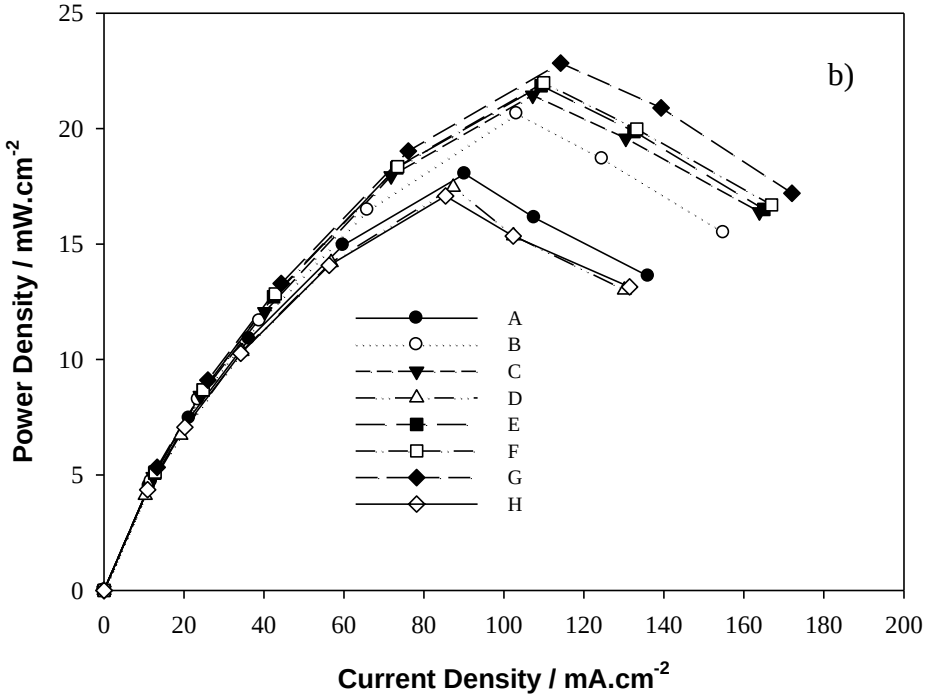

Figure 4.7 – Potential (a) and power density (b) obtained at the DMFC as a function of the current density for the different pre-treatment procedures (end of the activation procedure).

It can be seen that the untreated PEM (sample H) exhibits the worse performance. This indicates that the *in situ* loading procedure is not able to supply the adequate hydration when the PEM is not pre-treated. On the other hand, it can be concluded that when a PEM is pre-treated in concentrated sulfuric acid solutions (sample D), the final DMFC performance is also very poor. When the PEM is pre-treated simply immersing it in water at 55 ºC (sample A), the final DMFC performance is only slightly better. It is also observed that the rest of the tested pre-treatments lead to similar performances, although the best procedure seems to be boiling the PEM in water (G). On the other hand, Figure 4.7 shows that the final DMFC performance is more dependent upon pre-treatments that guarantee high conductivities rather than a low methanol crossover. Indeed, the pre-treatments E, F and G also lead to the best overall energy efficiencies, with a maximum around 11 %.

4.3.3. Comparison of Different Activation Methods

The ultimate objective of this work is to develop an effective activation procedure for MEAs not dependent on hydrogen. A few similar MEAs were then pre-treated following the same protocol (PEM and catalyst boiled in water during one hour) and then submitted to the previous activation procedure (*in situ* loading cycles) and two other *in situ* activation procedures reported in the literature: hydrogen anode conditioning [11], and hot-methanol conditioning [12]; the procedures were assessed based on the performance obtained by DMFC.

Figure 4.8 depicts the power density as a function of the current density at the end of an activation procedure for the three *in situ* procedures.

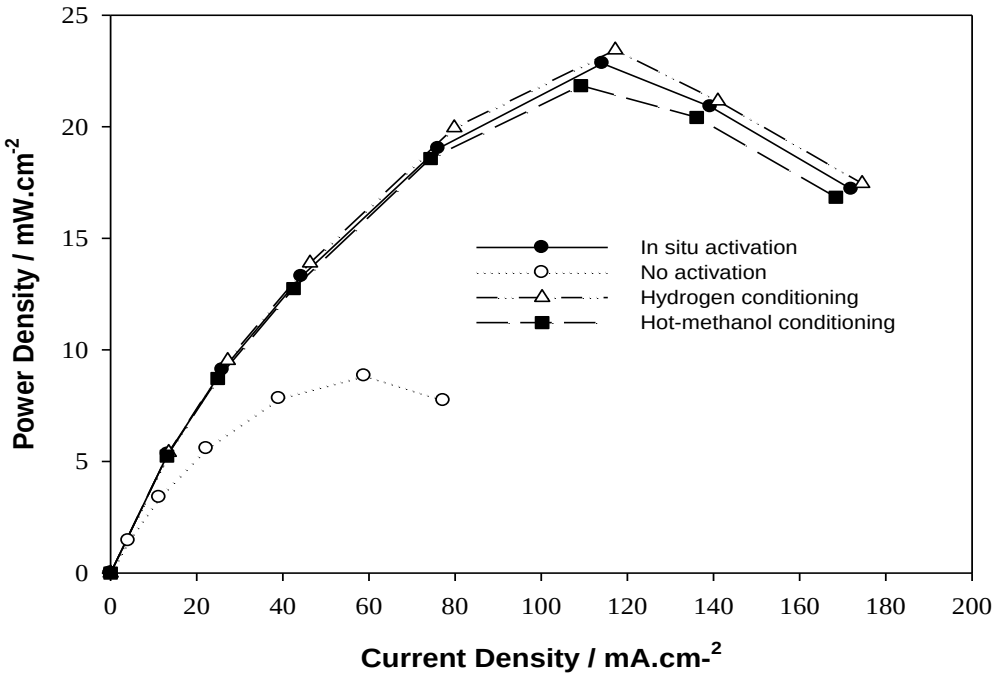

Figure 4.8 – Power density as a function of the current density at the end of the activation procedure.

From Figure 4.8 it can be observed that the hydrogen anode conditioning shows the best DMFC performance. The *in situ* loading cycles activation led to a slightly smaller DMFC performance when compared to the hydrogen conditioning activation. Despite that, the *in situ* loading cycles procedure is very attractive because it does not use hydrogen in a direct methanol system. The hot methanol activation procedure showed the lowest DMFC performance of the three *in situ* procedures. On the other hand, it was verified that when the MEA was not *in situ* activated, its performance was extremely poor.

The impedance spectra at 0.300 V vs DHE were also recorded at the end of the activation procedure. This allowed evaluating several impedance parameters that helped to understand the changes that both the anode catalyst and the PEM experienced. The

electric analogue shown in Figure 4.9 was found to be suitable to fit the data along the activation procedure [8].

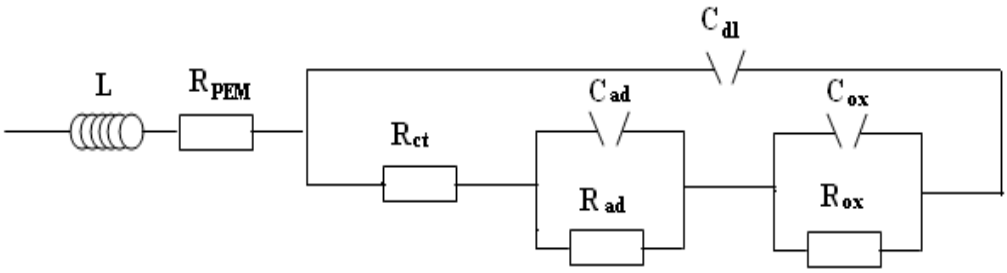

Figure 4.9 – Equivalent circuit of the fuel cell.

The inductance L takes into account the magnetic disturbance caused by spurious sources on the connection of the wires and on the metal plates. The resistance R_{PEM} can be assigned to the proton transport resistance across the PEM, R_{ct} is the resistance due to the charge transfer process, C_{dl} is the double layer capacitance, the $C_{ad}\,R_{ad}$ analogue can be assigned to the methanol oxidation reaction including the adsorption and dehydrogenation process and the $C_{ox}\,R_{ox}$ analogue can be associated to the surface bound residue oxidation process. In Table 4.7 are given the model parameters extracted fitting the model to the experimental Nyquist plots. From Table 4.7 it can be seen that the anode hydrogen conditioning presents the smallest methanol oxidation resistance suggesting that the reduction of surface oxides play an important role on the DMFC performance. Decreased charge transfer resistances and increased double layer capacitances are also observed in comparison with the other activation procedures. This indicates that this procedure promotes advantageous changes in the diffusion and catalyst layers. It can also be observed that higher rECA values are obtained for the hydrogen conditioning (the rECA values are normalized by the value obtained for the hydrogen conditioning) indicating a larger catalyst usage after this activation procedure.

Table 4.7 – Impedance parameters extracted fitting the model to the experimental Nyquist plots at 0.3 V versus DHE for the different activation procedures.

Activation Procedures	R_{Pem} / mΩ	R_{ct} / mΩ	C_{dl} / mF	R_{ad} / mΩ	rECA
***In situ* activation**	14.6	15.6	8.8	80.3	0.94
No activation	22.1	24.3	5.8	147.3	0.65
Hydrogen conditioning	14.5	13.4	10.2	74.1	1
Hot-methanol conditioning	14.7	15.4	8.7	81.3	0.93

4.4. Conclusions

The ultimate energy performance of a DMFC also depends on the activation protocol followed. This work concerns the study of different activation protocols, the optimization of a selected protocol and the corresponding study for understanding the reasons behind the improved power performance.

An activation procedure includes the PEM and catalyst pre-treatment but also a set of procedures to improve the performance of a MEA when the fuel cell is working (*in situ* activation). The *in situ* activation is mainly conditioned by the fuel cell operating conditions. To minimize the number of runs needed to obtain the optimal conditions, it was followed a Design of Experiments approach (surface responding method). The relevant factors, selected after a pre-screening study, were the temperature, the loading and the cathode air pressure. It was verified that the experimental data is well predicted by the second order response model and that the loading was the most significant factor on the final DMFC performance (evaluated in terms of maximum power density).

The pre-treated MEAs were compared evaluating the proton conductivity, the swelling and the methanol crossover. It was observed that the pre-treated MEAs with

higher proton conductivity also presented higher methanol crossover and swelling. So, all the pre-treated MEAs were submitted to the optimized *in situ* activation and it was observed that the best pre-treatment procedure was boiling the PEM in water (case G). The methanol pre-treatment is also able to produce good results. Indeed, when the PEMs were submitted to these pre-treatments, the overall energy efficiencies were also the higher ones, around 11 %.

The developed activation procedure was compared with two common protocols found in the literature; it was concluded that the hydrogen conditioning and the *in situ* loading activation procedure showed the best results.

The adopted DoE methodology contributed for obtaining the most favourable operating conditions based on a small set of experiments.

4.5. References

1. R. Dillon, S. Srinivasan, A. S. Aricò and V. Antonucci, *Journal of Power Sources*, 127, 112 (2004).
2. V. Neburchilov, J. Martin, H. Wang and J. Zhang, *Journal of Power Sources*, 169, 221 (2007).
3. P. Piela and P. Zelenay, *The Fuel Cells Review*, 1, 17 (2004).
4. C. S. Spiegel, *Designing & Building Fuel Cells*, Mc Graw Hill, New York (2007).
5. B. K. Kho, I. H. Oh, S. A. Hong and H. Y. Ha, *Electrochimica Acta*, 50, 781 (2004).

6. V. S. Silva, V. B. Silva, A. Mendes, L. M. Madeira, H. Silva, J. Michaelmann, B. Ruffmann and S. P. Nunes, *Separation Science Technology*, 42, 2909 (2007).

7. Z. Qi and A. Kaufman, *Journal of Power Sources*, 109, 227 (2002).

8. D. Chakraborty, I. Chorkendorff and T. Johannessen, *Journal of Power Sources*, 173, 110 (2007).

9. F. Liu and C. Y. Wang, *Electrochimica Acta*, 50, 1413 (2005).

10. J. H. Kim, H. I. Lee, S. A. Hong and H. Y. Ha, *Journal of Electrochemical Society*,152, A2345 (2005).

11. H. N. Dinh, X. Ren, F. H. Garzon, P. Zelenay and S. Gottesfeld, *Journal of Electroanalytical. Chemistry*, 491, 222 (2000).

12. A. K. Shukla, P. A. Christensen, A. J. Dickinson and A. Hamnett, *Journal of Power Sources*, 76, 54 (1998).

13. C. Rice, X. Ren, and S. Gottesfeld, Methods of Conditioning Direct Methanol Fuel Cells, United States Patent (2005).

14. D. C. Montgomery, *Design and Analysis of Experiments*, John Wiley & Sons, New York (2004).

15. J. Larminie and A. Dicks, *Fuel Cell Systems Explained*, John Wiley & Sons, Chichester (2003).

16. B. Sunden and M. Faghri, *Transport Phenomena in Fuel Cells*, WIT Press, United Kingdom (2005).

17. J. H. Kim, H. Y. Ha, I. H. Oh, S. A. Hong, H. N. Kim and H. I. Lee, *Electrochimica Acta*, 50, 801 (2004).

18. G. Alberti, M. Casciola, L. Massinelli and B. Bauer, *Journal of Membrane Science*, 185, 73 (2001).

19. E. Gülzow, S. Weißhaar, R. Reissner and W. Schröder, *Journal of Power Sources*, 118, 405 (2003).

20. M. Khayet, C. Cojocaru and C.Garcia-Payo, *Industrial & Engineering Chemical Research*, 46, 5676 (2007).

21. Z. Qi and A. Kaufman, *Journal of Power Sources*, 114, 21 (2003).

5. An Activation Procedure Applied to Fluorinated and Non-Fluorinated Proton Exchange Membranes*

Abstract

The effect of an activation procedure was studied considering membranes of different natures. They were selected proton exchange membranes (PEMs) of sulfonated poly(ether ether ketone) (sPEEK) (sulfonation degree, SD, of 42 %), plain and loaded with zirconium oxide (2.5 wt.% and 5.0 wt.%) and membranes of Nafion 112, 1135 and 117. The activation procedure considered two stages, a pre-treatment stage where the membrane electrode assembly (MEA) was boiled in water, and an *in situ* activation procedure stage where the MEA was submitted to a set of loading cycles with the MEA inserted in the fuel cell. The effect of the pre-treatment was evaluated performing proton conductivity measurements. On the other hand, the *in situ* activation procedure effect was followed by electrochemical impedance spectroscopy (EIS), cyclic voltammetry (CV), polarization curves, methanol crossover and electro-osmotic drag measurements. It was found that both pre-treatment and *in situ* activation were effective to increase the power density of all the MEAs even using different PEMs. The plain sPEEK membrane showed to be more sensitive to the pre-treatment and loading cycles than the Nafion. The composite sPEEK membranes showed the worst final power density and needed longer activation periods to achieve reasonable performances. Despite the higher power densities obtained by MEAs using thicker membranes, they need longer activation periods. The optimal temperature to set up the *in situ* activation is dependant on the nature and thickness of the PEM. Furthermore, the activation of the thicker membranes (Nafion 1135 and Nafion 117) benefits from higher activation temperatures, around 70 ºC, while the

thinner membranes (Nafion 112 and plain sPEEK) show the best performance when activated at a temperature closer to 55 ºC and 40 ºC, respectively.

---

*V. B. Silva, A. Mendes, submitted.

5.1. Introduction

There are a number of challenging problems to be resolved before successful commercialization of Direct Methanol Fuel Cells (DMFCs); among them the low methanol oxidation kinetics and the excessive methanol crossover [1]. Beyond these challenges, the development of quick and effective procedures to ensure maximum performance of the membrane electrode assembly (MEA) during the start-up or after resting periods is also important. However, these procedures have received less attention from the research community and little information is available in the open literature [2, 3]. It is known that a MEA performs below the nominal power whenever started from fresh or after a resting period [4]. It is then necessary to apply a set of procedures to activate the MEA. The improvement of the DMFC performance can be attained in two stages: pre-treatment and *in situ* activation procedures. The pre-treatment includes all actions carried on the proton exchange membrane (PEM) and electrodes that are made over a fresh MEA, while the *in situ* activation procedure are actions used to improve the performance of a MEA when the fuel cell is on a working state. Along the activation procedure, the proton exchange membrane and the diffusion and catalyst layers experiment strong changes in their properties [2, 3]. Thus, it is expectable that the optimal activation procedure renders different from MEA to MEA depending on the membrane and catalyst characteristics.

The most used electrolytes are ion exchange membranes predominantly formed of high-molecular weight perfluorosulfonic acid polymers, such as Nafion [5]. Nafion® polymer electrolyte membranes are available at different thicknesses [6]. It was verified that Nafion 112, a membrane of only 50 μm thick, shows lower proton transport resistance because the protons overall pathway to cross from the anode to the cathode is smaller [7] being also easily hydrated. On the other hand, an ideal ohmic conductor

should show a proton transport resistance independent from the thickness. However, it was found that when the proton resistance is normalized by the thickness, it increases for lower membrane thicknesses [8]. There are some reasons in the open literature explaining this trend [8, 9]. Paganin et al. [9] attributed this nonlinear response of the proton transport resistance as a function of the membrane thickness to an uneven water distribution across the proton membrane. However, the effect of an uneven water distribution can only be justified at high current densities. On the other hand, Slade et al. [8] identified the PEM production process(inhomogeneities) as the main reason for the unexpected specific conductivity decrease for thinner membranes. It is then expectable that different PEM thicknesses could also lead to different behaviours during the activation procedure.

Perfluorinated PEMs are however characterized by a high price and a significant methanol crossover [10]. Nevertheless, these problems can be minimized by developing new polymers [11 - 13] or modifying existing ones [14 - 16]. Presently, non-perfluorinated polymers show significant improvements in some of these criteria, and are therefore being thoroughly investigated [17 - 18]. The membrane made of these polymers can be used plain or modified either using organic or inorganic additives [19 - 22]. Organic or inorganic additives can be used advantageously to improve the mechanical stability and to reduce the methanol crossover. However, their use always leads to higher proton transport resistances that in general, result in lower power performances.

Non-fluorinated membranes based on sulfonated poly(ether ether ketone) (sPEEK) originated large expectations due to their high proton conductivity [18, 22]. It was found that when immersed in boiling water, plain sPEEK membranes increase more their proton conductivity than Nafion [18]. This can be explained by the different structure of sPEEK and Nafion polymers. Nafion® has a very hydrophobic and highly crystalline polymer

matrix with ionic clusters attached to flexible side chains favoring the formation of relatively large ionic clusters, separated from the matrix, where water and methanol can be easily sorbed. Simultaneously, this highly crystalline matrix avoids a significant dimensional change of the proton exchange membrane. On the other hand, sPEEK has sulfonic groups statistically distributed in a rigid aromatic backbone. The clusters are not well separated from the matrix, like in the case of Nafion, and water and methanol are then much better distributed over the membrane.

This paper studies the effect of an activation procedure on MEAs using PEMs of different natures and thicknesses. The PEMs considered are Nafion 112, 1135 and 117 (50 μm, 90 μm and 180 μm, respectively), sulfonated poly(ether ether ketone) (sPEEK) with a sulfonation degree of 42 % (55 μm) and composite sPEEK membranes (SD=42 %) doped with two different zirconium oxide loads, 2.5 wt. % (180 μm) and 5.0 wt. % (230 μm).

The effect of the pre-treatment on the selected PEMs was followed performing proton conductivity experiments. The *in situ* activation procedure was made by applying a set of loading cycles with the MEA inserted in the DMFC. Previous to each new loading cycle, the polarization curve was obtained. The impedance spectrum, cyclic voltammogram, methanol crossover and water electro-osmotic drag coefficient were evaluated before and after the *in situ* activation. These characterization techniques gave a comprehensive picture of how the activation protocol changes the MEA towards an improved and stable performance.

5.2. Experimental

5.2.1 Materials

The sPEEK membranes used along this study were previously produced by our research team in cooperation with the GKSS laboratory (Geesthacht, Germany). Poly(ether ether ketone) (PEEK) was supplied as pellets by Victrex and then sulfonated as described in the literature [23]. The final sulfonation degree obtained was 42 % (ion exchange capacity, IEC, of 1.27 $meq \cdot g^{-1}$), which was determined by elemental analysis and by H-NMR. Considering the composite sPEEK/zirconium oxide membranes, it was used zirconium tetrapropylate (70 wt. % solution in iso-propanol) and acetyl acetone (ACAC) that were purchased from Gelest. Zirconium tetrapropylate, $Zr(OPr)_4$, was used as precursor of the inorganic zirconium oxide modification and acetyl acetone was used as chelating agent to avoid the precipitation of the inorganic compound. In this study, they were used composite sPEEK/zirconium oxide membranes with two different zirconium oxide loads: 2.5 wt. % and 5 wt. %. Nafion membranes were purchased from Quintech.

5.2.2. MEA Pre-treatment

The backing and catalyst layers were boiled during one hour for improving the catalyst performance [24]. The proton exchange membrane samples were immersed in water at room temperature for 3 days to ensure total leaching. Then, the samples were immersed in boiling water (pre-treatment) during one hour before the characterization tests [18].

5.2.3. MEA Activation Protocol

The pre-treated MEAs were activated *in situ* submitting the DMFC to a set of loading cycles at 55 ºC and 200 mV. Each loading cycle lasted 180 minutes and was

interrupted to obtain a polarization curve. Before to apply the first loading cycle, a MEA characterization was obtained performing a polarization curve, an impedance spectrum, a cyclic voltammogram, and a methanol crossover and an electro-osmotic drag experiment. This characterization was also repeated at the end of the activation protocol. Between each cycle, it was allowed the MEA to rest at the open circuit condition during 30 min.

The activation procedure was finished whenever the changes in the current density became smaller than 3 % between successive loading cycles for the same corresponding voltages (the analysis was done for the complete voltage range).

5.2.4. Characterization Methods

5.2.4.1. Methanol Crossover Measurements

The methanol that crosses throughout the proton exchange membrane is wasted and it can not be used to produce effective work. The amount of wasted methanol can be computed by determining the parasitic current density, $I_{crossover}$ which can be related to the methanol crossover current density at the open circuit (OC), $I_{OCV,crossover}$, and to the anode mass-transport limiting current density, $I_{\lim}$, as follows [25]:

$$I_{crossover} = I_{OCV,crossover} \times \left(1 - \frac{I}{I_{\lim}}\right) \qquad (5.1)$$

To determine the parasitic current density at the open circuit condition, the DMFC anode was fed with a methanol aqueous solution (backpressure of 2.5 bar, 12 $mL \cdot min^{-1}$ and 1.5 M) and the cathode was fed with dry hydrogen (200 $mL_N \cdot min^{-1}$ and 2.5 bar); the cell was maintained at 55 °C. Scans were performed at 3 $mA \cdot s^{-1}$ between 0 and 0.8 V *vs* the reference electrode, in galvanostatic mode. Finally, the limiting current density was obtained at 0 V averaging 30 min reads.

5.2.4.2. *In situ* Cyclic Voltammetry (CV)

In situ cyclic voltammetry was performed with the MEA inserted in the DMFC at 55 °C. A dry hydrogen stream (200 $ml_N \cdot min^{-1}$ and 2.5 bar) was fed to the cathode side while a humidified nitrogen stream (200 $mL_N \cdot min^{-1}$, 100 % RH and 2.5 bar) was fed to the anode. The anode and cathode worked as working electrode and reference/counter electrode, respectively. The working electrode was swept at 50 $mV \cdot s^{-1}$ between -0.4 V and 1.3 V versus the reference electrode.

Relative anode electrochemical active areas (ECA) were obtained by calculating the areas of the hydrogen oxidation peaks from the cyclic voltammograms [26] using the following equation:

$$rECA = \frac{Q}{\mu_{Pt} \times L} \qquad (5.2)$$

where $rECA$ is the relative anode electrochemical active area, Q is the charge density of the atomic hydrogen adsorbed, μ_{Pt} is the charge needed to reduce a monolayer of protons at the polycrystalline Pt surface of 1 cm^2 (μ_{Pt} = 210 $mC \cdot cm^{-2}$ Pt) and L is the Pt load (1 $mg \cdot cm^{-2}$). Despite the absolute ECAs could not be obtained due to the Ru interference, it is possible to compare the relative surface areas [26] along the activation procedure.

5.2.4.3. Electrochemical Impedance Spectroscopy

Impedance spectra were obtained feeding the DMFC anode side with similar conditions as those used during the activation process (backpressure of 2.5 bar, 12 $mL \cdot min^{-1}$ and 1.5 M). The cathode side was fed with a dry hydrogen stream (200 $mL_N \cdot min^{-1}$ and 2.5 bar) making it a dynamic hydrogen electrode (DHE) by applying a voltage difference of 300 mV. The temperature of the fuel cell was maintained at 55 ˚C. The electrochemical impedance measurements were performed using a Zahner IM6e workstation coupled with a potentiostat (PP-240, Zahner). Impedance spectra were also

recorded at ten points per decade by superimposing a 5 mV ac signal over the frequency range from 100 kHz to 10 mHz.

5.2.4.4. Evaluation of the Electro-osmotic Water Drag Coefficient

The water electro-osmotic drag coefficients were determined feeding an aqueous methanol solution to the anode chamber and a dry oxygen stream to the cathode and operating the fuel cell at high current densities [27]. At these conditions, the water flux across the PEM is driven only by protonic drag.

The cell was operated at 55 °C and constant current with a 1.5 M methanol aqueous solution feed to the anode at 12 $mL \cdot min^{-1}$ and dry oxygen fed to the cathode at 300 $mL_N \cdot min^{-1}$. The anode and cathode backpressures were kept equal at 2.5 bar. Water vapour emerging with the cathode effluent was condensed in a U-shaped tube immersed in glycolated water at ca. -10 °C.

5.2.4.5. Proton Conductivity

Proton conductivity measurements were performed at 55 ºC in a house made cell. The proton conductivity was obtained from the high frequency interception with the real axis in the Nyquist plot. For increasing the precision of the measurements, it was used a stack of four membranes and then calculated the proton conductivity for one membrane. The membrane-membrane interface resistance was determined as described by Alberti et al. [28]. Samples were previously immersed in water at room temperature during 3 days to ensure total leaching. Then the samples were boiled during an hour before the proton conductivity evaluation. The spectrometer used was a Zahner IM6e workstation working in the frequency range between 0.1 and 10^5 Hz. The average error obtained using this procedure was 5.3 % (t distribution for 95 % confidence interval).

5.2.4.6. DMFC Tests

The studied MEAs were prepared by hot pressing the membrane samples, between two ElectroChem electrodes at 90 ºC and 150 bar for 150 s. Supported Pt-Ru (1 $mg \cdot cm^{-2}$ and 1:1 molar ratio) and Pt (0.5 $mg \cdot cm^{-2}$) were used on the anode and cathode, respectively. Single cell measurements were performed in a fuel cell with 25 cm^2 of active area. The DMFC was operated with a methanol aqueous solution (backpressure of 2.5 bar, 12 $mL \cdot min^{-1}$ and 1.5 M) at the anode side and with air (backpressure of 2.5 bar and 1000 $mL_N \cdot min^{-1}$) at the cathode side. The DMFC set-up is described elsewhere [29]. The cell temperature was maintained at 40 ºC, 55 ºC, 70 °C and 90 °C.

5.3. Discussion and Results

5.3.1. Proton Conductivity

An activation protocol was settle down comprising a pre-treatment step, consisting of immersing in boiling water the PEMs and the diffusion and catalyst layers for 1 h, and a set of loading cycles performed at 55 ºC named of *in situ* activation. The effect of the pre-treatment was evaluated performing ex situ proton conductivity experiments. All membranes were previously immersed in water for 3 days, at room temperature, to ensure total leaching. In Table 5.1 are listed the proton conductivity values of each PEM considering two cases: a) with no further treatment (named not pre-treated) and b) samples boiled during 1 hour in water previously to the proton conductivity evaluation (named pre-treated). From Table 5.1 it can be concluded that all not pre-treated membranes show a proton conductivity that is far lower than after boiling. Indeed, all proton exchange membranes were sensitive to the pre-treatment. However, this effect was more perceptible for the sPEEK-based membranes, namely for the plain sPEEK membrane.

Table 5.1 – Proton conductivity of the proton exchange membranes at 55 ºC: a) not pre-treated and b) pre-treated.

Proton Exchange Membranes	**Proton Conductivity / mS·cm^{-1}**		**Increase factor**
	Not pre-treated	**Pre-treated**	
Nafion 112	118.1	140.1	1.19
Nafion 1135	120.2	146.2	1.22
Nafion 117	132.9	159.2	1.20
sPEEK SD 42 %	43.4	154.7	3.56
sPEEK ZrO_2 2.5 wt.%	33.5	88.9	2.65
sPEEK ZrO_2 5.0 wt.%	19.2	37.2	1.94

Nafion membranes were less sensitive to the applied pre-treatment showing a proton conductivity increase by a factor of approximately 1.2. This increase was nearly constant as a function of the thickness of the Nafion membranes. It is noticeable that at the end of the pre-treatment the plain sPEEK membrane showed higher proton conductivity than Nafion 112 and Nafion 1135. Simultaneously, it seems that the incorporation of zirconium oxide in the sPEEK matrix prevents excessive dimensional changes being this effect more evident at high inorganic concentrations.

The number of water molecules accompanying the transport of each proton, i.e., the electro-osmotic drag coefficient of the water, was also obtained. Table 5.2 shows the water drag coefficient for the not pre-treated and pre-treated membranes before and after the activation procedure (in-situ activation), evaluated as described in section 5.2.4.4. From Table 5.2 it can be seen that the water drag coefficient was always higher for the pre-treated membranes. These results confirm that the increase of the proton conductivity after the pre-treatment is related to improved proton mobility most probably caused by broader water channels and larger ionic clusters, as suggested by Kreuer et al. [30].

The water drag coefficient of the plain sPEEK membrane increases considerably after the pre-treatment, becoming higher than the values obtained for Nafion 112 and Nafion 1135, which is in agreement with the proton conductivity experiments. This increase should be related with the absence of a highly crystalline matrix in the sPEEK membrane [31] allowing it to experience considerable dimensional changes along the pre-treatment, particularly if not modified with too high zirconium oxide loads. From Table 5.2 it can be observed that the *in situ* activation makes also the water drag coefficient to increase. It can then be expected that similarly to the pre-treatment, the *in situ* activation also enhances the proton mobility through the PEM.

Table 5.2 – Water electro-osmotic drag coefficient for the not pre-treated and pre-treated proton exchange membranes before and after the activation procedure.

Proton Exchange Membranes	**Water Electro-osmotic Coefficient Drag /** $\frac{mol\,H_2O}{mol\,H^+}$			
	Before the Activation		**After *In situ* Activation**	
	Not Pre-treaded	**Pre-treated**	**Not Pre-treaded**	**Pre-treated**
Nafion 112	1.19	1.63	1.82	2.12
Nafion 1135	1.27	1.74	1.93	2.23
Nafion 117	1.39	1.91	2.07	2.39
sPEEK SD 42 %	0.59	1.82	2.03	2.27
sPEEK ZrO_2 2.5 wt.%	0.32	0.83	0.93	1.09
sPEEK ZrO_2 5.0 wt.%	0.21	0.42	0.48	0.60

Figure 5.1 shows the proton conductivity of the studied membranes, a) not pre-treated and b) pre-treated, obtained by *in situ* impedance spectroscopy (with the MEA inserted in the fuel cell) before and after the activation procedure. From Figure 5.1 it can be seen that the not pre-treated membranes experience a higher proton conductivity increase along the *in situ* activation when compared with the previously boiled membranes. This fact seems to indicate that when a membrane is pre-treated it keeps part of the hydrated water, exhibiting increased proton conductivity at the beginning of the *in situ* activation procedure. On the other hand, it was also observed that the pre-treated membranes achieve high proton conductivity faster than the not pre-treated membranes, as shown later on.

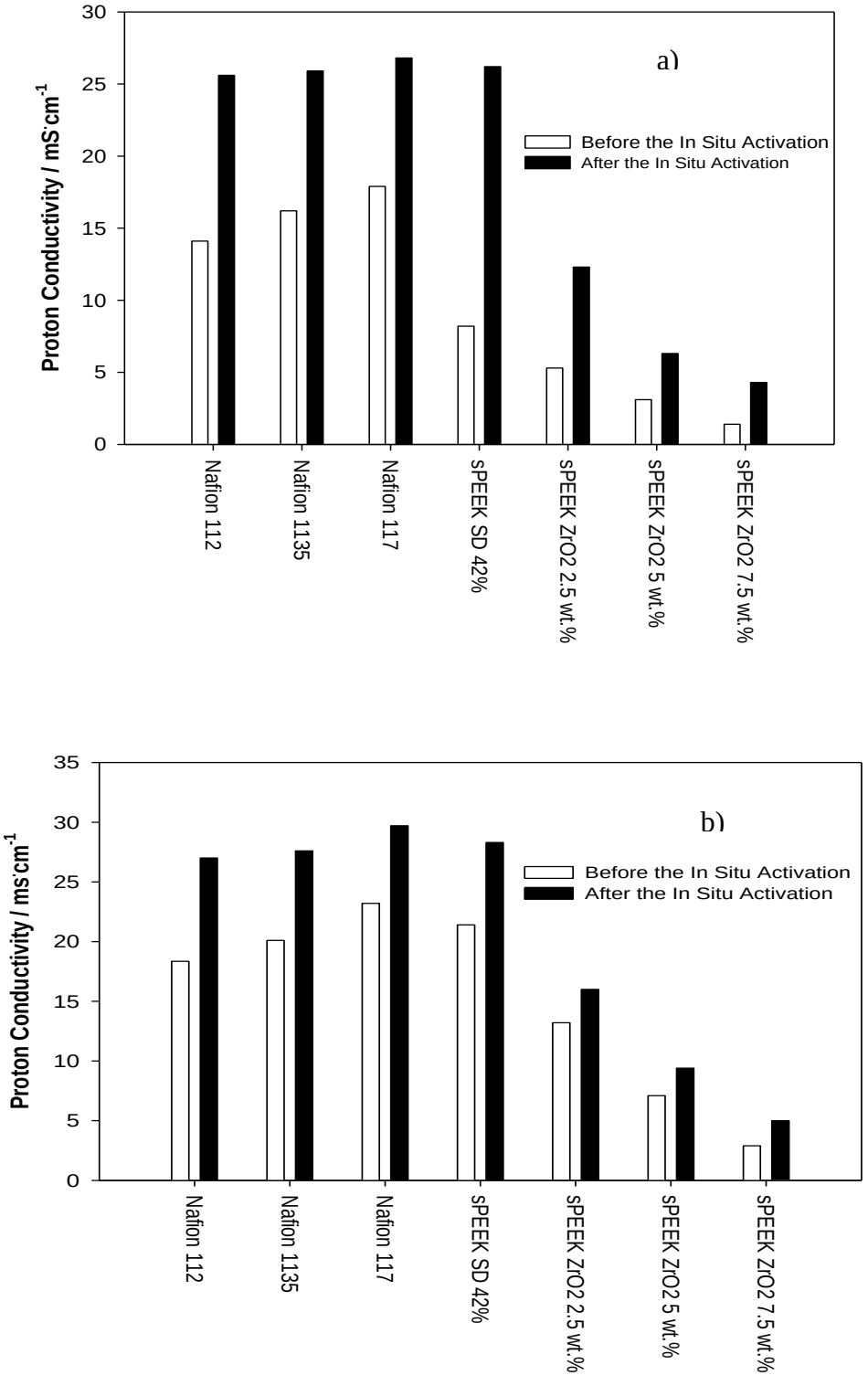

Figure 5.1 – Proton conductivity obtained by *in situ* EIS before and after the *in situ* activation procedure for the a) not pre-treated and b) pre-treated proton exchange membranes.

This figure also shows that the *in situ* activation is effective for all the studied membranes. However, as found for the ex situ proton conductivity characterization, the effect is less notorious for the Nafion membranes, particularly for the not pre-treated samples (Fig. 5.1a). Indeed, the large proton conductivity increase was obtained for the not pre-treated plain sPEEK. From the literature, it can be found that the proton conductivity of sPEEK based membranes depends on the sulfonation degree, thermal history, presence of residual solvent from the casting stage [32] but also on the applied pre-treatment [18]. The last factor was confirmed by our proton conductivity experiments.

5.3.2. Methanol Crossover, CV and EIS Experiments

Table 5.3 shows the open circuit voltage and the corresponding parasitic current density due to the methanol crossover through the proton exchange membranes before and after the *in situ* activation procedure using a) not pre-treated and b) pre-treated membranes. From Table 5.3, it can be seen that the activation procedure makes the proton exchange membranes more permeable towards methanol. Once again, the effect is more pronounced for the sPEEK-based membranes, which justifies their smaller increase of the OCV. It can be concluded that depending on the materials of the PEM, the corresponding MEA shows a different proton conductivity and methanol crossover history along the *in situ* activation.

Table 5.3 - Open circuit voltage and parasitic current density due to the methanol crossover through the proton exchange membrane before and after the *in situ* activation procedure for the not pre-treated and pre-treated membranes.

Proton Exchange Membranes	Open Circuit Voltage / V				Parasitic Current Density/ mA·cm^{-2}			
	Before the Activation		After the Activation		Before the Activation		After the Activation	
	Not-treated	Pre-treated	Not-treated	Pre-treated	Not-treated	Pre-treated	Not-treated	Pre-treated
Nafion 112	0.394	0.385	0.427	0.436	54.7	63.9	108.9	128.3
Nafion 1135	0.430	0.426	0.472	0.487	47.8	56.6	97.6	115.6
Nafion 117	0.555	0.552	0.594	0.613	28.6	34.2	47.3	60.9
sPEEK SD 42 %	0.541	0.526	0.528	0.552	21.3	44.3	100.1	115.9
sPEEK ZrO_2 2.5 wt.%	0.545	0.530	0.534	0.550	9.2	16.9	40.4	52.8
sPEEK ZrO_2 5.0 wt.%	0.547	0.538	0.540	0.545	5.0	7.2	14.3	19.2

Table 5.4 shows the relative electrochemical catalyst area from the studied MEAs before and after the *in situ* activation procedure, for the not pre-treated and pre-treated proton exchange membranes. It can be observed that the starting electrochemical catalyst areas from each MEA are different. Indeed, lower electrochemical catalyst areas were observed for the MEAs whose PEMs also show lower proton conductivities. Simultaneously, all the MEAs showed increased rECAs at the end of both the pre-treatment and activation procedure.

Table 5.4 – Relative electrochemical catalyst areas for the MEAs using not pre-treated and pre-treated proton exchange membranes at the beginning and at the end of the activation procedure.

Proton Exchange Membranes	**Electrochemical Catalyst Area / m^2 Pt ·g Pt^{-1}**			
	Before the Activation		**After the Activation**	
	Not pre-treated	**Pre-treated**	**Not pre-treated**	**Pre-treated**
Nafion 112	0.47	0.62	0.82	0.87
Nafion 1135	0.50	0.65	0.84	0.91
Nafion 117	0.51	0.75	0.89	1.00
sPEEK SD 42 %	0.27	0.71	0.86	0.94
sPEEK ZrO_2 2.5 wt.%	0.16	0.26	0.52	0.62
sPEEK ZrO_2 5.0 wt.%	0.09	0.15	0.23	0.29

*The values are normalized by that of pre-treated Nafion 117 after the activation protocol.

The impedance spectrum was obtained before and after the activation procedure for obtaining a more comprehensive picture of the occurring phenomena. The impedance data was fitted to an expanded Randle's analogous circuit as described elsewhere [33]. Table 5.5 shows the double layer capacitances from the MEAs comprising the not pre-treated and pre-treated PEMs before and after the activation procedure. From Tables 5.4 and 5.5, it is observed that higher ECAs are associated with higher double layer capacitances. The double layer capacitance is an indicator of the extension of interconnection of the PEM, the catalyst and the reactants [34]; its value is usually proportional to the catalyst active area [34].

Table 5.5 – Double layer capacitance of the studied MEAs before and after the activation procedure.

Proton Exchange Membranes	Double Layer Capacitance / mF			
	Before the Activation		After the Activation	
	Not pre-treated	Pre-treated	Not pre-treated	Pre-treated
Nafion 112	4.3	5.8	8.0	8.5
Nafion 1135	4.5	6.1	8.2	8.8
Nafion 117	4.6	7.1	8.4	9.3
sPEEK SD 42 %	2.9	6.8	8.3	9.0
sPEEK ZrO_2 2.5 wt.%	1.5	2.2	5.1	6.3
sPEEK ZrO_2 5.0 wt.%	0.8	1.2	2.1	2.6

The results obtained so far suggest that the PEM nature might play an important role on the MEA power density not only due to its proton conductivity and ability to prevent the methanol crossover but also because its influence on the protonic link between the catalyst and the membrane.

5.3.3. Polarization and Power Behaviour

Figure 5.2 plots the power density as a function of the current density for pre-treated membranes (a) before the activation procedure and (b) after the activation procedure. From Figure 5.2a, it can be seen that the power density of the pre-treated sPEEK membrane is higher than the obtained for the Nafion 112 and Nafion 1135 membranes. When the sPEEK membrane is not pre-treated, the corresponding power density is considerable smaller when compared with the same Nafion membranes (not shown). This indicates that the pre-treatment is more effective for the plain sPEEK membrane. In fact, the pre-treatment not only makes the power density to increase but also makes the *in situ* activation procedure to occur faster, as described below. Figure 5.2b shows that at the end of the applied activation procedure the performances of all membranes is better than before the activation and for most of them close to each other.

Finally, it can be concluded that the sPEEK membrane loaded with 2.5 wt. % of zirconium oxide shows the worst performance in both cases. For the sPEEK membrane loaded with 5.0 wt. % the obtained performance was even worst and then is not shown.

It was verified that each MEA needed a different number of loading cycles to meet the activation criteria defined before – changes in the current density smaller than 3 % between successive loading cycles for the complete voltage range. Table 5.6 shows the number of cycles needed to set-up the *in situ* activation for each MEA using not pre-treated and pre-treated PEMs. It can be seen that pre-treating the PEMs makes the *in situ* activation procedure faster, saving at least two activation-loading cycles. From all the PEMs considered during this study, the plain sPEEK membrane is the fastest to be activated; however, the inorganic modification readily makes the sPEEK membranes significantly slow activated. Concerning the Nafion membranes, it was observed that the thicker membranes need a longer time for activation.

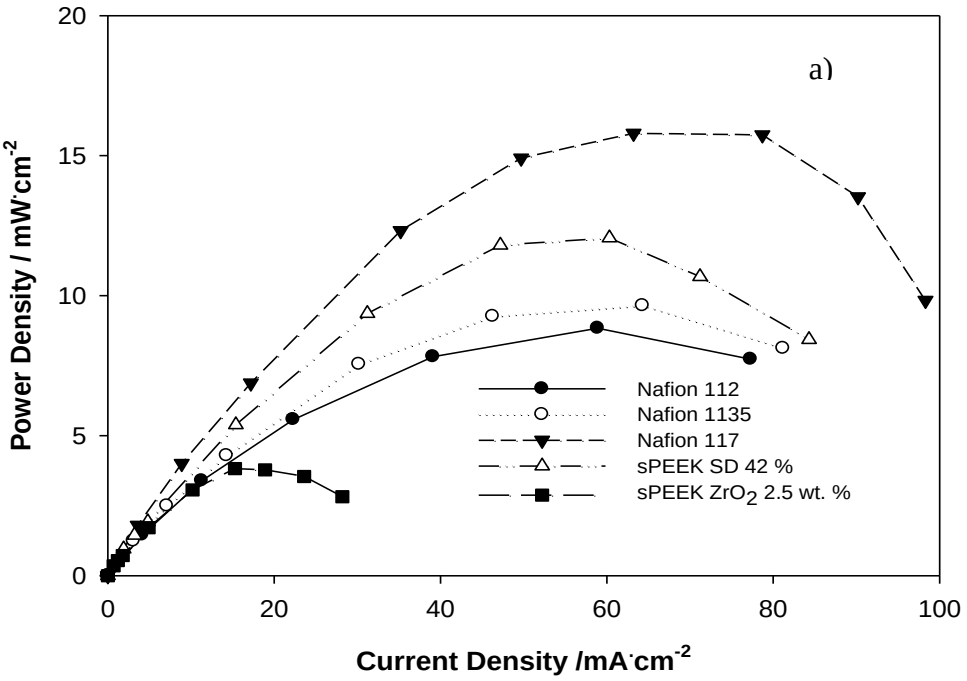

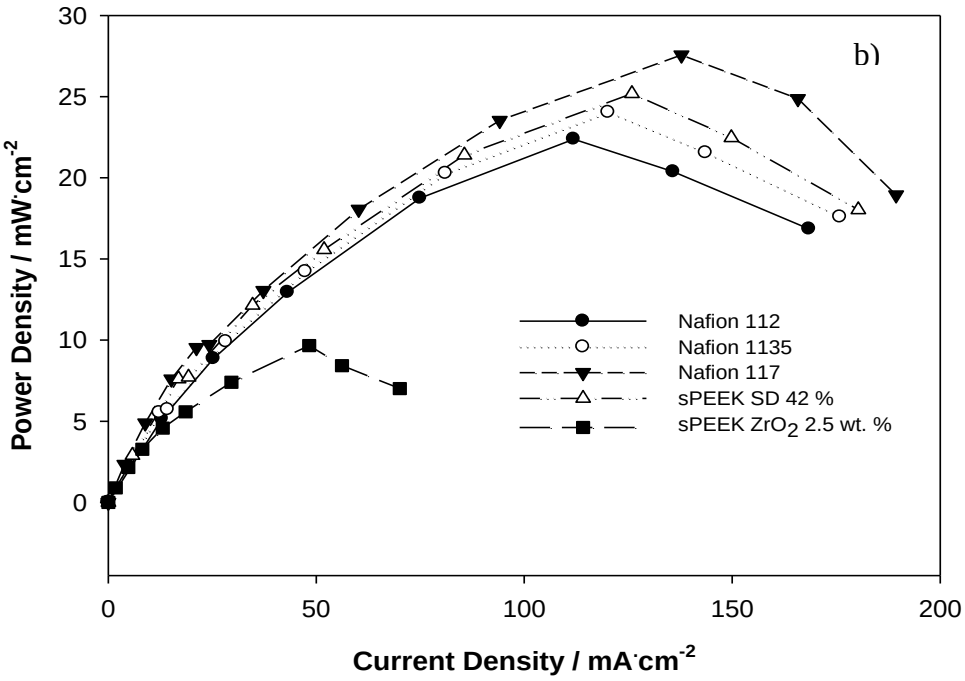

Figure 5.2 – Power density as a function of the current density (at 55 ºC) for the MEAs using pre-treated PEMs a) before the activation procedure and b) after the activation procedure.

Table 5.6 – Number of cycles needed to meet the MEAs activation criteria starting from not pre-treated and pre-treated PEMs.

Proton Exchange Membranes	**Number of Cycles**	
	Not pre-treated	**Pre-treated**
Nafion 112	8	6
Nafion 1135	9	7
Nafion 117	10	8
sPEEK SD 42 %	7	5
sPEEK ZrO_2 2.5 wt.%	11	8
sPEEK ZrO_2 5.0 wt.%	14	10

5.3.4. The Effect of the Temperature on the *In situ* Activation Procedure

Previous studies [2, 3] indicate that the temperature plays a crucial role on the *in situ* activation procedure, namely affecting the development of the triple phase boundary.

From the impedance experiments it was shown that using different proton exchange membranes results in different double layer capacitances after the activation procedure. This could mean that the optimum temperature to set-up the activation procedure depends on the proton exchange membrane in use. Figure 5.3 depicts the open circuit voltage at 55 ºC of each activated MEA as a function of the *in situ* activation temperature for the most promising PEMs. From this figure, one can realise that the OCV of the Nafion membranes increases with thickness being this difference more notorious for higher temperatures. This fact is probably related with the ability of the thicker membranes to prevent an excessive methanol crossover. On the other hand, and within the temperature range considered, the thicker membranes benefit from the activation procedure to occur at higher temperatures, while the thinner ones show an intermediate optimal activation temperature.

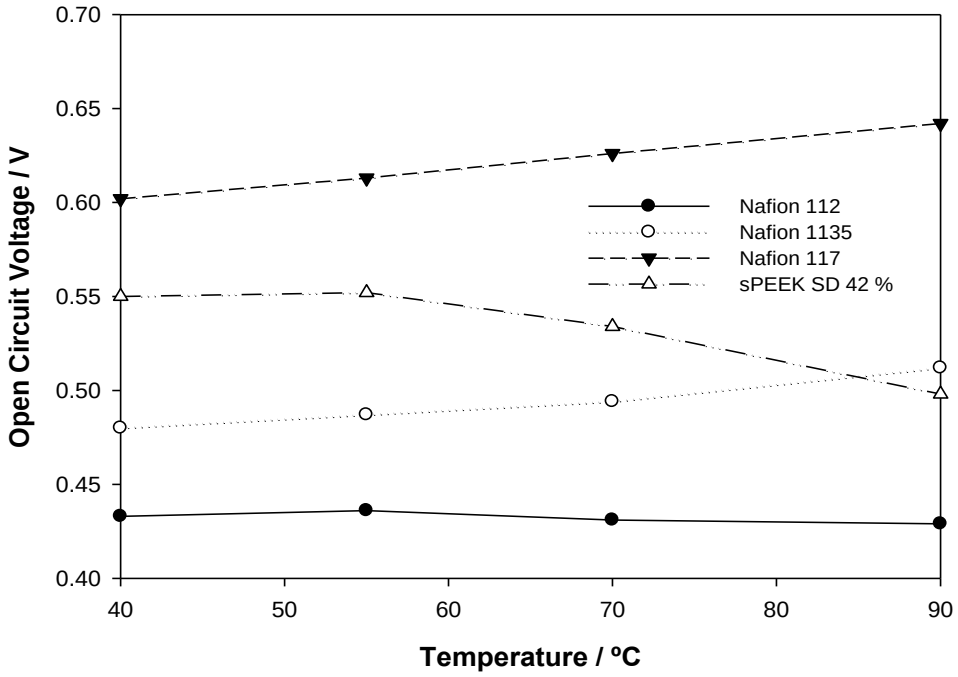

Figure 5.3 – Open circuit voltage evaluated at 55 ºC as a function of the MEA *in situ* activation temperature for pre-treated membranes.

In terms of the methanol crossover at open circuit condition, Figure 5.4 shows that the parasitic current density increases as a function of the activation temperature for all membranes. The sPEEK SD 42% and Nafion 112 membranes show the highest increase of methanol crossover after 55 °C. The reason for the optimum activation temperature up to 55 °C found for these membranes should be related with the methanol crossover that beyond this temperature increases more notoriously.

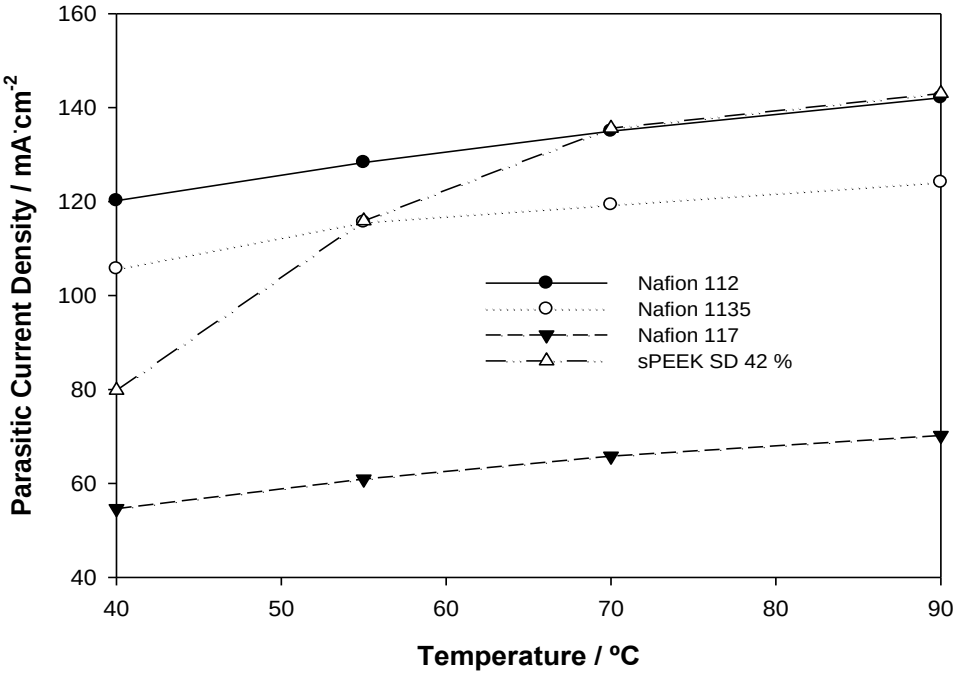

Figure 5.4 – Parasitic current density caused by the methanol crossover at open circuit condition and evaluated at 55 ºC as a function of the MEA *in situ* activation temperature.

Figure 5.5 plots the maximum power density at 55 ºC as a function of the *in situ* activation temperature. It can be observed that the maximum power density shifts to higher activation temperatures (70 ºC) when the thicker Nafion membranes (Nafion 1135 and Nafion 117) are considered while Nafion 112 and plain sPEEK show the best performance when activated at a temperature closer to 55 ºC and 40 ºC, respectively. At an activation temperature of 40 ºC, the performance of the plane sPEEK in terms of

maximum power output is pretty close to that reached by Nafion 117. Despite the higher power densities obtained by the MEAs using thicker membranes, they experience a slower activation procedure.

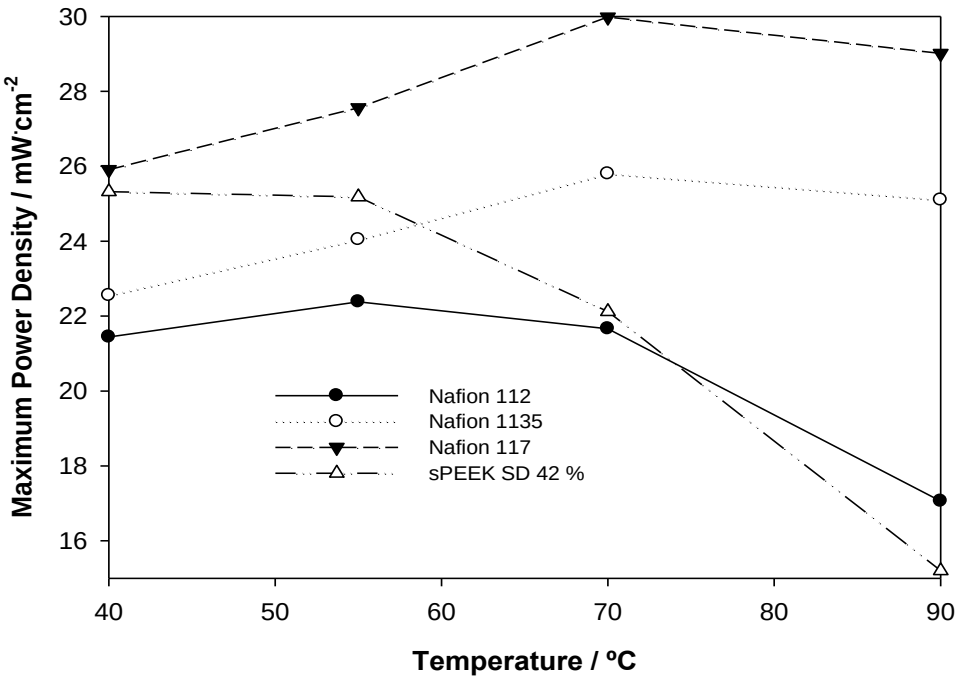

Figure 5.5 – Maximum power density obtained at 55 ºC with the MEAs activated at different *in situ* activation temperatures.

5.4. Conclusions

The present paper aims at to understand the effect of using different types of proton exchange membranes, sPEEK, sPEEK loaded with different zirconia contents (2.5 wt. % and 5.0 wt. %) and Nafion, during an activation procedure. Additionally, the effect of using membranes of Nafion with different thicknesses was also studied.

The activation procedure comprehends a pre-treatment of the PEMs (boiling in water) and an *in situ* activation of the MEAs (loading cycles). It was observed that all the MEAs were sensitive both to the pre-treatment and to the *in situ* activation. It was also concluded that the pre-treatment of the proton exchange membranes makes the activation

procedure faster. The pre-treatment effect on the proton conductivity and methanol crossover was more notorious for the plain sPEEK membrane. Concerning the Nafion membranes, they exhibited similar behaviors irrespectively to the thickness.

Proton exchange membranes (Nafion and sPEEK) play a critical role on the activation procedure not only because its proton conductivity but also because its ability to promote a better interconnection with the catalyst particles leading to the enlarging of the triple phase area.

The period of time for activation depends on the type and thickness of the membrane. It was observed that both sPEEK SD 42% and Nafion 112 membranes (thinner Nafion membrane) were activated in the shortest period of time. The composite sPEEK membranes showed the worst final power density and needed longer activation periods to achieve reasonable performances.

The optimum temperature to set-up the activation procedure was also dependent on the proton exchange membrane in use. It was concluded that the activation of the thicker membranes (Nafion 1135 and Nafion 117) benefits from higher activation temperatures.

5.5. References

1. R. Dillon, S. Srinivasan, A. S. Aricò and V. Antonucci, *Journal of Power Sources*, 127, 112 (2004).

2. J. H. Kim, H. I. Lee, S. A. Hong and H. Y. Ha, *Journal of Electrochemical Society*, 152, A2345 (2005).

3. F. Liu and C. Y. Wang, *Electrochimica Acta*, 50, 1413 (2005).

4. B. K. Kho, I. H. Oh, S. A. Hong and H. Y. Hong, *Electrochimica Acta*, 50, 781 (2004).

5. J. Larminie and A. Dicks, *Fuel Cell Systems Explained*, John Wiley & Sons, Chichester (2003).

6. M. N. Tsampas, A. Pikos, S. Brosda, A. Katsaounis and C. G. Vayenas, *Electrochimica Acta*, 51, 2743 (2006).

7. P. Dimitrova, K. A. Friedrich, B. Vogt and U. Stimming, *Journal of Electroanalytical Chemistry*, 532, 75 (2002).

8. S. Slade, S. A. Campbell, T. R. Ralph and F. C. Walsh, *Journal of Electrochemical Society*, 149, A1556 (2002).

9. V. A. Paganin, E. A. Ticianelli and E. R. Gonzalez, *Proton Conducting Membrane Fuel Cells*, The Electrochemical Society Proceedings Series, Pennington (1995).

10. V. Neburchilov, J. Martin, H. Wang and J. Zhang, *Journal of Power Sources*, 169, 221 (2007).

11. J. Wang, N. Li, Z. Cui, S. Zhang and W. Xing, *Journal of Membrane Science*, 341, 155 (2009).

12. H. Lin, C. Zhao, Z. Cui, W. Ma, T. Fu, H. Na and Wei Xing, *Journal of Power Sources*, 193, 507 (2009).

13. S. D. Bhat, A. K. Sahu, C. George, S. Pitchumani, P. Sridhar, N. Chandrakumar, K. K. Singh, N. Krishna and A. K. Shukla, *Journal of Membrane Science*, 340, 73 (2009).

14. Y. F. Lin, C. Y. Yen, C. H. Hung, Y. H. Hsiao and C. M. Ma, *Journal of Power Sources*, 168, 162 (2007).

15. X. Teng, Y. Zhao, J. Xi, Z. Wu, X. Qiu and L. Chen, *Journal of Membrane Science*, 341, 149 (2009).

16. M. H. Yildirim, A. R. Curòs, J. Motuzas, A. Julbe, D. F. Stamatialis and M. Wessling, *Journal of Membrane Science*, 338, 75 (2009).

17. P. Xing, G. P. Robertson, M. D. Guiver and S. D. Mikhailenko, *Journal of Membrane Science*, 229, 95 (2004).

18. V.S. Silva, V.B. Silva, A. Mendes, L.M. Madeira, H. Silva, J. Michaelmann, B. Ruffmann and S.P. Nunes, *Separation Science Technology*, 42, 2909 (2007).

19. Z. Gaowen and Z. Zhentao, *Journal of Membrane Science*, 261, 107 (2005).

20. A. F. Ismail, N. H. Othman and A. Mustafa, *Journal of Membrane Science*, 329, 18 (2009).

21. S. Sambandam and V. Ramani, *Journal of Power Sources*, 170, 259 (2007).

22. V. S. Silva, B. Ruffmann, H. Silva, Y. A. Gallego, A. Mendes, L. M. Madeira and S. P. Nunes, *Journal of Power Sources*, 140, 34 (2005).

23. R. Y. M. Huang, P. H. Shao, C. M. Burns and X. Feng, *Journal of Applied Polymer Science*, 82, 11 (2001).

24. Z. Qi and A. Kaufman, *Journal of Power Sources*, 109, 227 (2002).

25. B. Sunden and M. Faghri, *Transport Phenomena in Fuel Cells*, WIT Press, United Kingdom, 2005.

26. J. H. Kim, H. Y. Ha, I. H. Oh, S. A. Hong, H. N. Kim and H. I. Lee, *Electrochimica Acta*, 50, 801 (2004).

27. X. Ren, W. Henderson and S. Gottesfeld, *Journal of Electrochemical Society*, 144, L267.

28. G. Alberti, M. Casciola, L. Massinelli and B. Bauer, *Journal of Membrane Science*, 185, 73 (2001).

29. E. Gülzow, S. Weißhaar, R. Reissner and W. Schröder, *Journal of Power Sources*, 118, 405 (2003).

30. K. D. Kreuer, *Journal of Membrane Science*, 185, 29 (2001).

31. B. Yang and A. Manthiram, *Electrochemical Solid-State Letters*, 6, 229 (2003).

32. J. Rozière and D. J. Jones, *Annual Review of Materials Research*, 33, 503 (2003).

33. D. Chakraborty, I. Chorkendorff and T. Johannessen, *Journal of Power Sources*, 162, 1010 (2006).

34. Z. Siroma, *Journal of Electroanalytical Chemistry*, 546, 73 (2003).

Part IV

6. Optimizing the Operating Conditions of a DMFC using a Design of Experiments Methodology*

Abstract

The power density of a Direct Methanol Fuel Cell (DMFC) as a function of temperature, methanol concentration, air flow rate, methanol flow rate and air relative humidity was studied using a Response Surface Methodology (RSM). For a DMFC equipped with a membrane of Nafion 112, it was observed that only the temperature, methanol concentration and air flow rate were relevant factors or operating variables. A new design of experiments was done for a narrower range of these variables and the operating values that optimise the power density were obtained using the software JMP 7.0 (SAS). The predicted power density values were in agreement with the experimental results obtained for the optimized operating conditions. Then, the RSM was applied to membranes with different thicknesses, Nafion 112, Nafion 1135 and Nafion 117, and as a function of the temperature and methanol concentration. The DMFC was characterized for the open circuit voltage (OCV), methanol crossover at the OC, power density and global efficiency. The membrane showing the best compromise between power density and efficiency was Nafion 117.

*V. B. Silva, A. Mendes, submitted.

6.1. Introduction

Direct methanol fuel cell (DMFC) is a complex system that depends nonlinearly on a number of parameters to originate the observed power density and global efficiency [1]. The empirical understanding and optimization of a DMFC needs a large number of experiments performed at different operating conditions. This process can be long and a straightforward methodology is needed.

Traditional one by one experiment optimization is characterized by changing one independent variable under study while all the others are kept constant. This procedure can lead to misleading results due the superimposing of the interactions involved between the input parameters [2]. It should be noticed that sometimes these interactions can be more important than the effect produced by the independent variables. Furthermore, this procedure is also time-consuming because replications are highly recommended to prevent uncertainty and improve confidence in the obtained results. Then, the all procedure becomes time consuming and inaccurate being necessary a better approach.

On the other hand, when a full factorial design is applied the sample size grows exponentially in the number of factors [2] becoming too expensive to run for the most practical purposes; this could happen for DMFC systems where some parameters are involved. A fractional factorial experiment is then particular effective and highly suggested.

The Design of Experiments (DoE) is a fractional design approach that can be applied with advantage to the optimization and behavior understanding of a fuel cell [3, 4]. The DoE approach requires fewer runs and can handle simultaneously several factors. This allows the determination of high order interactions among these factors that may contribute to the final results. The relationship between the different input parameters or factors can then be identified and discussed. Additionally, the experiments are always

performed in a randomized way to minimize the occurrence of systematic experimental errors.

In the open literature, there are some studies considering the discussion and application of the DoE methodology to the DMFCs usage regarding both the operating conditions and the used materials. Lee et al. [5] used the DoE methodology to evaluate the electrical, mechanical and molding properties of graphite composite bipolar plates for Proton Exchange Membrane Fuel Cells (PEMFCs). Rahman et al [6] used a fractional factory analysis to optimize the preparation of gas-diffusion electrodes for Alkaline Fuel Cells (AFCs). It was concluded that the PFTE content, milling time and their interactions are the important parameters to achieve a better power performance.

The power output of a commercial PEMFC stack operating at atmospheric hydrogen pressure was also optimized using a fractional experimental design [3]. The experiments showed that not all the operating conditions delivered a stable power output with the considered hydrogen pressure, but that it was possible to stabilize it using higher oxygen flowrates.

Wahdame et al. [7] applied the DoE methodology to optimize a 5 kW fuel cell stack while Eccarius et al. [8] used the DoE coupled with a mathematical model to quantify the factors affecting the methanol crossover in a DMFC. The role and different possibilities offered by the DoE methodology in the fuel cell domain is also reported in the open literature [9].

The DMFC voltage versus current graph exhibits a S-shaped curve, which is related with the different limiting mechanisms that guide the DMFC behavior as a function of the current density changes [10]. This behavior can be predicted developing an analytical mathematical model that describes the governing equations associated to the physical or chemical processes for each current range. However, this procedure is

complex requiring considerable time periods and effort. At these circumstances, the DoE can be advantageously applied to generate an interpolating polynomial that describes the DMFC behaviour within the whole current range. One of the most implemented designs is the response surface method (RSM). The RSM includes several coupled statistical and mathematical methods that can predict effectively a system response that is dependant on some independent variables [11]. Simultaneously, it allows evaluating the optimal operating conditions and the corresponding responses.

To gain a better understanding about the DMFC behaviour using a Nafion 112 membrane, it was followed a RSM considering 5 factors, temperature, methanol concentration, air flow rate, methanol flow rate and air relative humidity, and three levels. It was used a commercial software, JMP from SAS, that indicated 36 experimental runs. This study allowed identifying the relevant factors. New experimental runs were then performed as a function of temperature, methanol concentration and air flow rate for a narrower range of these variables for obtaining the set of operating conditions that maximize the power density.

Finally, a new design was accomplished to inspect the power behaviour of a DMFC considering the use of Nafion membranes with different thicknesses and the relevant factors found in the previous designs. Additionally, the methanol crossover, open circuit voltage (OCV) and global efficiency were also experimentally obtained as a function of the temperature, methanol concentration and Nafion thickness (Nafion 112, Nafion 1135 and Nafion 117).

6.2. Experimental

6.2.1. MEA Pre-treatment

In this work were used membranes of Nafion 112, Nafion 1135 and Nafion 117. The samples were immersed in water at room temperature for 3 days to ensure total leaching. Then, the samples were immersed in boiling water (pre-treatment) during one hour before the characterization tests [12].

The backing and catalyst layers were also boiled during one hour for improving the catalyst performance [13].

6.2.2. *In situ* Activation Procedure

The *in situ* activation procedure was accomplished submitting the MEAs, inside the fuel cell at 55 ºC, to a set of sequential loading cycles. In each cycle, the cell was loaded during 180 minutes at 200 mV. Between each loading cycle it was allowed the MEA to rest for 30 minutes under the open circuit condition. The procedure was repeated for each cycle until the difference between two consecutive reads in the current density differ less than 3 % for the whole current range.

6.2.3. Design of Experiments: Selection of the optimum operating conditions

The operating variables pre-selected for the DMFC power density optimization were the temperature, methanol concentration, air flow rate, methanol flow rate and cathode humidification. The anode and the cathode pressure were kept constant at 2.5 bar. The operating range of each factor was selected taking into account the normal working conditions of a DMFC and for the pre-screening stage is listed in Table 6.1. To evaluate the response of the DMFC it was followed a RSM of three levels and with 5 central points. This first DoE allowed identifying the relevant factors for the range of operating conditions selected. A new DoE was then performed for a narrower operating conditions

range and with the relevant factors: temperature, methanol concentration and air flow rate. The new operating ranges are also given in Table 6.1.

Table 6.1 – Operating range conditions for the applied design of experiments.

Stage	**Methanol concentration / M**	**Air flowrate / $mL_N \cdot min^{-1}$**	**Methanol flowrate / $mL \cdot min^{-1}$**	**Temperature / ºC**	**Relative Humidity / %**
Screening	0.5 – 2.0	200 - 1000	4 - 20	50 - 90	0 -100
Optimization	1.2 – 1.6	600 - 1000	27	70 - 90	0

To study the role of the membrane thickness in the power density and global efficiency it was also used a DoE approach. The operating variables and ranges considered for this study are given in Table 6.2.

Table 6.2 – Operating variables and ranges for studying the role of the membrane thickness in the optimization of the power density and global efficiency.

Operating Conditions	**Methanol concentration / M**	**Temperature / ºC**	**PEM thickness / µm**
Range	1 - 3	50 - 90	50, 87.5 and 180

The anode and cathode pressures were kept constant and equal to 2.5 bar. It was concluded from the first set of experiments that the power density increases with the methanol flow rate; it was then chose the maximum value allowed by the experimental

set-up for this operating variable, 27 $mL \cdot min^{-1}$. The cathode was fed with air at 0 % of RH.

6.2.4. Characterization Methods

6.2.4.1. Methanol Crossover Measurements

The current density that results from the methanol that crosses the electrolyte ($I_{crossover}$) can be related with the anode mass-transport limiting current density ($I_{\lim}$) [14]:

$$I_{crossover} = I_{OCV,crossover} \times \left(1 - \frac{I}{I_{\lim}}\right) \quad (6.1)$$

where $I_{OCV,crossover}$ is the methanol crossover current density at the OCV and I is the operation current density.

To evaluate the parasitic current density at open circuit, the anode side of the DMFC was fed at similar conditions to the corresponding run (Table 6.3) and the cathode side was fed with a hydrogen stream at 200 $mL_N \cdot min^{-1}$, 2.5 bar and 0 % relative humidity. Scans were performed at a scan rate of 3 $mA \cdot s^{-1}$ between 0 and 0.8 V *vs* the reference electrode, in the galvanostatic mode. Finally, the limiting current density was obtained when the polarization curves were recorded.

6.2.4.2. DMFC Tests

MEAs were prepared by hot pressing the membrane samples, Nafion 112, Nafion 1135 and Nafion 117, between two ElectroChem electrodes at 90 ºC and 150 bar for 150 s. Supported PtRu (1 $mg \cdot cm^{-2}$ and 1:1 molar ratio) and Pt (0.5 $mg \cdot cm^{-2}$) were used on the anode and cathode, respectively. Single cell measurements were performed in a 25 cm^2 active area fuel cell. The open circuit voltage and the limiting current density were obtained operating the fuel cell in the respective conditions during 30 min and considering the steady state average value. The DMFC set-up is described elsewhere [15].

6.3. Discussion and Results

As mentioned before, the response surface method includes several mathematical and statistical techniques that can be applied advantageously to solve problems where a single or multiple responses are a function of a set of independent variables [11]. The effect of the independent variables on the process performance as well as the optimization of the responses can be evaluated without being necessary the developing of a phenomenological model that describes the governing equations associated to the physical and chemical phenomena. Indeed, the RSM models can be easily used for interpolating predicted values for different operating conditions and used for optimization purposes.

6.3.1. RSM Applied to a DMFC Operating at the Steady-state

6.3.1.1. Screening Experiments

In this study the RSM is applied to a DMFC operating at the steady-state for obtaining the power response surface. The design was generated considering five operating conditions (factors): temperature, methanol concentration, air flowrate, methanol flowrate and air relative humidity. The air pressure at the cathode was not included in the previous design because it was verified that inside the experimental set-up operating range, from 1 bar up to 2.5 bar, the power density increases monotonically with it. So, it was selected the pressure of 2.5 bar, the maximum pressure allowed by the experimental DMFC. All the DMFC design variables (active cell area among others) were kept constant for all runs.

The power density of the DMFC was obtained for 36 operating conditions, including 5 central points, generated randomly by the DoE software employed (JMP 7.0). The 5 central points are there to assess the experimental error. Table 6.3 shows the

DMFC operating conditions and the corresponding maximum power densities obtained experimentally.

Table 6.3 - DMFC operating conditions given by the DoE software and the corresponding maximum power densities.

Run #	Methanol concentration / M	Air Flow rate / $mL_N \cdot min^{-1}$	Methanol Flow rate / $mL \cdot min^{-1}$	Temperature / ºC	Relative Humidity / %	Maximum Power Density / $mW \cdot cm^{-2}$
1	2.00	200	12	50	0	18.1
2	0.50	600	4	70	50	28.7
3	2.00	600	12	90	50	61.2
4	1.25	600	12	70	50	41.3
5	2.00	200	4	70	50	34.3
6	1.25	1000	20	90	50	67.6
7	1.25	600	12	70	0	43.5
8	1.25	600	12	70	50	41.2
9	0.50	1000	12	90	0	49.5
10	0.50	600	20	90	100	49.1
11	1.25	1000	4	50	0	22.3
12	2.00	1000	12	70	100	35.0
13	1.25	600	12	70	50	41.8
14	1.25	200	4	90	0	65.5
15	1.25	600	20	70	100	39.8
16	1.25	600	12	70	50	36.1
17	2.00	1000	20	50	50	19.6
18	0.5	1000	12	50	100	16.0
19	2.00	600	20	70	0	37.6
20	0.50	200	4	50	100	13.1
21	0.50	1000	20	50	0	16.4
22	0.50	1000	4	90	100	48.4
23	1.25	600	4	90	100	65.8

24	2.00	600	4	50	100	18.9
25	0.50	200	20	50	50	14.0
26	1.25	200	20	90	0	63.9
27	2.00	200	20	90	100	58.2
28	1.25	200	12	70	100	38.1
29	0.50	200	4	50	0	13.8
30	2.00	200	20	50	100	17.1
31	1.25	1000	4	70	50	42.2
32	0.50	200	12	90	50	46.1
33	2.00	1000	4	90	0	62.8
34	1.25	600	12	70	50	41.5
35	1.25	600	12	50	50	21.9
36	1.25	600	12	70	50	41.2

In agreement with the experimental design, the parameters of a second order response model were obtained minimizing the sum of the residues square. The empirical model can be defined in terms of actual parameters as:

$$Y = B_0 + \sum_{i=1}^{5} B_i \times X_i + \sum_{i=1}^{5} B_{i,i} \times X_i^2 + \sum_{j=2}^{5} \sum_{i<j}^{5} B_{i,j} \times X_i \times X_j \qquad (6.2)$$

where Y is the power density, the X_i terms are the main factors $-1 \leq X_i \leq 1$,, temperature (1), methanol concentration (2), air flowrate (3), methanol flowrate (4) and air relative humidity (5) and the B_i terms are the equation coefficients related to the main factors. The B_0 term is the interception coefficient, the $B_{i,i}$ terms are the quadratic effects (give the curvature to the response surface) and the $B_{i,j}$ terms symbolize the cross interactions between factors

Table 6.4 shows the regression coefficients from the second order response model and their significance evaluated by the p-values.

Table 6.4 – Empirical coefficients of the second order polynomial model in terms of actual factors given by Equation (6.2) and their significance evaluated by the p-values. The coefficients with a p-value lower than 0.15 are in bold.

Parameters	Estimate	Prob > |t|
$\underline{B_0}$	41.1	0.00
B_1	**19.6**	**0.00**
B_2	**4.0**	**0.00**
B_3	**0.9**	**0.02**
B_4	0.5	0.16
B_5	**-0.5**	**0.13**
B_{11}	**3.6**	**0.00**
B_{12}	**2.5**	**0.00**
B_{22}	**-9.2**	**0.00**
B_{13}	**0.6**	**0.14**
B_{23}	-0.2	0.70
B_{33}	-0.8	0.22
B_{14}	-0.5	0.22
B_{24}	-0.3	0.54
B_{34}	0.6	0.17
B_{44}	**1.0**	**0.10**
B_{15}	-0.6	0.16
B_{25}	0.0	0.93
B_{35}	**0.7**	**0.12**
B_{45}	-0.3	0.41
B_{55}	0.0	0.95

The influence of the model parameters was assessed from the corresponding p-values. When the p-values are smaller than 0.05 indicates that the corresponding parameters have a significant effect on the response with a confidence level of more than 95 %. On the other hand, whenever the p-values are above 0.15 the parameters should be neglected. If the p-values sit between 0.05 and 0.15, then the parameters have a marginal effect on the response and should be taken into account in a first approach. This allows reformulating the fitting model and eventually upgrade some of these marginal parameters if their p-values become not greater than 0.05.

In Table 6.4 the parameters whose coefficient show a p-value lower than 0.15 are in bold; they are the temperature, methanol concentration, air flow rate and relative humidity. The quadratic factors are the temperature (B_{11}), methanol concentration (B_{22}) and anode flowrate (B_{44}) and the crossed factors are (B_{12}), temperature x methanol concentration, (B_{13}), temperature x air flowrate and (B_{35}), air flowrate x relative humidity. The new parameters obtained by fitting to the experimental data neglecting the parameters with p-values above 0.05 are given in Table 6.5. The interpolating polynomial after this two-step approach becomes:

$$Y = 40.9 + 19.6 \times X_1 + 4.0 \times X_2 + 1.0 \times X_3 + 3.3 \times X_1^2 - 9.0 \times X_2^2 + 2.3 \times X_1 \times X_2 \quad (6.3)$$

Table 6.5 – Empirical coefficients of Equation (6.3) and corresponding p-values.

Parameters	**Estimate**	**Prob > |t|**
$\underline{B_0}$	40.9	0.00
B_1	19.6	0.00
B_2	4.0	0.00
B_3	1.0	0.00
B_{11}	3.3	0.00
B_{12}	2.3	0.00
B_{22}	-9.0	0.00

An analysis of variance (ANOVA) was performed to verify the significance of this second order model. The *F* ratio, model mean square divided by the error mean square, is considerably high meaning that this model predicts well the experimental data. The model regression coefficient, R^2, is 0.99 indicating that almost all the data variance can be described by the empirical model. Furthermore, the R^2 values are not very different from the R^2 adjusted values; this indicates that the significant terms were included in the empirical model.

Figure 6.1 presents a parity plot of the experimental versus fitted vales. It can be seen that the polynomial model fits quite well the experimental data.

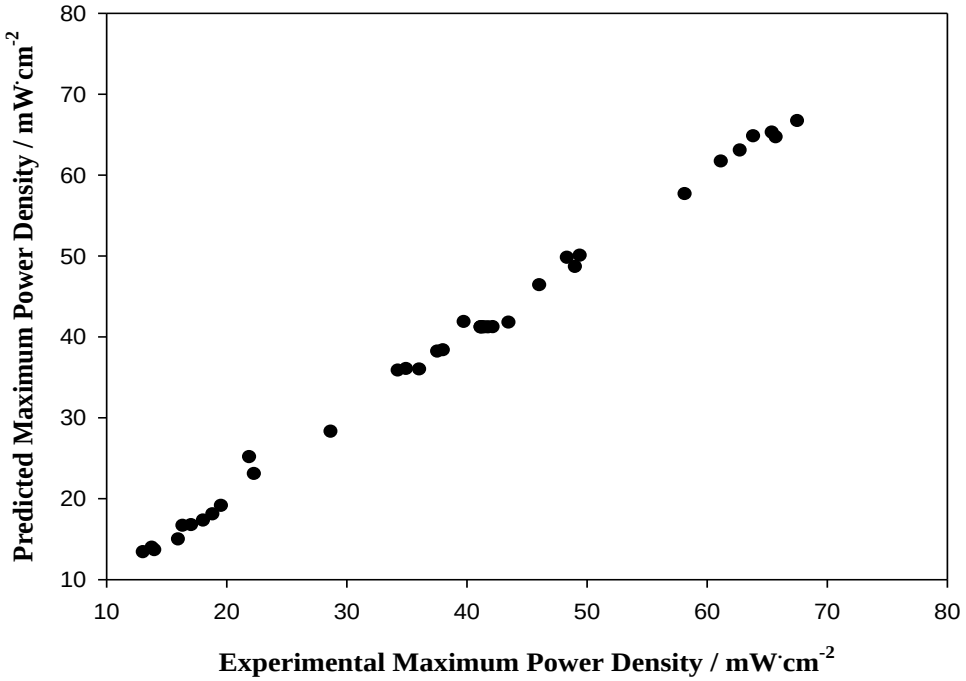

Figure 6.1 – Predicted maximum power density as a function of the experimental maximum power density.

Figure 6.2 plots the maximum power density at the optimum operating conditions (90 ºC, 1.5 M, air flowrate at 875 $mL_N \cdot min^{-1}$, methanol flowrate at 27 $mL \cdot min^{-1}$and 0 % relative humidity) as a function of the relevant parameters: a) temperature, b) methanol concentration and c) air flow rate. The maximum power density was obtained using the desirability function associated to equation (6.3).

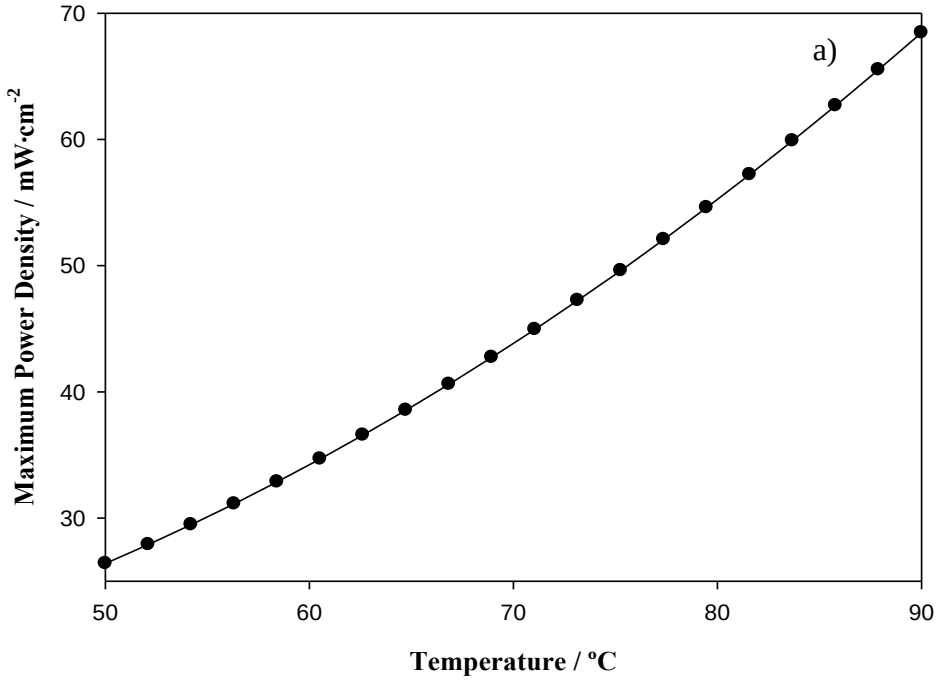
a)
Maximum Power Density / mW·cm-2
70
60
50
40
30
50
60
70
80
90
Temperature / ºC

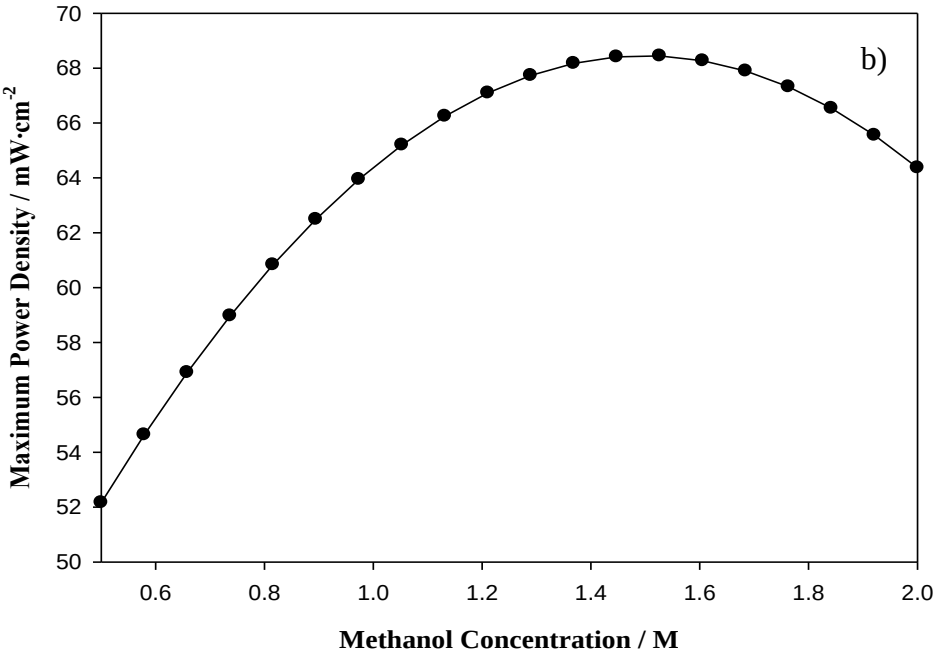
b)
Maximum Power Density / mW·cm-2
70
68
66
64
62
60
58
56
54
52
50
0.6
0.8
1.0
1.2
1.4
1.6
1.8
2.0
Methanol Concentration / M

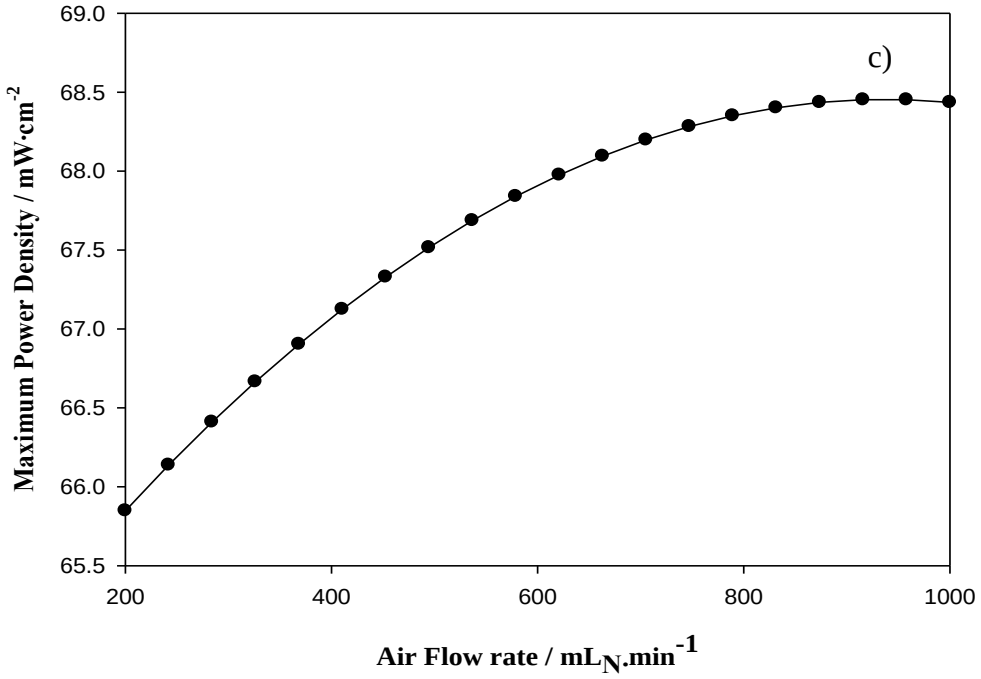

Figure 6.2 – Maximum power density at the optimum operating conditions (90 ºC, 1.5 M, air flowrate at 875 $mL_N \cdot min^{-1}$, methanol flowrate at 27 $mL \cdot min^{-1}$and 0 % relative humidity) as a function of the a) temperature b) methanol concentration and c) air flow rate.

From Figure 6.2a, it can be observed that the maximum power density increases with the temperature. In fact, the temperature plays a significant role on the improvement of the methanol oxidation and cathode reduction kinetics [1].

Figure 6.2b shows the power density as a function of the methanol concentration; the best methanol concentration is close to 1.5 M. When the anode feed is supplied with higher methanol aqueous solution concentrations the anode reaction (methanol oxidation) is favored; however the detrimental effect of the methanol crossover is also more pronounced. At higher methanol concentrations the main effect responsible for the power density is the methanol crossover. Indeed, when the fuel cell is supplied with methanol concentrations higher than 1.5 M, the maximum power density starts to decrease. This

fact is due to a lower equilibrium potential between the anode and the cathode and also due to the development of unavoidable parasitic reactions at the cathode generating a mixed potential.

Figure 6.2c shows that the performance of a DMFC increases with the air flow rate up to a maximum value. The performance of a DMFC increases with the air flow rate because it increases the oxidant concentration at the cathode side and controls the water concentration and then the excessive swelling. On the other hand, it vents more methanol from the cathode which presence is related to the mixed overpotential.

6.3.1.2. Optimization

The screening experiments were helpful to highlight the relevant parameters related with the maximum power density of the fuel cell. A new DoE was performed considering narrower ranges of the relevant operating conditions (Table 6.1); this should allow obtaining more accurately the optimum operating conditions. Table 6.6 lists the experiments performed and the corresponding fuel cell outputs: methanol crossover, limiting current density and maximum power density.

Table 6.6 – The DMFC operating conditions generated by a new design of experiment and the corresponding values.

Runs	Temperature / ºC	Methanol Concentration / M	Air Flow rate / $mL_N \cdot min^{-1}$	Methanol $Crossover_{OC}$ / $mA \cdot cm^{-2}$	Limiting Current Density / $mA \cdot cm^{-2}$	Maximum Power Density / $mW \cdot cm^{-2}$
1	90	1.2	800	158.2	319.2	69.1
2	80	1.4	800	144.7	293.2	57.1
3	90	1.4	1000	165.8	322.4	69.6
4	80	1.4	800	145.6	294.2	58.1
5	70	1.4	600	134.3	242.3	43.8
6	90	1.2	600	160.1	316.4	68.2
7	70	1.2	600	131.5	230.6	41.7
8	80	1.2	1000	140.2	285.6	55.8
9	70	1.4	800	139.3	245.3	44.2
10	90	1.4	800	166.2	321.3	69.4
11	80	1.6	600	150.2	278.3	53.4
12	80	1.4	800	145.8	293.2	58.2
13	80	1.6	1000	149.5	281.6	54.1

In Figure 6.3 the methanol crossover is plotted as a function of the temperature and methanol concentration keeping the airflow rate at 1000 $mL_N \cdot min^{-1}$. The most relevant factor affecting the methanol crossover is the temperature but the methanol concentration also plays a significant role. The methanol crossover is more sensitive to the methanol concentration at higher temperatures; these temperatures favour the formation of relatively large ionic clusters in the Nafion membrane. Water and methanol can be easily sorbed in these clusters and the swelled domains build percolate channel structures that favours the methanol crossover.

It was also observed that, as a general trend, the methanol crossover decreases with the air flowrate (not shown); indeed, the airflow sweeps the methanol that crosses the PEM and also the water, causing the OCV to increase.

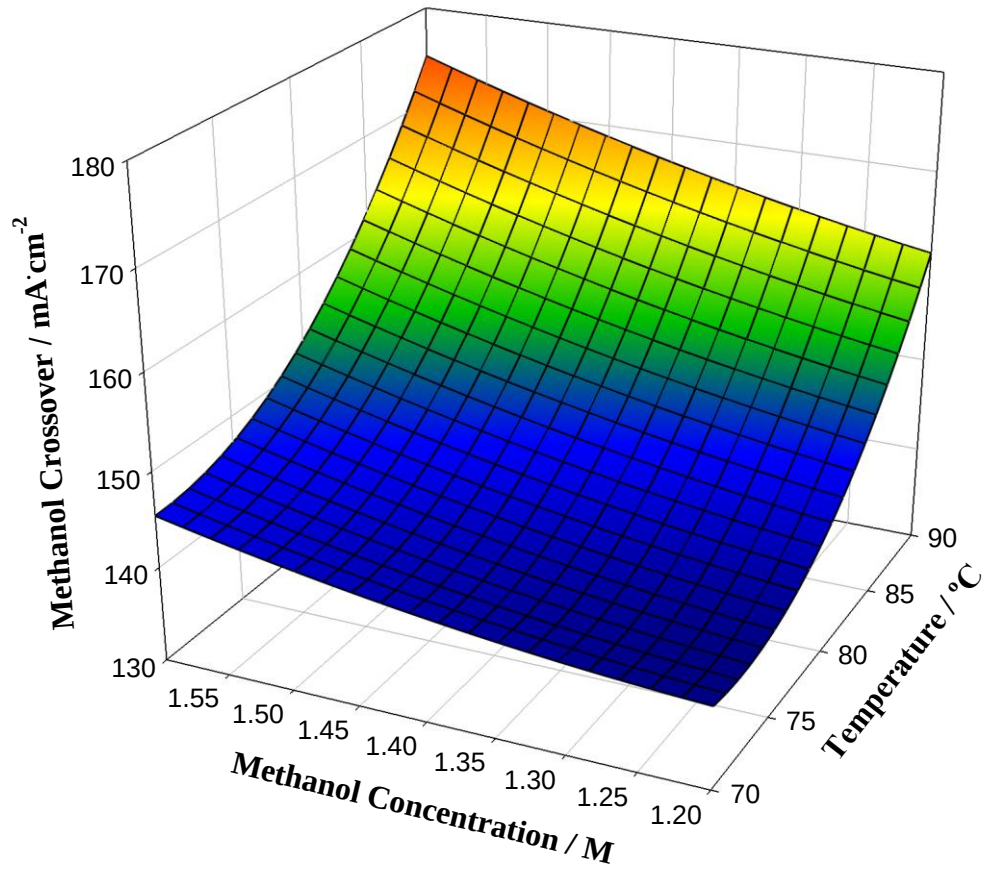

Figure 6.3 - Methanol crossover at OC as a function of the temperature and methanol concentration for 1000 $mL_N \cdot min^{-1}$ of air flow rate.

Figure 6.4 depicts the limiting current density as a function of the a) temperature and methanol concentration and as a function of the b) temperature and air flowrate. From Figure 6.4, it can be observed that the limiting current behaviour of a MEA using a Nafion membrane is mainly determined by the temperature and to a lesser extent by the methanol concentration and air flow rate. It was verified that the limiting current density increases with the temperature and achieves its maximum value at intermediates methanol concentrations. For high current densities, i.e. for higher temperatures and more concentrated methanol solutions, the increase amount of carbon dioxide produced at the

anode causes the partial blockage of the carbon cloth and diffusion layers pores, hindering the methanol access to the catalyst and then originating the current density decrease. Finally, it was observed that the limiting current density is only slightly affected by the airflow rate. This seems to indicate that in the considered range, the airflow rate was supplied above of the stoichiometry ratio as it can be confirmed by a molar and electrons balance.

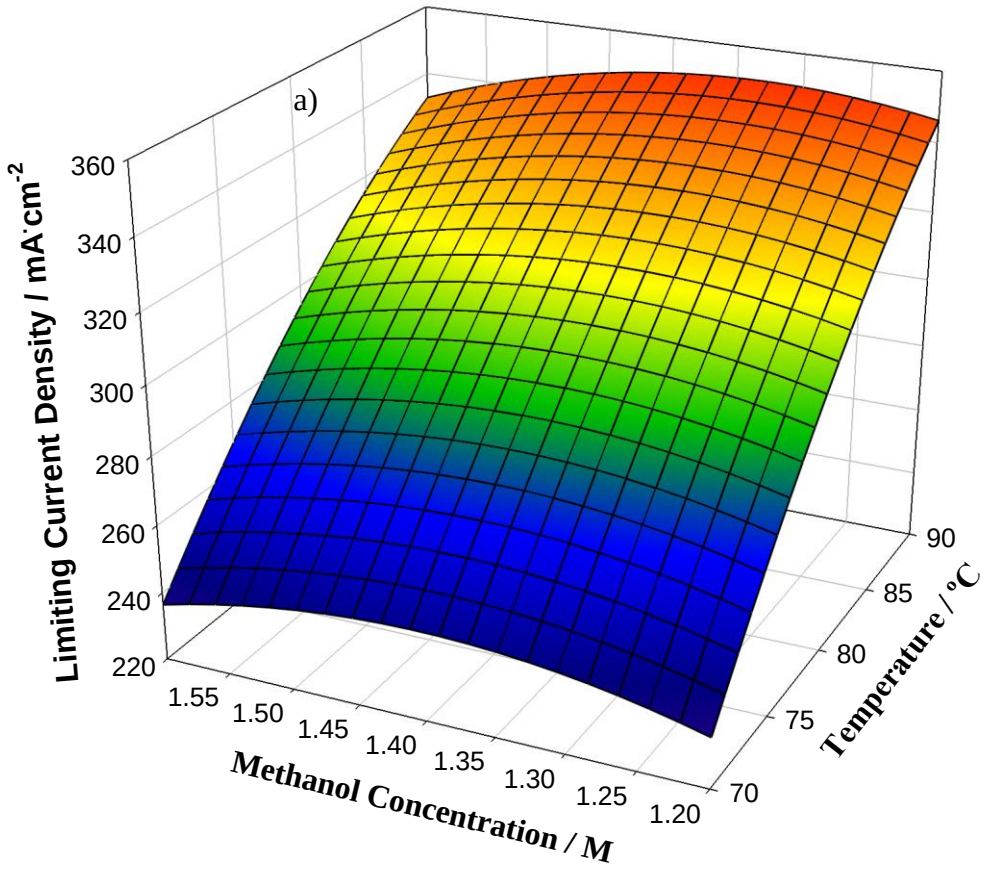

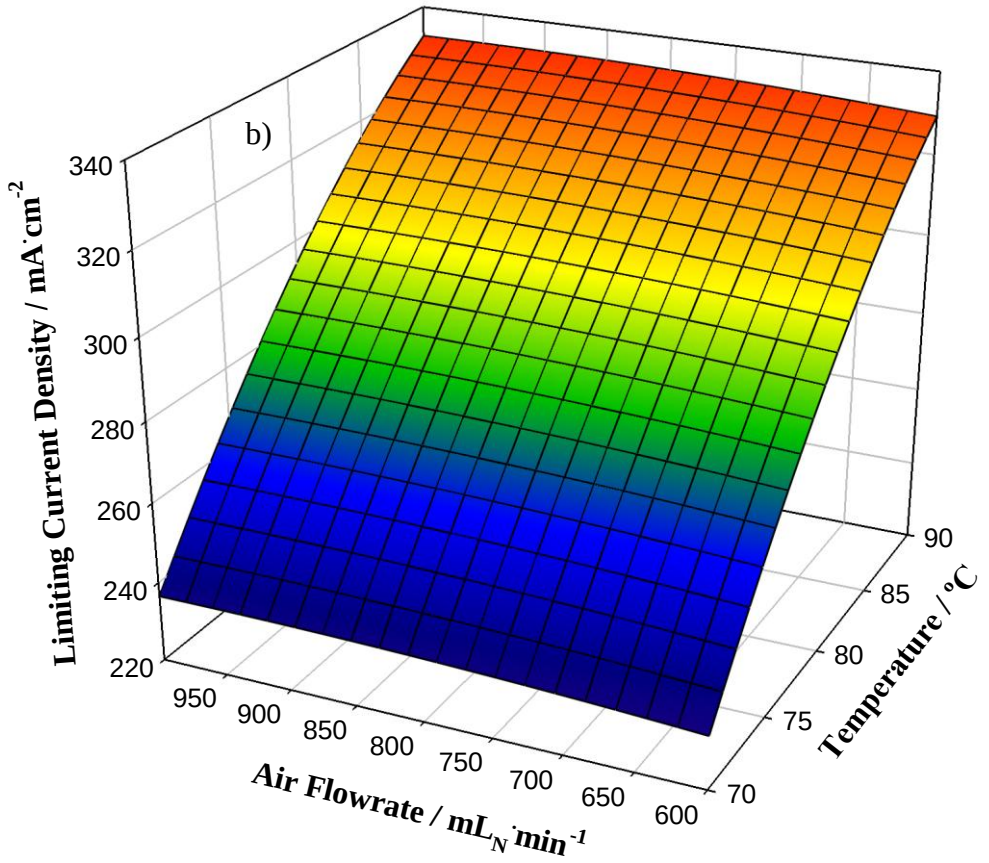

Figure 6.4 - Limiting current density as a function of the a) temperature and methanol concentration keeping the air flow rate at 1000 $mL_N \cdot min^{-1}$ and b) temperature and air flow rate keeping the methanol concentration at 1.6 M.

Using the empirical model, a maximum power density of 69.8 ± 2.9 $mW \cdot cm^2$ was computed for the following operating conditions: methanol concentration of 1.42 M, air flowrate of 850 $mL_N \cdot min^{-1}$ and operating temperature of 90 ºC – the other operating variables were: 27 $mL \cdot min^{-1}$ methanol feed flowrate and 0 % relative humidity. Finally, a new run was performed following the optimum operating conditions and it was observed that the experimental maximum power density (averaged of 4 runs) was 69.3 ± 0.6

$mW \cdot cm^{-2}$, within the predicted value. The average error was obtained using a t distribution for a 95 % confidence interval.

6.3.2. DoE applied to Proton Exchange Membranes with Different Thicknesses

The previous experiments were performed considering only Nafion 112 (50 μm). However, it is well known that the Nafion thickness affects the DMFC power density and efficiency [16, 17]. In fact, the membrane thickness should be selected carefully in order to achieve a compromise between different requirements, such as the proton conductivity, chemical stability, water and methanol permeability and cost of the membrane. Unfortunately, the membrane thickness affects each one of these properties in different ways, so the selection of the optimum thickness is a complex task.

Based in the previous experiments, it was concluded that the temperature and feed methanol concentration are much more relevant than the airflow rate in the performance of a DMFC. Following these conclusions, it was made a compact experimental design for highlight the role of the selected variables, methanol concentration, temperature and membrane thickness (Nafion 112, Nafion 1135 and Nafion 117), concerning the DMFC power density and global efficiency. In Table 6.7 are listed the operating conditions generated by the DoE (a custom design coupled with a response surface methodology was used because only discrete values were allowed to the Nafion thickness and not values within a range) and the corresponding experimental results for OCV, methanol crossover at OCV, power density and global efficiency.

Table 6.7 – Operating conditions generated by the DoE and the corresponding experimental values for OCV, methanol crossover, power density and global efficiency.

Runs	Temp. / ºC	Methanol Concent. / M	Thickness /µm	OCV / V	Methanol Crossover / mA·cm^{-2}	Maximum Power Density / mW·cm^{-2}	Maximum Global Efficiency / %
1	70	2	50	0.478	149.8	36.1	11.9
2	70	1	50	0.512	126.3	38.4	12.4
3	70	2	90	0.528	132.4	41.9	12.7
4	90	2	180	0.642	117.9	75.1	13.3
5	50	2	50	0.412	119.8	18.1	10.4
6	50	1	180	0.598	75.6	26.3	12.8
7	70	2	180	0.624	98.3	42.5	13.1
8	70	3	50	0.417	171.2	29.2	10.6
9	50	3	180	0.552	93.6	27.2	12.7
10	50	1	90	0.458	104.7	25.2	12.5
11	90	1	90	0.546	152.8	73.4	12.5
12	70	2	90	0.53	132.0	41.8	12.6
13	50	3	90	0.426	119.4	21.4	10.9
14	90	3	90	0.524	174.6	67.8	12.3
15	90	2	50	0.510	185.4	45.4	12.2

Figure 6.5 shows the OCV as a function of the a) temperature (at a feed methanol concentration of 2 M) and b) methanol concentration (at 80 ºC) for membranes Nafion 112, Nafion 1135 and Nafion 117. From Figure 6.5a, it can be observed that as a general trend, the open circuit voltage increases with the temperature independently of the membrane thickness. Thicker membranes (Nafion 117) show higher OCV values and a smaller temperature dependency.

From Figure 6.5b, it can be observed that thicker membranes behave better with higher methanol concentrations; at 3 M there is a significant difference between the OCV of Nafion 112 and the OCVs of the other membranes (Nafion 1135 and Nafion 117). At these circumstances, it is preferable to operate with thicker membranes (Nafion 1135 and Nafion 117) for preventing the excessive methanol permeability. On the other hand, the effect of the methanol crossover is more notorious at higher temperatures.

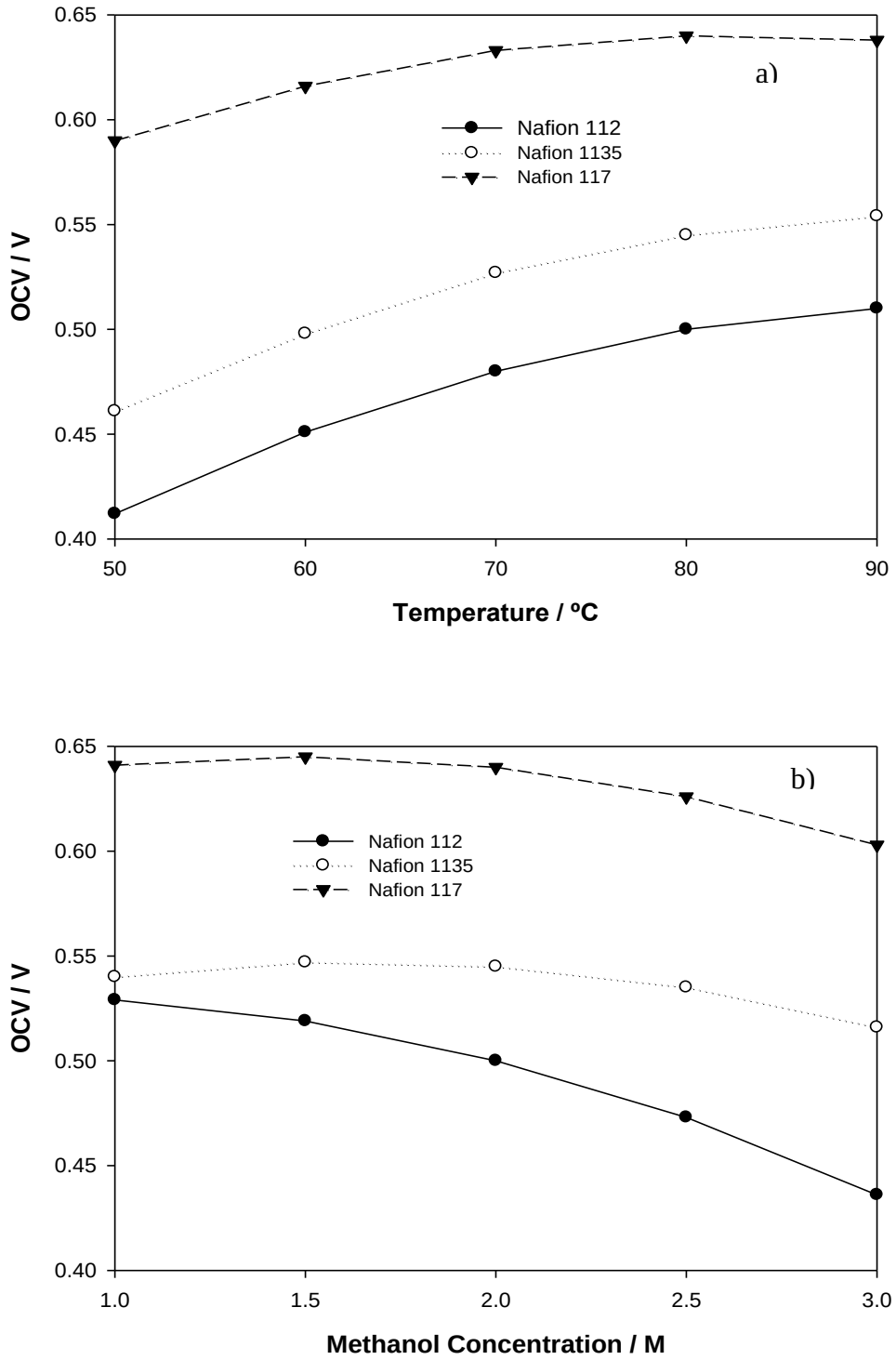

Figure 6.5 – Open circuit voltage as a function of the a) temperature (at a feed methanol concentration of 2 M) and of the b) methanol concentration (at 80 ºC).

Figure 6.6 shows the power density as a function of the a) temperature (at a feed methanol concentration of 2 M) and b) feed methanol concentration (at 80ºC) for Nafion membranes with different thicknesses. All membranes tested show higher power densities at higher temperatures (Fig. 6.6a). However, it can be observed that the thinner membrane (Nafion 112) experiences the smallest power increase probably due to the detrimental increase of the methanol crossover that is more notorious at higher temperatures. On the other hand, it can be observed that between 50 ºC and 70 ºC the obtained power densities are closer considering the Nafion 112 and the other two thicker membranes.

For thicker membranes, the optimum power density shifts towards higher methanol feed concentrations (Fig. 6.6b). Simultaneously, the performance of the thicker membranes, Nafion 117 and Nafion 1135, did not experience a significant decrease within the methanol concentration range considered, supporting severe conditions as 3 M without showing pronounced power losses.

Considering the global efficiency, it was verified that it does not vary considerably as a function of the operating variables within the selected ranges. This is probably because the potencial and faradaic efficiencies change inversely with the temperature, methanol concentration and membrane thickness. On the other hand, it was concluded that the maximum optimized global efficiency was 13.5 % and was obtained for the Nafion 117 membrane. Temperature is the factor that affects more the global efficiency.

The optimum for power density and global efficiency was obtained using membrane Nafion 117, this reveals that this membrane shows the best balance between permeability towards methanol and proton conductivity at the selected operating conditions. However, the power density and global efficiencies obtained using Nafion 1135 and Nafion 117 membranes were not very different.

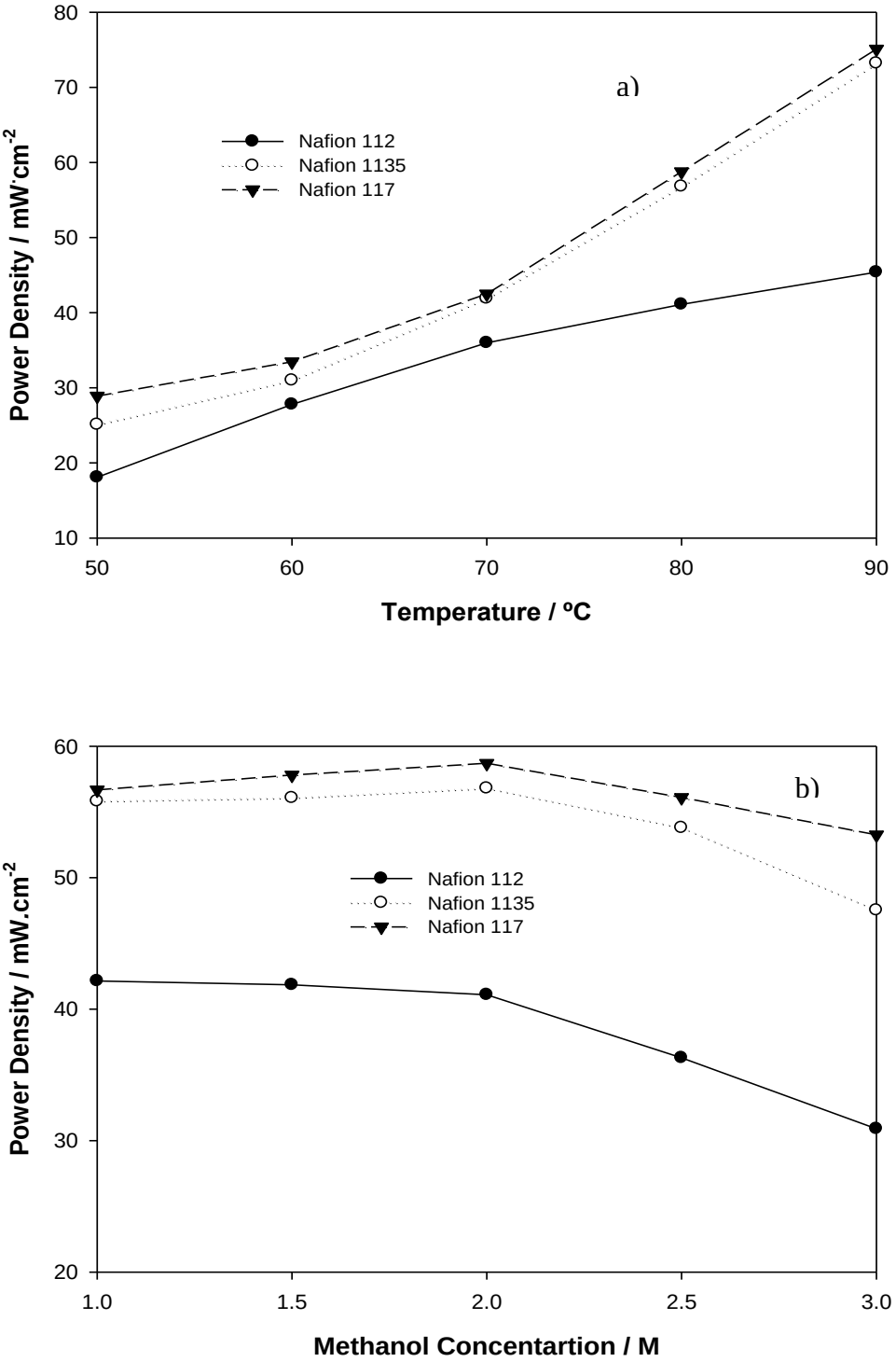

Figure 6.6 – Power density as a function of the a) temperature (at a feed methanol concentration of 2 M) and b) methanol concentration (at 80 ºC) for the Nafion 112, Nafion 1135 and Nafion 117 membranes.

6.4. Conclusions

The main factors that control the performance of a DMFC equipped with a membrane Nafion 112 were investigated using a response surface methodology. Initially they were selected 5 factors (temperature, methanol concentration, air flow rate, methanol flow rate and air relative humidity) and a set of 36 experiments performed. It was found that temperature, methanol concentration and air flow rate were the relevant factors affecting the power density of the fuel cell; the power density increased with the temperature in the range between 50 °C and 90 °C but showed a maximum with the air flow rate at 850 $mL \cdot min^{-1}$ and the methanol concentration at a concentration around 1.5 M. It was carried out a second design of experiments considering only the temperature, methanol concentration and air flow rate within a narrower set of ranges. This new design was used to obtain the operating conditions that originate the highest power density. The interpolating model predicted a maximum power density of 69.8 ± 2.9 $mW \cdot cm^{-2}$ for 90 °C, methanol concentration of 1.42 M and air flow rate of 875 $mL \cdot min^{-1}$, whereas the experimental value, averaged of four runs, was 69.7 ± 0.6 $mW \cdot cm^{-2}$.

Finally, the response surface method was also applied to membranes with different thicknesses (Nafion 112, Nafion 115 and Nafion 117), as a function of the temperature and methanol concentration. The DMFC equipped with thicker membranes (Nafion 1135 and Nafion 117) showed reasonable performances in the entire methanol concentration range. The maximum power density and global efficiency were obtained for the Nafion 117 membrane.

6.5. References

1. J. Ge and H. Liu, *Journal of Power Sources*, 142, 56 (2005)

2. D. C. Montgomery, *Design and Analysis of Experiments*, John Wiley & Sons, New York (1997).

3. R. C. Dante, J. L. Escamilla, V. Madrigal, T. Theuss, J. D. Caldéron, O. Solorza and R. Rivera, *International Journal of Hydrogen Energy*, 28, 343 (2003).

4. W. Lung, S. J. Wu and S. W. Shiah, *International Journal of Hydrogen Energy*, 33, 2311 (2008).

5. H. S. Lee, H. J. Kim, S. G. Kim and S. H. Ahn, *Journal of Materials Processing Technology*, 187, 425 (2007).

6. S. Rahman, M. A. Saleh and A. S. Al-Zakri, *Journal of Power Sources*, 72, 71 (1998).

7. B. Wahdame, D. Candusso, X. François, F. Harel, A. De Bernardis, J. M. Kauffmann and G. Coquery, *Fuel Cells*, 1, 47 (2007).

8. S. Eccarius, B. Garcia, C. Hebling and J. Weidner, *Journal of Power Sources*, 179, 723 (2008).

9. B. Wahdame, D. Candusso, X. François, F. Harel, J. M. Kauffmann and G. Coquery, *International Journal of Hydrogen Energy*, 34, 967 (2009).

10. V. Silva, PhD Thesis, Direct Methanol Fuel Cell: Analysis Based on Experimentation and Modeling, Porto, 2005.

11. R. H. Myers and D. C. Montgomery, *Response Surface Methodology: Process and Product Optimization Using Designed Experiments*, John Wiley & Sons, New York (2002).

12. V. S. Silva, V. B. Silva, A. Mendes, L. M. Madeira, H. Silva, J. Michaelmann, B. Ruffmann and S. P. Nunes, *Separation Science. Technology*, 42, 2909 (2007).

13. Z. Qi and A. Kaufman, *Journal of Power Sources*, 109, 227 (2002).

14. B. Sunden and M. Faghri, *Transport Phenomena in Fuel Cells*, WIT Press, United Kingdom, (2005).

15. E. Gülzow, S. Weißhaar, R. Reissner and W. Schröder, *Journal of Power Sources*, 118, 405 (2003).

16. P. Dimitrova, K. A. Friedrich, B. Vogt and U. Stimming, *Journal of Electroanalytical Chemistry*, 532, 75 (2002).

17. J. G. Liu, T. S. Zhao, Z. X. Liang and R. Chen, *Journal of Power Sources*, 153, 61, (2006).

Part IV

7. General Conclusions and Future Work

7.1. Conclusions

The present work aimed at studying the changes experienced by a MEA during an activation procedure of a proton exchange membrane fuel cell. Simultaneously, it was obtained the best DMFC operating conditions that maximize the efficiency and the power density. The optimization of the activation procedure as well as of the steady-state operating conditions of a fuel cell was obtained applying a DoE methodology.

7.1.1. Activation Procedure of a H_2-fed Fuel Cell

The *in situ* electrochemical techniques allowed to follow the induced changes by an applied loading program in a MEA along an activation procedure. It was verified that a set of loading cycles applied consecutively to a MEA makes it to increase the power density and global efficiency. It was verified that this procedure was effective even at 25 ^{o}C.

Polarization curves showed that the maximum power density of the Nafion 112-based MEA almost doubles from the 1st cycle to the last. It was observed a significant increase on the catalyst activity and catalytic area available to perform the electrochemical reactions. This was confirmed by an increase on the Tafel slope (obtained from the linear regression of the iR-compensated polarization curves) and by an increase of the electrochemical catalyst area obtained by cyclic voltammetry experiments. The open circuit voltage increases along the activation procedure mainly because of the mixed potential effect, which decreases accordingly. This was confirmed by linear sweep voltammetry and EIS data.

EIS experiments allowed concluding that the proton exchange membrane resistance decreases along the activation procedure due to an increase in the PEM water content. Actually, the PEM was hydrated along this procedure. The double layer capacitance increase along the loading cycles indicated that there was an enlargement of the triple phase boundary (catalyst/reactant/electrolyte), confirming a catalyst activity improvement. In fact, it was also verified that the increase of the catalyst activity was the main responsible factor for the increase of the MEA performance. The overall energy efficiency is also increased with the activation procedure.

7.1.2. Activation Procedure of a DMFC

Similarly to the H_2-fed fuel cell, whenever a MEA is inserted in a DMFC, it does not reach the best performance immediately after starting up. It was observed that when the activation procedure was applied to the DMFC, it undergoes a gradual increase on the power density and global efficiency. Indeed, the maximum power density of a MEA based on a Nafion 112 membrane increased about 2.5 times along the activation. On the other hand, the increase in the DMFC global energy efficiency was more notorious at high current densities due to a significant increase on the potential efficiency. Once again, the changes that a MEA experiences along the activation procedure were followed performing a set of *in situ* electrochemical tests and techniques, such as power curves (gives the history of the maximum power density), linear sweep voltammetry (gives the history of the methanol crossover), cyclic voltammetry (gives the history of the relative electrochemical catalyst area) and electrochemical impedance spectroscopy (gives the history of the PEM and catalyst resistances as well as the double layers' capacitance).

Despite the methanol crossover increase along the activation procedure; the open circuit voltage also increased due to a strong increase on the catalyst activity. This was

also confirmed by EIS experiments which showed a decrease of the anode resistances related to the adsorption and dehydrogenation phenomena associated to the methanol oxidation. In fact, the catalyst resistances decrease showed to be the main responsible factor for the maximum power density increase along the activation procedure. On the other hand, the role played by the PEM was also important not only due to its increased proton conductivity but also because it allowed a better interconnection and enlargement of the triple phase boundary.

The activation procedure can be divided in two main stages: pre-treatment and *in situ* activation, the later consisting in this work of a set of consecutive loading cycles. Concerning, the pre-treatment, it was verified that boiling the PEM in distilled water was the most effective procedure among the standard pre-treatments tested. This strategy was effective because it makes the membrane proton conductivity to increase significantly. On the other hand, the selected operating conditions during the *in situ* activation affect the DMFC final performance. In fact, the number of the loading cycles needed to achieve a stable performance of a DMFC can be reduced using optimized operating conditions. To minimize the number of activation cycles needed to obtain the maximum power density at steady-state conditions, it was used a Design of Experiments approach (surface response method). It was verified that for the *in situ* activation applied, the loading, the temperature and the cathode air pressure are the main factors affecting the power density of a DMFC. The loading is particularly effective when low voltages are used, i.e. less than 200 mV. Indeed, when the DMFC is activated at open circuit voltage, the final maximum power density is considerably lower. The DMFC should be also activated at intermediates temperatures, around 55 ºC. The DMFC power density is detrimentally affected when the activation procedure is performed at higher temperatures, probably due to an excessive

swelling on the ionomer that is interconnected with the catalyst. Finally, for the range of operating conditions considered, the cathode pressure always increases the power density.

The DoE methodology allowed to select the most favourable operating conditions. The boiling pre-treatment applied to the MEA and the *in situ* activation performed at the optimum operating conditions given by the DoE methodology allowed obtaining power densities very similar to the ones reached by the hydrogen conditioning, which is accepted as the most effective *in situ* activation procedure.

It was observed that the applied pre-treatment and *in situ* activation are also effective for MEAs using different types of proton exchange membranes, namely sPEEK, sPEEK loaded with different zirconium oxide contents (2.5 wt.% and 5 wt.%) and Nafion of different thicknesses.

The pre-treatment shorts the period needed for an activation procedure for all the selected proton exchange membranes. However, it was verified that the period of time for activation depends on the type and thickness of the membrane. Indeed, it was observed that the thinner membranes were activated faster.

The optimum temperature to perform the activation procedure also depends on the nature of the proton exchange membrane.

7.1.3. Optimization of the DMFC Operating Conditions

The performance of a DMFC depends largely on the applied operating conditions. Indeed, the temperature, the methanol concentration, the air flow rate, the methanol flow rate and the air relative humidity affect the maximum power density that can be extracted from a DMFC.

The response surface methodology can be applied advantageously to generate a semi-empiric second order model. Using this methodology, it was concluded that for a

DMFC equipped with a membrane of Nafion 112, the temperature, the methanol concentration and the air flow rate were the relevant operating variables.

The same methodology applied to DMFCs equipped with membranes of different thicknesses (Nafion 112, Nafion 1135 and Nafion 117) showed that the membrane that maximizes the power density and global efficiency was made of Nafion 117.

7.2. Future Work

There are several reports studying different approaches to obtain better performances at the start-up of a PEMFC. However, only few studies provide phenomenological support for the observed increase of performance during the activation procedure. In this work, a set of *in situ* electrochemical characterization methods were applied to better understand the changes experienced by the MEA, namely for MEAs equipped with different PEMs. However, the same methodology was not applied to MEAs equipped with different catalysts. Furthermore, there are no studies directed to understand the effect of changing the parameters related to the diffusion and catalyst layers (catalyst load, diffusion and catalyst layers thickness or the amount of electrolyte covering the catalyst particles, among others) during an activation procedure. This is a topic which certainly deserves further attention and research efforts.

The application of the DoE methodology for learning the role of catalytic-related design conditions could be very useful for understanding the catalyst phenomena and for shortening the activation period needed for PEMFCs equipped with different types of catalyst. On the other hand, it could contribute to find best protocols based on the selected diffusion and catalyst layers.

A model generated by the DoE approach could be also useful for helping the development of an analytical model that could describe some of the phenomena behind an activation procedure, such as, the electrochemical catalyst area changes, the catalyst

particle size evolution and the history of the catalyst coverage of oxides and PEM proton conductivity .

The development of a DMFC steady-state model coupled with the activation phenomena will allow not only to obtain a powerful diagnosis tool for power and energy efficiency optimization but also a diagnosis tool for design improvement.